# Quantum Optical State Comparison Amplification

Electra Eleftheriadou

Department of Physics and SUPA

University of Strathclyde

A thesis presented in the fulfilment of the requirements

for the degree of

*Doctor of Philosophy*

February 2015

# Copyright

This thesis is the result of the author's original research. It has been composed by the author and has not been previously submitted for examination which has led to the award of a degree.

The copyright of this thesis belongs to the author under the terms of the United Kingdom Copyright Acts as qualified by University of Strathclyde Regulation 3.50. Due acknowledgement must always be made of the use of any material contained in, or derived from, this thesis.

# Synopsis

Quantum signals have intriguing properties and a characteristic feature of them is their intrinsic noise. This results in uncertainty relations restricting our ability to measure conjugate variables with absolute precision simultaneously. In the context of amplification, this noise forbids an unknown quantum signal to be amplified perfectly in a deterministic manner.

In the first part of this thesis we propose a method to amplify coherent states probabilistically. Our method is based on coherent state comparison and photon subtraction. We found that for an input chosen at random from a binary set of states, under certain circumstances the fidelity can reach $100\%$. The probability of success is very high ($\sim 10 - 40\%$) and it increases with gain.

We tested the experimental performance of our protocol for a gain of $g^2 = 1.8$ and verified that the experimental results were in line with the theoretical predictions. For an input state chosen from a binary set the fidelity was $> 98\%$ and the success rate of our amplifier was $> 26000$ amplified states per second.

In the second part of the thesis we propose a new form of orbital angular momentum and angle states. These states consist of a sum of overlapping Gaussians in the angular position representation. We calculated both the uncertainty product and the entropic uncertainty relation for orbital angular momentum and angle. We found that in both cases our new states have a lower uncertainty than the intelligent states.

Bringing all results together, our proposals have implications in quantum communications: as our amplification protocol gives a perfect fidelity while maintaining a high success probability it can find application as a quantum optical repeater, and as our overlapping Gaussian states are well-defined for any value of the angular uncertainty and have lower uncertainty relations than the intelligent states, they could find applications in protocols exploiting the high-dimensional basis of orbital angular momentum states.

# Contents

Contents

# List of Figures

Introduction

S IGNAL AMPLIFICATION is often a necessary process in order to compensate for the attenuation of signals along long transmission distances. Amplifiers, devices that receive a weak signal and output a stronger signal, are placed either upon transmission, or upon reception of a signal, and in-between long transmission lines so that the signal is maintained at a practical level for detection.

Communication always attracted interest because of its ubiquity in everyday life. However, the interest in quantum communications and quantum technologies in general is at its peak these years. The unique properties that are inherent on quantum signals, open exciting new prospects for applications that never seemed feasible before. First and foremost, quantum key distribution promises to provide unconditional security that cannot be surpassed even by the most efficient classical supercomputers. Teleportation of information is possible for longer distances as years go by. Quantum digital signatures, quantum dense coding and a myriad of other applications will be accessible due to advances in quantum computing and quantum communications.

This thesis deals with two questions related to quantum communications. Both questions arise because of the characteristic intrinsic noise present in quantum signals.

The first part considers the amplification of quantum signals. Any device that amplifies a quantum signal deterministically, also amplifies the quantum noise and adds some noise as well. The amplification of the noise is not desirable as it swamps the quantum properties of the signal. However, it is possible to amplify a quantum signal with the amount of noise kept at its minimum, only if the amplification is non-deterministic. This means that the device will not always work, but when it works the resulting amplified signal will have the same amount of noise it had before amplification.

There are two main quality factors that characterise non-deterministic amplifiers: the fidelity of the amplified state with the desired amplified state that does not have any added noise and the success probability of the device. These measures compete. Current protocols either amplify with high fidelity and low probability of success, or

compromise on the fidelity for higher success rates. In addition, most current protocols rely on quantum resources and they do not amplify states with high amplitude or high gain.

These challenges lead us to the first research question: how can we amplify quantum optical states with a high fidelity and a high probability of success? In addition, can we do so without the use of quantum resources, with high gain, or for high input state amplitudes?

The second part of this thesis is related to the precision with which we can measure incompatible observables. Uncertainty relations govern quantum mechanics, limiting our ability to measure incompatible observables with absolute precision simultaneously. One possible observable is the orbital angular momentum of light. This provides a high-dimensional basis for encoding information. The conjugate variable of orbital angular momentum is angular position (or angle). Notably, the properties of light are correlated in orbital angular momentum and the angular position. This means that states carrying orbital angular momentum could be used extensively in quantum communication protocols based on entanglement.

The uncertainty relation for orbital angular momentum and angle observables has a state-dependent lower bound. Consequently, the states that minimise that uncertainty relation for linear position and linear momentum, the intelligent states, do not necessarily minimise the uncertainty relation for angular position and orbital angular momentum. Additionally, the constrained minimum uncertainty product states that minimise the uncertainty relation are complex and they are not well-defined.

The need for a better form of states leads us to the second question: are there any orbital angular momentum and angular position states that have are well-defined and minimise the uncertainty relation?

## 1.1   Aims and objectives

This thesis aims to answer both questions, with more emphasis given to the topic of amplification. The main achievements are as follows:

- We present a new protocol that amplifies quantum optical states probabilistically, using the techniques of coherent state comparison and photon subtraction

    - It provides a high fidelity and high success probability
    - It does not use complex quantum resources
      and it is easy to implement experimentally

- We realise our amplification protocol experimentally

    - It provides high fidelity and high success rate, in agreement with theory

- We present a new form of orbital angular momentum and angle states

    - They are well-defined for all values of the angular uncertainty
    - They have a lower uncertainty product than the intelligent states
    - They have a lower entropic uncertainty relation than the intelligent states
    - They have no significant difference to numerically optimised states

## 1.2  Thesis structure

Original contributions:

- **Chapter 4** Quantum Optical State Comparison Amplifier

  The theoretical protocol for quantum optical state comparison amplification.

  *Physical Review Letters* **111**, 213601
  [Eleftheriadou, Barnett, and Jeffers, 2013]

- **Chapter 5** Experimental implementation of the state comparison amplifier

  The experiment was
  planned by John Jeffers, Robert J. Collins and Gerald S. Buller,
  designed by Ross. J. Donaldson, R.J.C. and G.S.B.,
  and analysed and the design enhanced by Electra Eleftheriadou.
  The experimental implementation was assembled and operated by
  R.J.D., R.J.C. and G.S.B. at Heriot-Watt University, Edinburgh, U.K.
  Analysis of the experimental data was performed by E.E. and J.J.

  A peer-reviewed version of this work has been accepted for publication
  in *Physical Review Letters*.

- **Chapter 6** Gaussian Entropy-Minimising States (GEMS)

  The new form of orbital angular momentum and angle states
  that improve upon previous bounds of uncertainty relations.

  The numerical optimisation algorithm was written by
  Prof. Miles J. Padgett at the University of Glasgow, U.K.

  *Journal of Optics* **16**, 105404
  [Yao, Brougham, Eleftheriadou, Padgett, and Barnett, 2014]

Background

- **Chapter 2** The basics
  The tools in quantum optics.

- **Chapter 3** Amplification of quantum optical states
  The existing protocols for quantum state amplification.

The end

- **Chapter 7** Conclusion
  The summary of the main results.

# PART I

---

# Quantum optical state comparison amplification

---

C OMMON TOOLS that are used in quantum mechanics, such as state vectors, operators, phase space distributions, etc, are introduced in this first chapter with the intention to set the ground for the rest of this thesis.

## 2.1 Preliminaries: States, operators and observables

### 2.1.1 State vectors

We express all the information we have about a physical system in what we call the *state* of the system. The states live in a complex vector space, the Hilbert space, so they can be described by vectors, usually referred to as state vectors. One of the nice properties of the Hilbert space is that we can define an inner product (or scalar product) between two vectors, say $\vec{\phi}, \vec{\psi}$,

$$\langle \vec{\phi}, \vec{\psi} \rangle = \langle \vec{\psi}, \vec{\phi} \rangle^* = c \tag{2.1}$$

where $c$ is a complex number. Dirac wrote the inner product as $\langle \phi | \psi \rangle$ which became known as the "Dirac bracket notation". We can think of the "bracket" as a combination of the "bra" $\langle \phi |$ and "ket" $| \psi \rangle$, where the ket $| \psi \rangle$ is another notation for the vector $\vec{\psi}$. Therefore the state vector $| \psi \rangle$ is defined as a superposition of some basis states, say $| \psi_n \rangle$,

$$| \psi \rangle = \sum_n c_n | \psi_n \rangle, \tag{2.2}$$

where $c_n$ is a complex number. It follows that the bra $\langle \phi |$ must live in the dual space of $| \psi \rangle$, in order for their inner product be a complex number. The Hilbert space is isomorphic to its dual (by Riesz Lemma), therefore there is a one-to-one correspondence between the bras and the kets. The bra is thus defined as,

$$\langle \phi | = \sum_n \langle \phi_n | c_n^*, \tag{2.3}$$

where $c_n^*$ is the complex conjugate of $c_n$ and in this notation the inner product (or overlap) between two states is

$$\langle\phi|\psi\rangle = \langle\psi|\phi\rangle^*. \tag{2.4}$$

The inner product of a state with itself is real and positive,

$$\langle\psi|\psi\rangle > 0, \tag{2.5}$$

and in particular when it is equal to one,

$$\langle\psi|\psi\rangle = 1, \tag{2.6}$$

we say that the state is normalised. For states that are both orthogonal, $\langle\psi_m|\psi_n\rangle = 0$ and normalised, $\langle\psi_n|\psi_n\rangle = 1$, such as the basis states, we say that they are orthonormal. It follows that the amplitudes $c_n$ are given by the overlaps

$$\langle\psi_n|\psi\rangle = c_n = \langle\psi|\psi_n\rangle^*. \tag{2.7}$$

If we set a normalisation condition and require that the probability amplitudes $|c_n|^2$ sum to one,

$$\sum_n |c_n|^2 = 1, \tag{2.8}$$

we can interpret $|c_n|^2$ as the probability that a measurement of the state $|\psi\rangle$ in the $\psi_n$ basis would yield $|\psi_n\rangle$.

### 2.1.2 Operators

Operators are applied to a state to give another state,

$$\hat{A}|\psi\rangle = |\phi\rangle, \tag{2.9}$$

where we will use the symbol $\hat{\ }$ to indicate that a function is an operator. The adjoint of an operator is defined as

$$\langle\phi|\hat{A}|\psi\rangle = \langle\psi|\hat{A}^\dagger|\phi\rangle^* \tag{2.10}$$

in Dirac notation and has the following properties:

$$(\hat{A}^\dagger)^\dagger = \hat{A} \tag{2.11}$$
$$(\lambda\hat{A})^\dagger = \lambda^*\hat{A}^\dagger \tag{2.12}$$
$$(\hat{A}\hat{B})^\dagger = \hat{B}^\dagger\hat{A}^\dagger \tag{2.13}$$
$$(\hat{A} + \hat{B})^\dagger = \hat{A}^\dagger + \hat{B}^\dagger. \tag{2.14}$$

Sometimes it is more convenient to express the operators in their matrix form. An operator acting on an $N$-dimensional Hilbert space can be described by an $N \times N$ square matrix. A vector is equivalent to a single column matrix and so the kets can be expressed as column vectors and the bras as row vectors.

A very important class of operators are the *self-adjoint* operators. An operator is self-adjoint if it is equal to its adjoint, $\hat{A} = \hat{A}^\dagger$ and so $\langle\phi|\hat{A}|\psi\rangle = \langle\psi|\hat{A}|\phi\rangle^*$.

## Eigenvalue equation

We say that $|\psi_n\rangle$ is an eigenstate (or eigenvector) of $\hat{A}$ with eigenvalue $\alpha_n$ if the following equation is satisfied

$$\hat{A}|\psi_n\rangle = \alpha_n|\psi_n\rangle, \tag{2.15}$$

known as an eigenvalue equation (or $\langle\psi_n|\hat{A}^\dagger = \langle\psi_n|\alpha_n^*$), where $\alpha_n$ is a complex number in general. A function of an operator $f(\hat{A})$ is also an operator and

$$\text{if } \hat{A}|\psi_n\rangle = \alpha_n|\psi_n\rangle,$$
$$\text{then } f(\hat{A})|\psi_n\rangle = f(\alpha_n)|\psi_n\rangle. \tag{2.16}$$

If $\hat{A}$ is a self-adjoint operator, $\hat{A} = \hat{A}^\dagger$, then the eigenvalues are real. Consequently, one of the postulates of quantum mechanics states that physical observables are represented by self-adjoint operators. Additionally, it can be shown that the eigenstates corresponding to different eigenvalues must be orthogonal. Therefore the eigenstates of a self-adjoint operator form a complete orthonormal basis and any state in the Hilbert space can be expanded uniquely as a linear combination of the eigenstates, as in (2.2).

## Mean and Variance

The expectation value (or mean) of measuring an observable $A$ associated with the (self-adjoint) operator $\hat{A}$ acting on the eigenstate $|\psi\rangle$ is given by

$$\langle\hat{A}\rangle = \langle\psi|\hat{A}|\psi\rangle \tag{2.17}$$

or more generally

$$\langle\hat{A}\rangle = \frac{\langle\psi|\hat{A}|\psi\rangle}{\langle\psi|\psi\rangle}, \tag{2.18}$$

if the state is not initially normalised, or if the operator, when applied to the state, results in a change of its magnitude. The expectation value $\langle\hat{A}\rangle$ is equivalent to the average of the measurements of identically prepared systems. The spread of the results from the mean is given by the variance,

$$(\Delta A)^2 = \langle\hat{A}^2\rangle - \langle\hat{A}\rangle^2$$
$$= \langle\psi|\hat{A}^2|\psi\rangle - \langle\psi|\hat{A}|\psi\rangle^2. \tag{2.19}$$

The square root of the variance is known as the uncertainty or standard deviation, $\Delta A$.

## Commutators

Another fundamental operator in quantum mechanics is the commutator. The commutator of two self-adjoint operators, $\hat{A}$ and $\hat{B}$, is given by the following relation,

$$[\hat{A}, \hat{B}] = \hat{A}\hat{B} - \hat{B}\hat{A}, \tag{2.20}$$

whilst the anti-commutator is given by

$$\{\hat{A}, \hat{B}\} = \hat{A}\hat{B} + \hat{B}\hat{A}. \tag{2.21}$$

The adjoint of the commutator of two self-adjoint operators is equal to the negative of the commutator:

$$
\begin{aligned}
[\hat{A}, \hat{B}]^{\dagger} &= (\hat{A}\hat{B} - \hat{B}\hat{A})^{\dagger} \\
&= \hat{B}^{\dagger}\hat{A}^{\dagger} - \hat{A}^{\dagger}\hat{B}^{\dagger} \\
&= \hat{B}\hat{A} - \hat{A}\hat{B}
\end{aligned}
$$
$$[\hat{A}, \hat{B}]^{\dagger} = -[\hat{A}, \hat{B}]. \tag{2.22}$$

We say that if

$$[\hat{A}, \hat{B}] = 0, \;\; \hat{A} \text{ and } \hat{B} \text{ commute} \tag{2.23}$$

$$[\hat{A}, \hat{B}] \neq 0, \;\; \hat{A} \text{ and } \hat{B} \text{ do not commute}. \tag{2.24}$$

Commutators indicate how a measurement of one observable influences the other or whether we can measure both observables simultaneously with absolute precision. In particular, when observables do not commute, then a measurement of one observable will introduce noise to the measurement of the other. This has as a consequence an uncertainty principle relating the standard deviations of two quantities A and B to the commutator of their operators by

$$\Delta A \Delta B \geq \frac{1}{2}|\langle [\hat{A}, \hat{B}] \rangle|, \tag{2.25}$$

of which the most well-known is Heisenberg's uncertainty principle

$$\Delta x \Delta p \geq \frac{\hbar}{2}, \tag{2.26}$$

where $\Delta x, \Delta p$ are the uncertainties in position, $\hat{x}$ and momentum, $\hat{p}$ and $\hbar = h/(2\pi)$ where $h$ is Planck's constant.

## Baker-Campbell-Hausdorff formula

According to (2.13) the adjoint of the operators $e^{\hat{A}}e^{\hat{B}}$ is

$$(e^{\hat{A}}e^{\hat{B}})^{\dagger} = e^{\hat{B}^{\dagger}}e^{\hat{A}^{\dagger}}. \tag{2.27}$$

However, if we wish to add the exponents there is a general formula we must use that involves the commutator of $\hat{A}$ and $\hat{B}$, known as the Baker-Campbell-Hausdorff

formula. If we consider the specific case where the commutator of two operators commutes with each of them,

$$[\hat{A}, [\hat{A}, \hat{B}]] = 0 = [\hat{B}, [\hat{B}, \hat{A}]], \tag{2.28}$$

then the following relation is true,

$$e^{\hat{A}} e^{\hat{B}} = e^{\hat{A} + \hat{B} + \frac{1}{2}[\hat{A}, \hat{B}]}. \tag{2.29}$$

## Ordering

It is evident that the order in which operators appear is very important. We group the operators depending on the position an annihilation operator, $\hat{a}$, has with respect to a creation operator, $\hat{a}^\dagger$ [Barnett and Radmore, 2002]:

- Normal order (indicated by the symbols ::):
  All creation operators are to the left of the annihilation operators,
  *e.g.* $: \hat{a} \hat{a}^\dagger \hat{a}^\dagger \hat{a} := \hat{a}^\dagger \hat{a}^\dagger \hat{a} \hat{a}$

- Anti-normal order (indicated by the symbols $\vdots \vdots$):
  All creation operators are to the right of the annihilation operators,
  *e.g.* $\vdots \hat{a} \hat{a}^\dagger \hat{a}^\dagger \hat{a} \vdots = \hat{a} \hat{a} \hat{a}^\dagger \hat{a}^\dagger$

- Symmetric order (indicated by $S(.)$):
  is the average of all possible orderings of the operators
  *e.g.* $S(\hat{a} \hat{a}^\dagger \hat{a}^\dagger \hat{a})$
  $= \frac{1}{6} \left( \hat{a}^\dagger \hat{a}^\dagger \hat{a} \hat{a} + \hat{a}^\dagger \hat{a} \hat{a}^\dagger \hat{a} + \hat{a}^\dagger \hat{a} \hat{a} \hat{a}^\dagger + \hat{a} \hat{a}^\dagger \hat{a}^\dagger \hat{a} + \hat{a} \hat{a}^\dagger \hat{a} \hat{a}^\dagger + \hat{a} \hat{a} \hat{a}^\dagger \hat{a}^\dagger \right)$

Operators in these specific orderings are used to define different quasiprobability distributions of the phase space. For example, the $P$-function, $Q$-function and Wigner function, are the distributions that can be defined when the operators are in normal, anti-normal and symmetric ordering, respectively [Schleich, 2011].

## Unitary operators

A *unitary* operator is the operator whose adjoint is equal to its inverse,

$$\hat{U}^\dagger = U^{-1}. \tag{2.30}$$

It follows that

$$\hat{U}^\dagger \hat{U} = \hat{\mathbb{1}} = \hat{U} \hat{U}^\dagger, \tag{2.31}$$

where $\hat{\mathbb{1}}$ is the identity operator. The eigenvalues of a unitary operator are in general complex numbers of modulus one and the eigenstates corresponding to different eigenvalues are orthogonal. This follows from the fact that unitary operators preserve the scalar product of the states under transformation,

$$\langle \phi | \psi \rangle = \langle \hat{U} \phi | \hat{U} \psi \rangle = \langle \phi | \hat{U}^\dagger \hat{U} \psi \rangle = \langle \phi | \psi \rangle, \tag{2.32}$$

and also they preserve the norm of a state. This makes the act of a unitary operator analogous to the rotation of vectors. Unitary operators appear in the description of the evolution of a quantum state, in systems with time-reversal symmetry and others. We will use to them describe the state transformation at a beamsplitter.

### 2.1.3 Mixed states and density operators

Sometimes we may not have all the information we need to express the quantum state in its state vector form, (2.2), but instead we may know only the probabilities $P_n$ that the system is in a normalised state $|\psi_n\rangle$. Therefore the average value of some observable $A$ associated with the operator $\hat{A}$ is the ensemble average

$$\langle \hat{A} \rangle = \sum_n P_n \langle \psi_n | \hat{A} | \psi_n \rangle. \tag{2.33}$$

The statistical mixture of states is represented by the density operator $\hat{\rho}$, that we define as

$$\hat{\rho} = \sum_n P_n |\psi_n\rangle\langle\psi_n|. \tag{2.34}$$

We require that the probabilities $P_n$ sum to unity, $\sum_n P_n = 1$, but if one of them is equal to one, $P_n = 1$, then the density matrix $\hat{\rho}$ reduces to

$$\hat{\rho} = |\psi_n\rangle\langle\psi_n|, \tag{2.35}$$

which is the corresponding description of (2.2) in the density operator formalism. The density operator in (2.34) is said to represent a mixed state, while the density operator in (2.35) is said to describe a pure state. Operators represent the outer product of two states, $|\psi\rangle\langle\phi|$.

### Completeness relation

If we sum over a set of basis states and obtain the identity,

$$\hat{\mathbb{1}} = \sum_m |\phi_m\rangle\langle\phi_m|, \tag{2.36}$$

we say that this set of states is complete. Equation (2.36) is a very useful tool known as the completeness relation or the resolution of the identity. Often it is used in order to change the basis of a function. For example, we can use the completeness relation, (2.36), to express the ensemble average, (2.33), as

$$\langle \hat{A} \rangle = \sum_n P_n \langle \psi_n | \hat{A} \hat{\mathbb{1}} | \psi_n \rangle$$

$$= \sum_n P_n \langle \psi_n | \hat{A} \left( \sum_m |\phi_m\rangle\langle\phi_m| \right) |\psi_n\rangle$$

$$= \sum_m \langle \phi_m | \left( \sum_n P_n |\psi_n\rangle\langle\psi_n| \right) \hat{A} |\phi_m\rangle$$

$$= \sum_m \langle \phi_m | \hat{\rho} \hat{A} | \phi_m \rangle$$

$$= \mathrm{Tr}\{\hat{\rho}\hat{A}\}, \tag{2.37}$$

where $\mathrm{Tr}$ is the trace operation that, as we have shown, can be evaluated in any basis.

## 2.2 The phase space

It's not easy to visualise something as abstract as a quantum state, but with the aid of the so-called *phase space* we can gain some insight into the structure of the density operator describing a quantum state [Schleich, 2011]. We will introduce the phase space depicting the properties of a classical system and then we will see how we can use the phase space to describe the properties of a quantum system.

### 2.2.1 Classical harmonic oscillator

Let's consider a simple harmonic oscillator, such as the periodic motion of a mass on a spring. From Newton's second law of motion the force acting on the mass is proportional to $\ddot{x}$, $F(x) = m\ddot{x}$. As this force is restoring, it is derivable from a potential $F(x) = -dV(x)/dx$. Here the potential is $V(x) = (1/2)m\omega^2 x^2$, where $\omega = \sqrt{k/m}$ is the natural frequency of oscillation and $k$ is the spring constant. By deriving the force, $F(x) = -m\omega^2 x$, we arrive to the relation

$$\ddot{x} = -\omega^2 x. \tag{2.38}$$

This is a second order differential equation and it is advantageous to define $\dot{x} = v$ in order to get a pair of coupled first order differential equations:

$$\dot{x} = v$$
$$\dot{v} = -\omega^2 x. \tag{2.39}$$

By specifying the initial conditions, $x(0)$ and $\dot{x}(0)$, we get a unique solution. The phase space of this system is the plot of the velocity, $\dot{x}(t)$, as a function of position, $x(t)$. The initial conditions $x(0), \dot{x}(0)$ give the first point on this plane. This point changes as a function of time and it traces a trajectory called the phase trajectory. We use an arrow on the phase trajectory to show how the system evolves in time. A closed phase trajectory describes a periodic motion, though note that the phase trajectory does not intersect itself and in this sense classical systems are deterministic.

We can either solve the two equations in (2.39) and use the initial conditions to get a unique solution, or we can find a general solution by evaluating the slope of the phase trajectory. Let's find the general solution first. If we divide the two equations in (2.39) and rearrange,

$$\frac{dv}{dx} = -\frac{\omega^2 x}{v}$$
$$vdv + \omega^2 x dx = 0, \tag{2.40}$$

and then integrate (2.40), we find

$$\frac{1}{2}v^2 + \frac{1}{2}\omega^2 x^2 = C \tag{2.41}$$

where $C$ is a constant. We can multiply this by $m$ to get the total energy, $E$, of the system:

$$\frac{1}{2}mv^2 + \frac{1}{2}m\omega^2 x^2 = E, \tag{2.42}$$
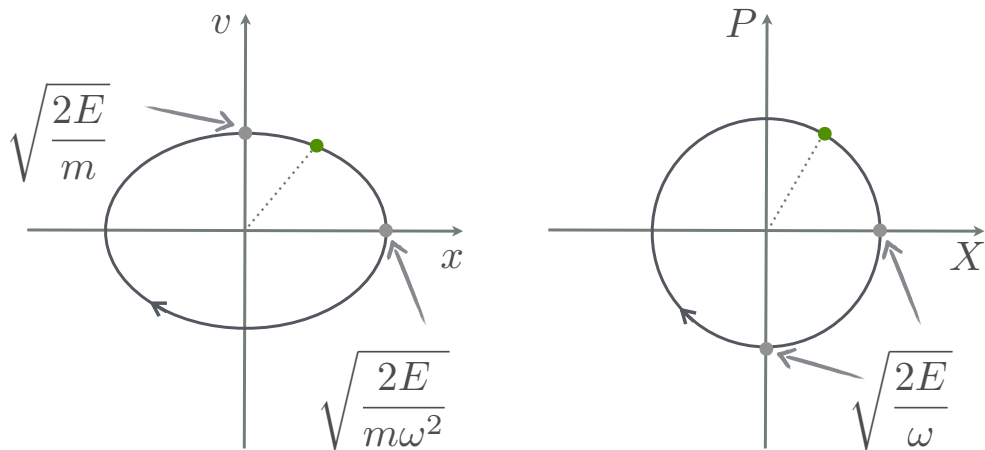
Figure 2.1: Each point on the phase space, $(x_i(t), v_i(t))$ or $(X_i(t), P_i(t))$, determines the state of the system completely at any instant of time. The arrow on the phase trajectory shows how the system evolves in time.

For periodic motion the phase trajectory is a closed loop and in particular for a harmonic oscillator the phase trajectory is an ellipse. We can rescale the axes to get circular phase trajectories.

where the first term on the left hand side of (2.42) is the kinetic energy and the second term is the potential energy. In the phase space, of $v$ vs $x$, this is an ellipse (Figure 2.1). An oscillator with a slightly higher or lower energy will be a concentric ellipse to this one. Like with any oscillatory motion, the time period is independent of the amplitude. If we wish we can multiply (2.42) by $m$ to get the ellipse on the momentum vs position phase space,

$$\frac{1}{2m}p^2 + \frac{1}{2}m\omega^2 x^2 = E. \tag{2.43}$$

We have seen how we can use the phase space to study a system, without the need to find the solutions to the equations of motion. This can be very useful if the system is more complex than a simple harmonic oscillator.

On the other hand, if we solve the equations of motion, we will get the following solutions,

$$\begin{aligned} x(t) &= A\cos\left(\omega t + \phi\right) \\ v(t) &= -\omega A\sin\left(\omega t + \phi\right) \end{aligned} \tag{2.44}$$

and

$$p(t) = -m\omega A\sin\left(\omega t + \phi\right) \tag{2.45}$$

for the momentum. We can define a function that represents position and momentum in the complex phase space. We choose the real axis to represent the position and

the imaginary axis to represent the momentum of the oscillator and so we define

$$\alpha(t) = x(t) + ip(t). \tag{2.46}$$

The axes of the phase plane can be rescaled, by multiplication of position by $\sqrt{m\omega}$ and momentum by $1/\sqrt{m\omega}$,

$$\alpha(t) = \sqrt{m\omega}A\cos{(\omega t + \phi)} + i\frac{(-1)}{\sqrt{m\omega}}m\omega A\sin{(\omega t + \phi)}$$
$$\alpha(t) = \sqrt{m\omega}Ae^{-i(\omega t + \phi)}$$
$$\alpha(t) = X(t) + iP(t) \tag{2.47}$$

to guarantee circular, rather than elliptical, phase trajectories (Figure 2.1). $X(t)$ and $P(t)$ are the rescaled $x(t)$ and $p(t)$ axes and now they have the same dimensions. The evolution of this function in time is

$$\dot{\alpha}(t) = -i\omega\alpha(t). \tag{2.48}$$

In this notation, the energy of the oscillator is equal to

$$E = \frac{1}{2}m\omega^2 A^2 \sin^2{(\omega t + \phi)} + \frac{1}{2}m\omega^2 A^2 \cos^2{(\omega t + \phi)}$$
$$E = \frac{\omega}{2}\left(P^2 + X^2\right)$$
$$E = \frac{\omega}{2}|\alpha(t)|^2, \tag{2.49}$$

and we know that it is constant in time.

### 2.2.2 Normal modes as harmonic oscillators

In this subsection we briefly state the form of the normal modes of an optical system in order to appreciate their mathematical equivalence to the harmonic oscillator. A detailed discussion of these points can be found in Grynberg et al. [2010].

It is known we can define a new field $\mathbf{A}(\mathbf{x}, t)$ called the vector potential that describes both the electric, $\mathbf{E}(\mathbf{x}, t)$ and magnetic, $\mathbf{B}(\mathbf{x}, t)$, fields in free space. It turns out that we can express the vector potential as a sum of functions, $\alpha_i(t)$,

$$\mathbf{A}(\mathbf{x}, t) = \sum_{i=-\infty}^{\infty} \frac{\mathbf{e}_i}{\sqrt{\omega_i}} C_i \left[\alpha_i(t)e^{i\mathbf{k}_i\mathbf{x}} + \alpha_i^*(t)e^{-i\mathbf{k}_i\mathbf{x}}\right], \tag{2.50}$$

where $\mathbf{e}_i$ are transverse polarisation vectors, the multi-index $i = (\mathbf{k}, s)$ contains three indices for the components of the $\mathbf{k}$-vector and one index for the two polarisation directions of each $\mathbf{k}$, $\omega_i = c|\mathbf{k_i}| = ck_i$ and $C_i$ is a constant. The normal modes $\alpha_i(t)$ are defined as

$$\alpha_i(t) = \frac{1}{2C_i}\left[\sqrt{\omega_i}\tilde{A}_i(t) + \frac{i}{\sqrt{\omega_i}}\dot{\tilde{A}}_i(t)\right], \tag{2.51}$$

where $\tilde{A}_i(t)$ are the scalar plane wave amplitudes. We find that the evolution of a normal mode in time is

$$\dot{\alpha}_i(t) = -iw_i\alpha_i(t), \tag{2.52}$$

which shows that each normal mode evolves independently from other modes. In fact, the real and imaginary parts are coupled,

$$\frac{\partial}{\partial t}\mathrm{Re}(\alpha_i) = w_i\mathrm{Im}(\alpha_i)$$

$$\frac{\partial}{\partial t}\mathrm{Im}(\alpha_i) = -w_i\mathrm{Re}(\alpha_i). \tag{2.53}$$

As time passes by, the real part of $\alpha_i(t)$ becomes the imaginary part and the imaginary part becomes a negative real. Equations (2.52) and (2.53) have the same form as those describing the harmonic oscillator, (2.48) and (2.39). Hence we reach an important conclusion: mathematically, a normal mode is equivalent to a harmonic oscillator, with the real part of $\alpha_i(t)$ interpreted as the position and the imaginary part as the momentum of a harmonic oscillator. As each normal mode evolves on its own, (2.52), we can treat them independently; in fact, we can treat the electromagnetic field as a sum of independent harmonic oscillators.

With this observation we note that we can use the phase space to plot the properties of the normal modes in the same way as we do for harmonic oscillators. We find the energy of the radiation field

$$H = \frac{\epsilon_0}{2}\int_V d^3r \left(|\mathbf{E}|^2 + c^2|\mathbf{B}|^2\right), \tag{2.54}$$

by expressing the electric, $\mathbf{E}(\mathbf{x}, t)$ and magnetic, $\mathbf{B}(\mathbf{x}, t)$, fields in terms of normal modes:

$$\mathbf{E}(\mathbf{x}, t) = -\dot{\mathbf{A}} = \sum_{i=-\infty}^{\infty} i\mathbf{e}_i\sqrt{\omega_i}C_i \left[\alpha_i(t)e^{i\mathbf{k}_i\mathbf{x}} - \alpha_i^*(t)e^{-i\mathbf{k}_i\mathbf{x}}\right] \tag{2.55}$$

$$\mathbf{B}(\mathbf{x}, t) = \nabla \times \mathbf{A} = \sum_{i=-\infty}^{\infty} i\mathbf{e}'_i\sqrt{\omega_i}C_i \left[\alpha_i(t)e^{i\mathbf{k}_i\mathbf{x}} - \alpha_i^*(t)e^{-i\mathbf{k}_i\mathbf{x}}\right], \tag{2.56}$$

where $\mathbf{e}'_i = 1/k_i(\mathbf{k}_i \times \mathbf{e}_i)$ and eventually we arrive at the expression that the total energy in the radiation field is

$$H = 4\epsilon_0 V \sum_i C_i^2 \frac{\omega_i}{2} |\alpha_i(t)|^2. \tag{2.57}$$

As it is expected, the energy of a each mode has the same form as the energy of the complex function we defined in (2.47) for the harmonic oscillator, (2.49).

In this subsection we mentioned the important analogy that one can draw between the normal modes of light and harmonic oscillators. Mathematically they are equivalent: the real and imaginary parts of a normal mode are coupled like the velocity (or momentum) and position of a harmonic oscillator. By convention, we keep the "position" and "momentum" labels in the phase space. It follows that the quantised normal modes behave like quantised harmonic oscillators. In the next subsection we will see that the "position" and "momentum" axes on the phase space give their way to the "position" and "momentum" operators.

### 2.2.3 Quantum harmonic oscillator

In this subsection we present the procedure to quantise the classical harmonic oscillator. Firstly, we find the positions, $x_i$ and momenta, $p_i$, of our system, as in subsection 2.2.1 or equivalently by using Hamilton's equations:

$$\dot{x}_i = \frac{\partial H}{\partial p_i}$$
$$\dot{p}_i = -\frac{\partial H}{\partial x_i}, \tag{2.58}$$

where the Hamiltonian, $H = T + V$, is the sum of the kinetic, $T$ and potential, $V$, energies. Then we replace the positions and momenta by the operators $\hat{x}_i$ and $\hat{p}_i$. Lastly, we require that these position and momentum operators obey the following commutation relations:

$$[\hat{x}_i, \hat{p}_j] = \delta_{ij} i\hbar, \tag{2.59}$$
$$[\hat{x}_i, \hat{x}_j] = [\hat{p}_i, \hat{p}_j] = 0, \tag{2.60}$$

known as the *canonical commutation relations*. From this we can find the famous uncertainty relation,

$$\Delta x \Delta p \geq \frac{1}{2} |\langle [\hat{x}_i, \hat{p}_i] \rangle|$$
$$\Delta x \Delta p \geq \frac{\hbar}{2}, \tag{2.61}$$

where $\Delta x$, $\Delta p$ are the uncertainties (or standard deviations) in position and momentum respectively.

The phase space plot of quantum states reflects the effect of the uncertainty principle. Let's look, for example, how the equilibrium point for a classical system and, analogously, the vacuum state for a quantum system are represented. For a classical system, the equilibrium point corresponds to the total energy being equal to zero. Thus on the phase space the equilibrium state is a point at the origin (Figure 2.2). However, we cannot pinpoint the state of a quantum system on the phase space in the same way as we can for a classical one. Heisenberg's uncertainty principle limits our ability to determine conjugate variables with absolute precision. Each point on the phase space becomes a circle of minimum uncertainty. The vacuum state is centred at the origin, with the quantum fluctuations symmetrically distributed around the centre (Figure 2.2). We will justify the last statement and see what different quantum states of light look like on the phase space in the following sections.
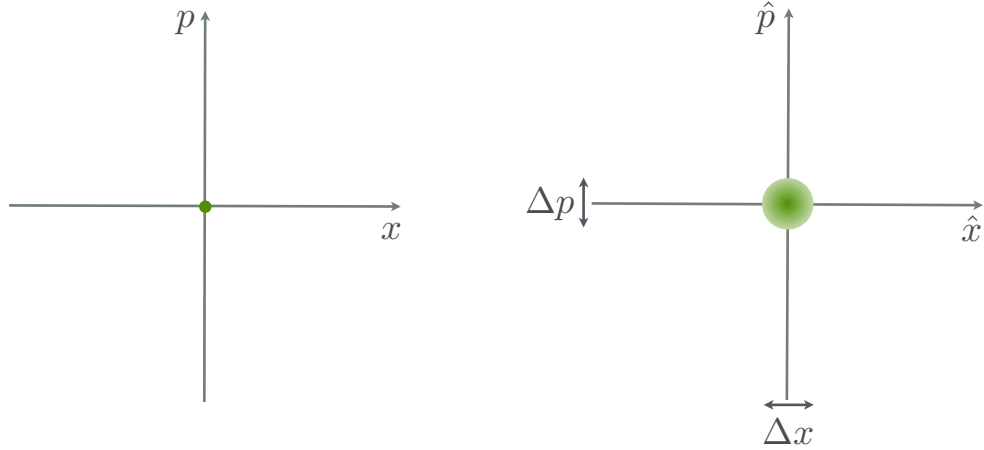
Figure 2.2: On the phase space, the equilibrium state of a classical system is represented by a single point at the origin. For a quantum system, the vacuum state is represented by a blob of uncertainty centred at the origin of the phase space.

The minimum quantum fluctuations are due to Heisenberg's uncertainty principle.

### 2.2.4 Creation and annihilation operators

Recall the function we defined for the normal mode, $\alpha_i = X_i + iP_i$. According to the rules of quantisation, we need to replace the "position" and "momentum" by their corresponding operators, which obey the canonical commutation relations. We choose to rescale the real and imaginary parts of $\alpha_i$ by $1/\sqrt{2\hbar}$ and so we define the operator for the normal mode:

$$\hat{a}_i = \frac{1}{\sqrt{2\hbar}} \left( \hat{x}_i + i\hat{p}_i \right), \tag{2.62}$$

with adjoint

$$\hat{a}_i^\dagger = \frac{1}{\sqrt{2\hbar}} \left( \hat{x}_i - i\hat{p}_i \right). \tag{2.63}$$

They have the following commutation relations,

$$
\begin{aligned}
[\hat{a}_i, \hat{a}_j^\dagger] &= \frac{1}{2\hbar} \left( \hat{x}_i + i\hat{p}_i \right) \left( \hat{x}_j - i\hat{p}_j \right) - \frac{1}{2\hbar} \left( \hat{x}_j - i\hat{p}_j \right) \left( \hat{x}_i + i\hat{p}_i \right) \\
&= \frac{1}{2\hbar} \left( \hat{x}_i\hat{x}_j - i\hat{x}_i\hat{p}_j + i\hat{p}_i\hat{x}_j + \hat{p}_i\hat{p}_j - \hat{x}_j\hat{x}_i - i\hat{x}_j\hat{p}_i + i\hat{p}_j\hat{x}_i - \hat{p}_j\hat{p}_i \right) \\
&= \frac{-i}{\hbar} [\hat{x}_i, \hat{p}_j] \\
&= \delta_{i,j}, 
\end{aligned}
\tag{2.64}
$$

and $[\hat{a}_i, \hat{a}_j] = [\hat{a}_i^\dagger, \hat{a}_j^\dagger] = 0.$ \hfill (2.65)

Their anti-commutator is

$$\{\hat{a}_i, \hat{a}_j^\dagger\} = \frac{1}{2\hbar}\left(\hat{x}_i + i\hat{p}_i\right)\left(\hat{x}_j - i\hat{p}_j\right) + \frac{1}{2\hbar}\left(\hat{x}_j - i\hat{p}_j\right)\left(\hat{x}_i + i\hat{p}_i\right)$$

$$= \frac{1}{2\hbar}\left(\hat{x}_i\hat{x}_j - i\hat{x}_i\hat{p}_j + i\hat{p}_i\hat{x}_j + \hat{p}_i\hat{p}_j + \hat{x}_j\hat{x}_i + i\hat{x}_j\hat{p}_i - i\hat{p}_j\hat{x}_i + \hat{p}_j\hat{p}_i\right), \quad (2.66)$$

therefore

$$\{\hat{a}_i, \hat{a}_i^\dagger\} = \frac{1}{\hbar}\left(\hat{x}_i^2 + \hat{p}_i^2\right). \quad (2.67)$$

It follows that the Hamiltonian operator for a mode of the quantum harmonic oscillator is

$$\hat{H}_i = \frac{\omega_i}{2}\left(x_i^2 + \hat{p}_i^2\right)$$

$$= \frac{\omega_i}{2}\hbar\left(\hat{a}_i\hat{a}_i^\dagger + \hat{a}_i^\dagger\hat{a}_i\right)$$

$$= \hbar\omega_i\left(\hat{a}_i^\dagger\hat{a}_i + \frac{1}{2}\right), \quad (2.68)$$

and the Hamiltonian operator of the radiation field is then the sum of all contributions.

Given the Hamiltonian, we can determine the eigenvalues of the energy eigenstates. Let us give a special name to the operator $\hat{a}_i^\dagger a_i$ appearing in the Hamiltonian,

$$\hat{n}_i = \hat{a}_i^\dagger a_i, \quad (2.69)$$

and let's suppose that the state $|n_i\rangle$ is an eigenstate of $\hat{n}_i$, such that

$$\hat{n}_i|n_i\rangle = n_i|n_i\rangle, \quad (2.70)$$

with eigenvalue $n_i$. With the help of $\hat{n}_i$ we can show how $\hat{a}_i^\dagger$ and $\hat{a}_i$ act on the state $|n_i\rangle$:

$$\hat{n}_i\hat{a}_i^\dagger|n_i\rangle = \hat{a}_i^\dagger a_i\hat{a}_i^\dagger|n_i\rangle$$

$$= \hat{a}_i^\dagger(1 + \hat{a}_i^\dagger a_i)|n_i\rangle$$

$$= \hat{a}_i^\dagger(1 + \hat{n}_i)|n_i\rangle$$

$$= (n_i + 1)\hat{a}_i^\dagger|n_i\rangle \quad (2.71)$$

$$\hat{n}_i\hat{a}_i|n_i\rangle = \hat{a}_i^\dagger a_i\hat{a}_i|n_i\rangle$$

$$= (\hat{a}\hat{a}_i^\dagger - 1)\hat{a}_i|n_i\rangle$$

$$= (\hat{n}_i - 1)\hat{a}_i|n_i\rangle$$

$$= (n_i - 1)\hat{a}_i|n_i\rangle. \quad (2.72)$$

The state $\hat{a}_i^\dagger|n_i\rangle$ is an eigenstate of $\hat{n}_i$ with eigenvalue $(n_i + 1)$ and $\hat{a}_i|n_i\rangle$ is an eigenstate of $\hat{n}_i$ with eigenvalue $(n_i - 1)$ and so

$$\hat{a}_i^\dagger|n_i\rangle = c_1|n_i + 1\rangle, \quad (2.73)$$

$$\hat{a}_i|n_i\rangle = c_2|n_i - 1\rangle. \quad (2.74)$$

Hence, the operator $\hat{a}^\dagger$ is called the *creation* (or raising) operator and the operator $\hat{a}$ is called the *annihilation* (or lowering, destruction) operator. The states $|n_i\rangle$ are normalised, $\langle n_i | n_i \rangle = 1$ and the constants $c_1, c_2$ are found to be

$$\langle n_i | \hat{a}_i \hat{a}_i^\dagger | n_i \rangle = \langle n_i + 1 | c_1^* c_1 | n_i + 1 \rangle$$
$$\langle n_i | (1 + \hat{a}_i^\dagger \hat{a}_i) | n_i \rangle = |c_1|^2$$
$$\langle n_i | (1 + \hat{n}_i) | n_i \rangle = |c_1|^2$$
$$(1 + n_i) = |c_1|^2, \tag{2.75}$$

$$\langle n_i | \hat{a}_i^\dagger \hat{a}_i | n_i \rangle = \langle n_i - 1 | c_2^* c_2 | n_i - 1 \rangle$$
$$\langle n_i | \hat{n}_i | n_i \rangle = |c_2|^2$$
$$n_i = |c_2|^2. \tag{2.76}$$

As $\hat{a}$ and $\hat{a}^\dagger$ are the conjugate of each other, the phases of the constants $c_1, c_2$ must be conjugate too,

$$\hat{a}|n\rangle = e^{-i\phi_n}\sqrt{n}|n-1\rangle, \tag{2.77}$$
$$\hat{a}^\dagger|n\rangle = e^{i\phi_n}\sqrt{n+1}|n+1\rangle, \tag{2.78}$$

where we include the possibility that the phases could depend on $n$. By using the commutation relation $[\hat{a}, \hat{a}^\dagger] = 1$, we have that

$$[\hat{a}, \hat{a}^\dagger]|n\rangle = \left( e^{i\phi_n}\sqrt{n+1}\hat{a}|n+1\rangle - e^{-i\phi_n}\sqrt{n}\hat{a}^\dagger \right)|n-1\rangle$$
$$= \left[ e^{i(\phi_n - \phi_{n+1})}(n+1) - e^{i(\phi_{n-1} - \phi_n)}n \right]|n\rangle = |n\rangle \tag{2.79}$$

and so the quantity in the square brackets must be equal to one for every $n$. For $n = 0$ we have that

$$e^{i(\phi_0 - \phi_1)} = 1 \tag{2.80}$$
$$\Rightarrow \phi_0 = \phi_1. \tag{2.81}$$

Similarly for $n = 1$ we have that

$$2e^{i(\phi_1 - \phi_2)} - 1 = 1 \tag{2.82}$$
$$e^{i(\phi_1 - \phi_2)} = 1$$
$$\Rightarrow \phi_1 = \phi_2 \tag{2.83}$$

and so on. Therefore that all the phases must be equal. However, as this phase is global it is physically insignificant, therefore we can choose the phase to be zero.

## Quadrature operators

It may be useful to express the "position" and "momentum" operators in terms of the normal mode operators, by rearranging (2.62) and (2.63),

$$\hat{x}_i = \sqrt{\frac{\hbar}{2}}\left( \hat{a}_i^\dagger + \hat{a}_i \right) \tag{2.84}$$

$$\hat{p}_i = i\sqrt{\frac{\hbar}{2}}\left( \hat{a}_i^\dagger - \hat{a}_i \right). \tag{2.85}$$

We can rescale them at our convenience, by multiplying by $1/\sqrt{2\hbar}$,

$$\hat{X}_i = \frac{1}{2}\left(\hat{a}_i^\dagger + \hat{a}_i\right)$$

$$\hat{P}_i = i\frac{1}{2}\left(\hat{a}_i^\dagger - \hat{a}_i\right), \tag{2.86}$$

so that $\hat{a}_i = \hat{X}_i + i\hat{P}_i$ and $\hat{a}_i^\dagger = \hat{X}_i - i\hat{P}_i$. The operators $\hat{X}_i$ and $\hat{P}_i$ are called the *quadrature* operators and as they are self-adjoint they correspond to observables. Their commutator is

$$
\begin{aligned}
[\hat{X}_i, \hat{P}_j] &= \frac{i}{4}\left[\left(\hat{a}_i^\dagger + \hat{a}_i\right)\left(\hat{a}_j^\dagger - \hat{a}_j\right) - \left(\hat{a}_j^\dagger - \hat{a}_j\right)\left(\hat{a}_i^\dagger + \hat{a}_i\right)\right] \\
&= \frac{i}{4}\left(\hat{a}_i^\dagger\hat{a}_j^\dagger - \hat{a}_i^\dagger\hat{a}_j + \hat{a}_i\hat{a}_j^\dagger - \hat{a}_i\hat{a}_j - \hat{a}_j^\dagger\hat{a}_i^\dagger - \hat{a}_j^\dagger\hat{a}_i + \hat{a}_j\hat{a}_i^\dagger + \hat{a}_j\hat{a}_i\right) \\
&= \frac{i}{4}\left([\hat{a}_i, \hat{a}_j^\dagger] + [\hat{a}_j, \hat{a}_i^\dagger]\right) \\
&= \frac{i}{2}[\hat{a}_i, \hat{a}_j^\dagger] \\
&= \frac{i}{2}
\end{aligned}
\tag{2.87}
$$

and the uncertainty product is

$$\Delta X_i \Delta P_i \geq \frac{1}{4}. \tag{2.88}$$

## Electric and magnetic field operators

One can find the operators for the vector potential, (2.50), the electric, (2.55) and magnetic fields, (2.56), through the transformation $\alpha_i(t) \rightarrow \hat{a}_i$,

$$\hat{\mathbf{A}}(\mathbf{x}, t) = \sum_{i=-\infty}^{\infty} \mathbf{e}_i \sqrt{\frac{\hbar}{2\epsilon_0 V \omega_i}}\left[\hat{a}_i e^{i\mathbf{k}_i\mathbf{x}} + \hat{a}_i^\dagger e^{-i\mathbf{k}_i\mathbf{x}}\right], \tag{2.89}$$

$$\hat{\mathbf{E}}(\mathbf{x}, t) = \sum_{i=-\infty}^{\infty} i\mathbf{e}_i \sqrt{\frac{\hbar\omega_i}{2\epsilon_0 V}}\left[\hat{a}_i e^{i\mathbf{k}_i\mathbf{x}} - \hat{a}_i^\dagger e^{-i\mathbf{k}_i\mathbf{x}}\right], \tag{2.90}$$

$$\hat{\mathbf{B}}(\mathbf{x}, t) = \sum_{i=-\infty}^{\infty} \frac{i\mathbf{e}'_i}{c} \sqrt{\frac{\hbar\omega_i}{2\epsilon_0 V}}\left[\hat{a}_i e^{i\mathbf{k}_i\mathbf{x}} - \hat{a}_i^\dagger e^{-i\mathbf{k}_i\mathbf{x}}\right], \tag{2.91}$$

It is useful to define the electric field quadrature operators as

$$
\begin{aligned}
\hat{E}_{xi} &= \sqrt{\frac{\hbar\omega_i}{2\epsilon_0 V}}\left(\hat{a}_i^\dagger + \hat{a}_i\right) \\
&= \sqrt{\frac{\hbar\omega_i}{2\epsilon_0 V}}\sqrt{\frac{2}{\hbar}}\,\hat{x}_i,
\end{aligned}
\tag{2.92}
$$

$$
\begin{aligned}
\hat{E}_{pi} &= i\sqrt{\frac{\hbar\omega_i}{2\epsilon_0 V}}\left(\hat{a}_i^\dagger - \hat{a}_i\right) \\
&= \sqrt{\frac{\hbar\omega_i}{2\epsilon_0 V}}\sqrt{\frac{2}{\hbar}}\,\hat{p}_i,
\end{aligned}
\tag{2.93}
$$

that are a rescaled version the "position" and "momentum" quadrature operators $\hat{x}_i$ and $\hat{p}_i$ defined above. Their commutator is

$$\begin{aligned}
[\hat{E}_{xi}, \hat{E}_{pj}] &= \frac{\hbar\omega_i}{2\epsilon_0 V}\,\frac{2}{\hbar}\,[\hat{x}_i, \hat{p}_j] \\
&= \frac{\hbar\omega_i}{2\epsilon_0 V}\,\frac{2}{\hbar}\,i\hbar \\
&= 2i\,\frac{\hbar\omega_i}{2\epsilon_0 V},
\end{aligned} \tag{2.94}$$

and the uncertainty product is

$$\Delta\hat{E}_{xi}\Delta\hat{E}_{pi} \geq \frac{\hbar\omega_i}{2\epsilon_0 V}. \tag{2.95}$$

## 2.3 The quantised modes of light

We have shown that the quantised modes of light are given by the *annihilation* and *creation* operators,

$$\begin{aligned}
\hat{a}_i|n_i\rangle &= \sqrt{n_i}\,|n_i - 1\rangle \\
\hat{a}_i^\dagger|n_i\rangle &= \sqrt{n_i + 1}\,|n_i + 1\rangle.
\end{aligned} \tag{2.96}$$

The creation operator, $\hat{a}_i^\dagger$, acts on a state to reach states with higher energies indefinitely, but the annihilation operator, $\hat{a}_i$, must satisfy the equation

$$\hat{a}_i|0\rangle = 0, \tag{2.97}$$

as there can be no state with lower energy than the ground state. Also we have found that the Hamiltonian operator for the quantised radiation field is

$$\hat{H} = \sum_i \hbar\omega_i\left(\hat{n}_i + \frac{1}{2}\right), \tag{2.98}$$

where $\hat{n}_i = \hat{a}^\dagger\hat{a}$ is known as the number operator. The eigenstates of the number operator are the states $|n_i\rangle$, $\hat{n}_i|n_i\rangle = n_i|n_i\rangle$ and consequently they are the energy eigenstates, $\hat{H}|n_i\rangle = E|n_i\rangle$. These states form a complete orthonormal basis, *i.e.* the following relations hold $\langle n_i|n_j\rangle = \delta_{i,j}$ and $\sum_{n_i}^\infty |n_i\rangle\langle n_i| = \hat{\mathbb{1}}$.

### 2.3.1 Number states

It follows that the $n$th eigenstate, $|n_i\rangle$, can be reached by applying the creation operator on the vacuum state a certain number of times and normalising appropriately,

$$|n_i\rangle = \frac{(\hat{a}_i^\dagger)^{n_i}}{\sqrt{n_i!}}|0\rangle. \tag{2.99}$$

The eigenvalue equation

$$\hat{H}_i|n_i\rangle = E_{n_i}|n_i\rangle \tag{2.100}$$

yields,

$$
\begin{aligned}
\hat{H}_i|n_i\rangle &= \hbar\omega_i\left(\hat{n}_i + \frac{1}{2}\right)|n_i\rangle \\
&= \hbar\omega_i\left(n_i + \frac{1}{2}\right)|n_i\rangle,
\end{aligned} \tag{2.101}
$$

showing that the energy eigenvalue is proportional to the number of quanta (or excitations, or photons). These eigenstates, (2.99), are known as the *number* states (or Fock states).

We can find some of their properties by examining the uncertainty in the photon number, the electric field and quadrature operators. By using the eigenvalue equation (2.70) we find that the variance in the photon number is zero,

$$
\begin{aligned}
(\Delta n_i)^2 &= \langle\hat{n}_i^2\rangle - \langle\hat{n}_i\rangle^2 \\
&= \langle n_i|\hat{n}_i^2|n\rangle - \langle n_i|\hat{n}_i|n_i\rangle^2 \\
&= n_i^2 - n_i^2 \\
&= 0.
\end{aligned} \tag{2.102}
$$

In other worlds, these states have a well-defined number of photons. The orthonormality condition $\langle n_i|n_j\rangle = \delta_{i,j}$ forces the following relations to be equal to zero:

$$
\begin{aligned}
\langle n_i|\hat{a}|n_i\rangle &= \sqrt{n_i}\langle n_i|n_i - 1\rangle = 0 \\
\langle n_i|\hat{a}^\dagger|n_i\rangle &= \sqrt{n_i + 1}\langle n_i|n_i + 1\rangle = 0,
\end{aligned} \tag{2.103}
$$

and consequently we find that the average electric field vanishes,

$$\langle n_i|\hat{\mathbf{E}}_i|n_i\rangle = 0. \tag{2.104}$$

However, the variance of the electric field, given by

$$
\begin{aligned}
(\Delta\mathbf{E}_i)^2 &= \langle\hat{\mathbf{E}}_i^2\rangle - \langle\hat{\mathbf{E}}_i\rangle^2 \\
&\equiv \langle n_i|\hat{\mathbf{E}}_i^2|n_i\rangle - \langle n_i|\hat{\mathbf{E}}_i|n_i\rangle^2,
\end{aligned} \tag{2.105}
$$

is not zero, but instead it is proportional to the number of quanta:

$$
\begin{aligned}
\langle n_i|\hat{\mathbf{E}}_i^2|n_i\rangle &= -\frac{\hbar\omega_i}{2\epsilon_0 V}\langle n_i|\hat{a}_i^2 - \hat{a}_i\hat{a}_i^\dagger - \hat{a}_i^\dagger\hat{a}_i + \hat{a}_i^{\dagger 2}|n_i\rangle \\
&= -\frac{\hbar\omega_i}{2\epsilon_0 V}\langle n_i|\hat{a}_i^2 + \hat{a}_i^{\dagger 2} - (1 + 2\hat{a}_i^\dagger\hat{a}_i)|n_i\rangle \\
&= \frac{\hbar\omega_i}{2\epsilon_0 V}\langle n_i|1 + 2\hat{n}|n_i\rangle \\
&= \frac{\hbar\omega_i}{2\epsilon_0 V}(1 + 2n_i).
\end{aligned} \tag{2.106}
$$

This means that the electric field fluctuates, but on average it has zero fluctuations. This is true even for the vacuum state (Figure 2.2). Similarly, we can find the uncertainty in the quadratures, where the expectation values of the quadrature operators, $\hat{X}_i$, $\hat{P}_i$, (2.86), are

$$\langle n_i | \hat{X}_i | n_i \rangle = 0,$$
$$\langle n_i | \hat{P}_i | n_i \rangle = 0, \tag{2.107}$$
$$\tag{2.108}$$

but the variance is

$$\langle n_i | \hat{X}_i^2 | n_i \rangle = \frac{1}{4} \left( 1 + 2n_i \right),$$
$$= \frac{1}{2} \left( n_i + \frac{1}{2} \right),$$
$$\langle n_i | \hat{P}_i^2 | n_i \rangle = \frac{1}{2} \left( n_i + \frac{1}{2} \right). \tag{2.109}$$

Therefore, the uncertainty product reads

$$\Delta X_i \Delta P_i = \frac{1}{2} \left( n_i + \frac{1}{2} \right), \tag{2.110}$$

which means that it increases with the number of quanta. Once again we note that the variance of the quadrature operators is not zero for the vacuum state and the uncertainty product is equal to $1/4$ which is the minimum possible value that the uncertainty product in the quadrature operators allows, (2.88). This means that the vacuum is a *quadrature minimum - uncertainty state*.

We will describe a number state in the representation used so far but we note that this plot must be taken with caution in this special case. The representation is accurate in the limit of large quantum numbers [Schleich, 2011]. The two quadratures have the same properties, (2.109) and the zero average fluctuations, (2.107), imply that the phase of the number states is completely undefined (Figure 2.3).

## 2.3.2 Coherent states

From the definitions for the creation and annihilation operators, (2.96), we note that the creation operator cannot have eigenstates, *i.e.* satisfy the eigenvalue equation

$$\hat{a}^\dagger | \psi \rangle \overset{?}{=} \lambda | \psi \rangle. \tag{2.111}$$

For an arbitrary state $|\psi\rangle$ defined in the number state basis, $|\psi\rangle = \sum_{n=0}^{\infty} c_n |n\rangle$, we have

$$\hat{a}^\dagger \sum_{n=0}^{\infty} c_n |n\rangle = \sum_{n=0}^{\infty} c_n \sqrt{n+1} |n+1\rangle, \tag{2.112}$$
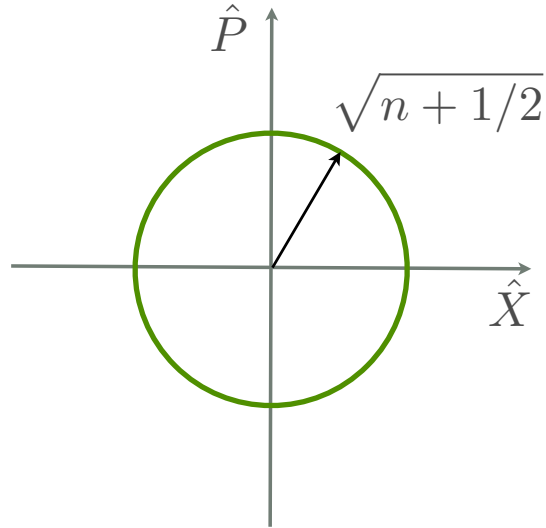
Figure 2.3: The number state has a well-defined energy, $n + 1/2$ and a completely undefined phase.

but this does not contain the vacuum state. Therefore equation (2.111) cannot be valid. However, the annihilation operator does have eigenstates,

$$\hat{a}|\psi\rangle = \alpha|\psi\rangle$$

$$\hat{a}\sum_{n=0}^{\infty} c_n|n\rangle = \sum_{n=1}^{\infty} c_n\sqrt{n}|n-1\rangle = \alpha\sum_{n=0}^{\infty} c_n|n\rangle \qquad (2.113)$$

and by equating the coefficients of the last two terms we get

$$c_n = \frac{\alpha}{\sqrt{n}}c_{n-1}. \qquad (2.114)$$

We can express the $n$th term in terms of the first one,

$$c_n = \frac{\alpha^n}{\sqrt{n!}}c_0, \qquad (2.115)$$

and by normalising, $\sum_n |c_n|^2 = 1$, we get the $0$th term,

$$|c_0|^2 \sum_n \frac{|\alpha|^{2n}}{n!} = |c_0|^2 e^{|\alpha|^2} = 1$$

$$\Rightarrow |c_0| = e^{-\frac{|\alpha|^2}{2}}. \qquad (2.116)$$

Therefore the annihilation operator has eigenstates

$$\hat{a}|\alpha\rangle = \alpha|\alpha\rangle, \qquad (2.117)$$

where the states $|\alpha\rangle$ are known as the *coherent* states (or Glauber states) [Glauber, 1963] and can be expressed as a linear superposition of number states:

$$|\alpha\rangle = e^{-\frac{1}{2}|\alpha|^2} \sum_{n=0}^{\infty} \frac{\alpha^n}{\sqrt{n!}}|n\rangle. \tag{2.118}$$

The annihilation operator is not self-adjoint so the eigenvalues $\alpha$ are complex: $\alpha = |\alpha|e^{i\theta}$, where $|\alpha|$ is referred to as the amplitude and $\theta$ as the phase of the coherent state (Figure 2.4). Coherent states are the left eigenstates of the creation operator,
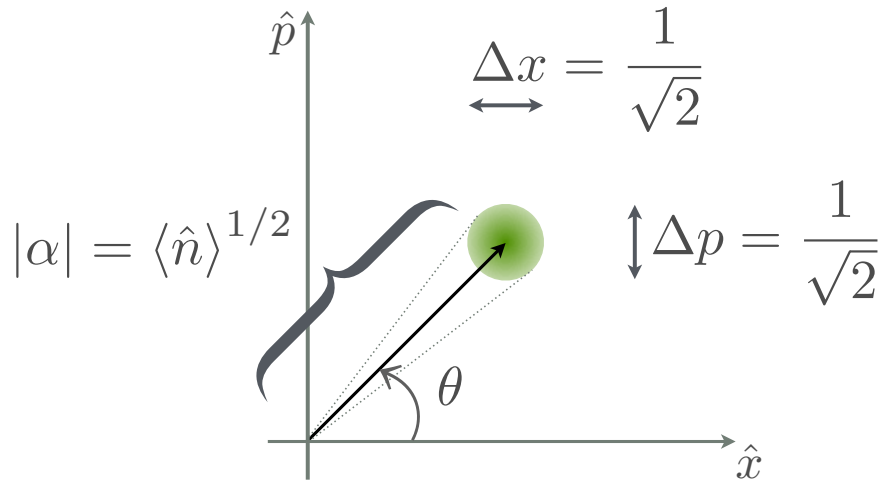


Figure 2.4: The coherent state as a displaced vacuum state, at a complex amplitude $|\alpha|$ from the origin and at a angle $\theta$ to the real axis of the phase space.

Coherent states are the minimum uncertainty states.

$$\langle\alpha|a^{\dagger} = \langle\alpha|\alpha^*. \tag{2.119}$$

From the definition of a coherent state as a superposition of number states, (2.118), we can show that coherent states are normalised

$$\begin{aligned} \langle\alpha|\alpha\rangle &= e^{-\frac{1}{2}|\alpha|^2}e^{-\frac{1}{2}|\alpha|^2} \sum_{n,m=0}^{\infty} \frac{\alpha^{*m}}{\sqrt{m!}} \frac{\alpha^n}{\sqrt{n!}} \langle m|n\rangle \\ &= e^{-|\alpha|^2} \sum_{n,m=0}^{\infty} \frac{\alpha^{*m}}{\sqrt{m!}} \frac{\alpha^n}{\sqrt{n!}} \delta_{m,n} \\ &= e^{-|\alpha|^2} \sum_{n=0}^{\infty} \frac{|\alpha|^{2n}}{n!} \\ &= e^{-|\alpha|^2}e^{|\alpha|^2} = 1, \end{aligned} \tag{2.120}$$

but they are not orthogonal,

$$\langle \alpha | \beta \rangle = e^{-\frac{1}{2}|\alpha|^2} e^{-\frac{1}{2}|\beta|^2} \sum_{n,m=0}^{\infty} \frac{\alpha^{*m}}{\sqrt{m!}} \frac{\beta^n}{\sqrt{n!}} \langle m | n \rangle$$

$$= e^{-\frac{1}{2}|\alpha|^2} e^{-\frac{1}{2}|\beta|^2} \sum_{n,m=0}^{\infty} \frac{\alpha^{*m}}{\sqrt{m!}} \frac{\beta^n}{\sqrt{n!}} \delta_{m,n}$$

$$= e^{-\frac{1}{2}|\alpha|^2} e^{-\frac{1}{2}|\beta|^2} \sum_{n=0}^{\infty} \frac{(\alpha^* \beta)^n}{n!}$$

$$= e^{-\frac{1}{2}|\alpha|^2 - \frac{1}{2}|\beta|^2 + \alpha^* \beta}$$

$$(2.121)$$

or

$$|\langle \alpha | \beta \rangle|^2 = e^{-|\alpha - \beta|^2}. \tag{2.122}$$

States that are complete but not orthogonal form an over-complete set. Coherent states are an example of such a set. They resolve the identity in the following way:

$$\int d^2\alpha |\alpha\rangle\langle\alpha| = \sum_{n,m=0}^{\infty} \frac{|n\rangle\langle m|}{\sqrt{n!m!}} \int d^2\alpha \ \alpha^n \alpha^{*m} e^{-|\alpha|^2} \tag{2.123}$$

where the integration is over the real and imaginary parts of $\alpha$, $d^2\alpha = d\alpha_R d\alpha_I$. The integral is therefore equal to

$$\int d^2\alpha \ \alpha^n \alpha^{*m} e^{-|\alpha|^2} = \int d\alpha_R \int d\alpha_I \ (\alpha_R + i\alpha_I)^n (\alpha_R - i\alpha_I)^m e^{-(\alpha_R^2 + \alpha_I^2)}$$

$$= \int_0^{\infty} |\alpha| d|\alpha| \int_0^{2\pi} d\theta |\alpha|^n e^{in\theta} |\alpha|^m e^{-im\theta} e^{-|\alpha|^2}$$

$$= \int_0^{\infty} d|\alpha| \ |\alpha|^{n+m+1} e^{-|\alpha|^2} \int_0^{2\pi} d\theta \ e^{i(n-m)\theta}$$

$$= 2\pi \delta_{n,m} \int_0^{\infty} d|\alpha| \ |\alpha|^{n+m+1} e^{-|\alpha|^2}$$

$$= 2\pi \delta_{n,m} \int_0^{\infty} d|\alpha| \ |\alpha|^{n+m+1} e^{-|\alpha|^2}$$

$$= 2\pi \delta_{n,m} \int_0^{\infty} \frac{dx}{2\sqrt{x}} x^{(n+m+1)/2} e^{-x}$$

$$= \pi \delta_{n,m} \int_0^{\infty} dx \, x^{(n+m)/2} e^{-x}$$

$$= \pi \delta_{n,m} \Gamma\left(\frac{n+m}{2} + 1\right)$$

$$= \pi n! \delta_{n,m} \tag{2.124}$$

where we introduced the integration variable $x = |\alpha|^2$ and used the Gamma function $\Gamma$ defined as

$$\Gamma(n+1) = \int_0^{\infty} dx \, x^n e^{-x} = n!. \tag{2.125}$$

Therefore,

$$\int \mathrm{d}^2\alpha |\alpha\rangle\langle\alpha| = \sum_{n,m=0}^{\infty} \frac{|n\rangle\langle m|}{\sqrt{n!m!}} \pi n! \delta_{n,m}$$

$$= \pi \sum_{n}^{\infty} |n\rangle\langle n|$$

$$= \pi \hat{\mathbb{1}} \tag{2.126}$$

and so for the coherent states the identity is resolved as

$$\hat{\mathbb{1}} = \frac{1}{\pi} \int \mathrm{d}^2\alpha |\alpha\rangle\langle\alpha|. \tag{2.127}$$

Now that we have a definition for the completeness relation, we can use it twice to write a general density operator $\hat{\rho}$ in the coherent state representation,

$$\hat{\rho} = \frac{1}{\pi} \int \mathrm{d}^2\alpha |\alpha\rangle\langle\alpha| \, \hat{\rho} \, \frac{1}{\pi} \int \mathrm{d}^2\beta |\beta\rangle\langle\beta|$$

$$= \frac{1}{\pi^2} \int \mathrm{d}^2\alpha \int \mathrm{d}^2\beta \, \langle\alpha|\hat{\rho}|\beta\rangle |\alpha\rangle\langle\beta|. \tag{2.128}$$

One can find the diagonal representation of a coherent state,

$$\hat{\rho} = \int \mathrm{d}^2\alpha P(\alpha) |\alpha\rangle\langle\alpha|, \tag{2.129}$$

by defining the function $P(\alpha)$ known as the P-function (or the Glauber-Sudershan P-distribution),

$$P(\alpha) \equiv \frac{1}{\pi} \sum_{n,m} \rho_{n,m} \alpha^n \alpha^{*m}, \tag{2.130}$$

where $\rho_{n,m}$ are the matrix elements of an anti-normally ordered density operator. The P-function is not a true probability distribution. This can be seen from the following example: for the coherent state $|\bar{\alpha}\rangle$, represented by the density operator

$$\hat{\rho} = |\bar{\alpha}\rangle\langle\bar{\alpha}|, \tag{2.131}$$

the $P$-function in equation (2.129) must be given by a Dirac delta function

$$P(\bar{\alpha}) = \delta^2(\alpha - \bar{\alpha}), \tag{2.132}$$

where $\delta^2(\alpha) = \delta(\alpha_R)\delta(\alpha_I)$.

Furthermore, by using the definition for a number state, (2.99), we can write the coherent states, (2.118), as

$$|\alpha\rangle = e^{-\frac{1}{2}|\alpha|^2} \sum_{n=0}^{\infty} \frac{\alpha^n}{\sqrt{n!}} \frac{(\hat{a}^\dagger)^n}{\sqrt{n!}} |0\rangle$$

$$= e^{-\frac{1}{2}|\alpha|^2} \sum_{n=0}^{\infty} \frac{(\alpha\hat{a}^\dagger)^n}{n!} |0\rangle$$

$$= e^{-\frac{1}{2}|\alpha|^2} e^{\alpha\hat{a}^\dagger} |0\rangle. \tag{2.133}$$

The operator $e^{-\frac{1}{2}|\alpha|^2}e^{\alpha\hat{a}^\dagger}$ is not particularly useful (nor physically meaningful) because it is not unitary: ideally we would like its adjoint to take the vacuum state into state $|-\alpha\rangle$, instead of $e^{-\frac{1}{2}|\alpha|^2}(e^{\alpha\hat{a}^\dagger})^\dagger|0\rangle = e^{-\frac{1}{2}|\alpha|^2}e^{\alpha^*\hat{a}}|0\rangle = e^{-\frac{1}{2}|\alpha|^2}|0\rangle$. By multiplying it on the right by $e^{-\alpha^*\hat{a}}$, it becomes unitary,

$$e^{-\frac{1}{2}|\alpha|^2}e^{\alpha\hat{a}^\dagger}e^{-\alpha^*\hat{a}}|0\rangle = e^{-\frac{1}{2}|\alpha|^2}e^{\alpha\hat{a}^\dagger}|0\rangle$$
$$= |\alpha\rangle$$
$$(e^{-\frac{1}{2}|\alpha|^2}e^{\alpha\hat{a}^\dagger}e^{-\alpha^*\hat{a}})^\dagger|0\rangle = e^{-\frac{1}{2}|\alpha|^2}e^{-\alpha\hat{a}^\dagger}e^{\alpha^*\hat{a}}|0\rangle$$
$$= e^{-\frac{1}{2}|\alpha|^2}e^{-\alpha\hat{a}^\dagger}|0\rangle$$
$$= |-\alpha\rangle. \tag{2.134}$$

By using the Baker-Campbell-Hausdorff formula, introduced in the first section (2.29), we simplify this operator to

$$e^{-\frac{1}{2}|\alpha|^2}e^{\alpha\hat{a}^\dagger}e^{-\alpha^*\hat{a}} = e^{-\frac{1}{2}|\alpha|^2}e^{\alpha\hat{a}^\dagger-\alpha^*\hat{a}+\frac{1}{2}[\alpha\hat{a}^\dagger,-\alpha^*\hat{a}]}$$
$$= e^{-\frac{1}{2}|\alpha|^2}e^{\alpha\hat{a}^\dagger-\alpha^*\hat{a}+\frac{1}{2}|\alpha|^2}$$
$$\hat{D}(\alpha) \equiv e^{\alpha\hat{a}^\dagger-\alpha^*\hat{a}}, \tag{2.135}$$

which is known as the *displacement* operator $\hat{D}(\alpha)$. By using the same formula again we can show that the adjoint of the displacement operator is

$$e^{-\frac{1}{2}|\alpha|^2}e^{-\alpha\hat{a}^\dagger}e^{+\alpha^*\hat{a}} = e^{-\frac{1}{2}|\alpha|^2}e^{-\alpha\hat{a}^\dagger+\alpha^*\hat{a}+\frac{1}{2}[-\alpha\hat{a}^\dagger,+\alpha^*\hat{a}]}$$
$$= e^{-\frac{1}{2}|\alpha|^2}e^{-\alpha\hat{a}^\dagger+\alpha^*\hat{a}+\frac{1}{2}|\alpha|^2}$$
$$\hat{D}(\alpha)^\dagger = e^{-\alpha\hat{a}^\dagger+\alpha^*\hat{a}}, \tag{2.136}$$

and easily verify that it is unitary, $\hat{D}(\alpha)^\dagger = \hat{D}(-\alpha)$. Therefore we have that

$$|\alpha\rangle = \hat{D}(\alpha)|0\rangle, \tag{2.137}$$

and so we introduced the coherent state as a displaced vacuum state (Figure 2.4). This is further justified by examining the noise properties of a coherent state.

The expectation value of the quadrature operators are the real and imaginary values of $\alpha$ in $\hat{X}$ and for $\hat{P}$ respectively,

$$\langle\hat{X}\rangle = \langle\alpha|\hat{X}|\alpha\rangle$$
$$= \frac{1}{2}\langle\alpha|\hat{a}^\dagger + \hat{a}|\alpha\rangle$$
$$= \frac{1}{2}\left(\langle\alpha|\hat{a}^\dagger|\alpha\rangle + \langle\alpha|\hat{a}|\alpha\rangle\right)$$
$$= \frac{1}{2}\left(\alpha^* + \alpha\right)$$
$$= \frac{1}{2}\left(\mathrm{Re}(\alpha) - i\mathrm{Im}(\alpha) + \mathrm{Re}(\alpha) + i\mathrm{Im}(\alpha)\right)$$
$$= \mathrm{Re}(\alpha), \tag{2.138}$$

$$\begin{aligned}
\langle \hat{P} \rangle &= \langle \alpha | \hat{P} | \alpha \rangle \\
&= \frac{i}{2} \langle \alpha | \hat{a}^\dagger - \hat{a} | \alpha \rangle \\
&= \frac{i}{2} \left( \alpha^* - \alpha \right) \\
&= \frac{i}{2} \left( \mathrm{Re}(\alpha) - i\mathrm{Im}(\alpha) - \mathrm{Re}(\alpha) - i\mathrm{Im}(\alpha) \right) \\
&= \frac{i}{2} \left( -2i\mathrm{Im}(\alpha) \right) \\
&= \mathrm{Im}(\alpha).
\end{aligned} \tag{2.139}$$

The spread is

$$\begin{aligned}
\langle \hat{X}^2 \rangle &= \frac{1}{4} \langle \alpha | \left( \hat{a}_i^{\dagger 2} + \hat{a}_i^2 + 2\hat{a}_i^\dagger \hat{a}_i + 1 \right) | \alpha \rangle \\
&= \frac{1}{4} \left( \alpha^{*2} + \alpha^2 + 2|\alpha|^2 + 1 \right),
\end{aligned} \tag{2.140}$$

and

$$\begin{aligned}
\langle \hat{P}^2 \rangle &= -\frac{1}{4} \langle \alpha | (\hat{a}_i^{\dagger 2} + \hat{a}_i^2 - 2\hat{a}_i^\dagger \hat{a}_i - 1) | \alpha \rangle \\
&= -\frac{1}{4} \left( \alpha^{*2} + \alpha^2 - 2|\alpha|^2 - 1 \right)
\end{aligned} \tag{2.141}$$

and consequently the variances are

$$\begin{aligned}
(\Delta X)^2 &= \langle \hat{X}^2 \rangle - \langle \hat{X} \rangle^2 \\
&= \frac{1}{4} \left( \alpha^{*2} + \alpha^2 + 2|\alpha|^2 + 1 \right) - \frac{1}{4} \left( \alpha^{*2} + 2|\alpha|^2 + \alpha^2 \right) \\
&= \frac{1}{4}.
\end{aligned} \tag{2.142}$$

$$\begin{aligned}
(\Delta P)^2 &= \langle \hat{P}^2 \rangle - \langle \hat{P} \rangle^2 \\
&= -\frac{1}{4} \left( \alpha^{*2} + \alpha^2 - 2|\alpha|^2 - 1 \right) + \frac{1}{4} \left( \alpha^{*2} - 2|\alpha|^2 + \alpha^2 \right) \\
&= \frac{1}{4}
\end{aligned} \tag{2.143}$$

Therefore the uncertainty product is

$$\Delta X \Delta P = \frac{1}{4}, \tag{2.144}$$

and like the vacuum state, (2.110), the coherent state is also a quadrature minimum - uncertainty state, with symmetric fluctuations in $\hat{X}$ and $\hat{P}$.

The average number of photons in a coherent state is

$$\begin{aligned}
\langle \hat{n} \rangle &= \langle \alpha | \hat{n} | \alpha \rangle \\
&= \langle \alpha | \hat{a}^\dagger \hat{a} | \alpha \rangle \\
&= |\alpha|^2.
\end{aligned} \tag{2.145}$$

As

$$\begin{aligned}\langle \hat{n}^2 \rangle &= \langle \alpha | \hat{n}\hat{n} | \alpha \rangle \\ &= \langle \alpha | \hat{a}^\dagger \hat{a} \hat{a}^\dagger \hat{a} | \alpha \rangle \\ &= \langle \alpha | \hat{a}^\dagger (1 + \hat{a}^\dagger \hat{a}) \hat{a} | \alpha \rangle \\ &= |\alpha|^2 + |\alpha|^4,\end{aligned} \tag{2.146}$$

the variance in a coherent state is equal to the average number of photons

$$\begin{aligned}(\Delta n)^2 &= \langle n^2 \rangle - \langle n \rangle^2 \\ &= |\alpha|^2 + |\alpha|^4 - |\alpha|^4 \\ &= |\alpha|^2.\end{aligned} \tag{2.147}$$

## 2.4   The beamsplitter

We can analyse the structure of a quantum state by looking at the outcome of its interference with another wave. Most interference techniques rely on an optical device known as the beamsplitter. As the name suggests, this device takes an incident beam and splits it, by reflecting some of the light and transmitting the rest. If the device is lossy then it absorbs some of the incident light. Here we will describe the simplest model of a beamsplitter, that is, a beamsplitter that exhibits no loss.

The action of a (lossless) beamsplitter on the modes of the incoming field is unitary, (2.30) and we can represent it by a matrix $\hat{U}$, known as the beamsplitter transformation matrix [Loudon, 2000]. For a beamsplitter with two input and two output modes for example, the beamsplitter transformation matrix relates the output modes to the input modes in the following way:

$$\begin{pmatrix} \hat{a}_{out} \\ \hat{b}_{out} \end{pmatrix} = \hat{U} \begin{pmatrix} \hat{a}_{in} \\ \hat{b}_{in} \end{pmatrix}. \tag{2.148}$$

In general, an asymmetric beamsplitter has different beamsplitter coefficients on each side (Figure 2.5), so that

$$\begin{pmatrix} \hat{a}_{out} \\ \hat{b}_{out} \end{pmatrix} = \begin{pmatrix} t_2 & r_1 \\ r_2 & t_1 \end{pmatrix} \begin{pmatrix} \hat{a}_{in} \\ \hat{b}_{in} \end{pmatrix}, \tag{2.149}$$

or equivalently,

$$\begin{aligned}\hat{a}_{out} &= t_2 \hat{a}_{in} + r_1 \hat{b}_{in} \\ \hat{b}_{out} &= r_2 \hat{a}_{in} + t_1 \hat{b}_{in}.\end{aligned} \tag{2.150}$$

The transmission and reflection coefficients are complex, $t_j = |t_j| e^{i\theta_j}$, $r_j = |r_j| e^{i\phi_j}$ and the transmitted and reflected intensities are given by $|t_j|^2$ and $|r_j|^2$, respectively. We can rearrange (2.148) in order to express the input modes in terms of the output modes,

$$\begin{aligned}\begin{pmatrix} \hat{a}_{in} \\ \hat{b}_{in} \end{pmatrix} &= \hat{U}^\dagger \begin{pmatrix} \hat{a}_{out} \\ \hat{b}_{out} \end{pmatrix} \\ &= \begin{pmatrix} t_2^* & r_2^* \\ r_1^* & t_1^* \end{pmatrix} \begin{pmatrix} \hat{a}_{out} \\ \hat{b}_{out} \end{pmatrix}.\end{aligned} \tag{2.151}$$
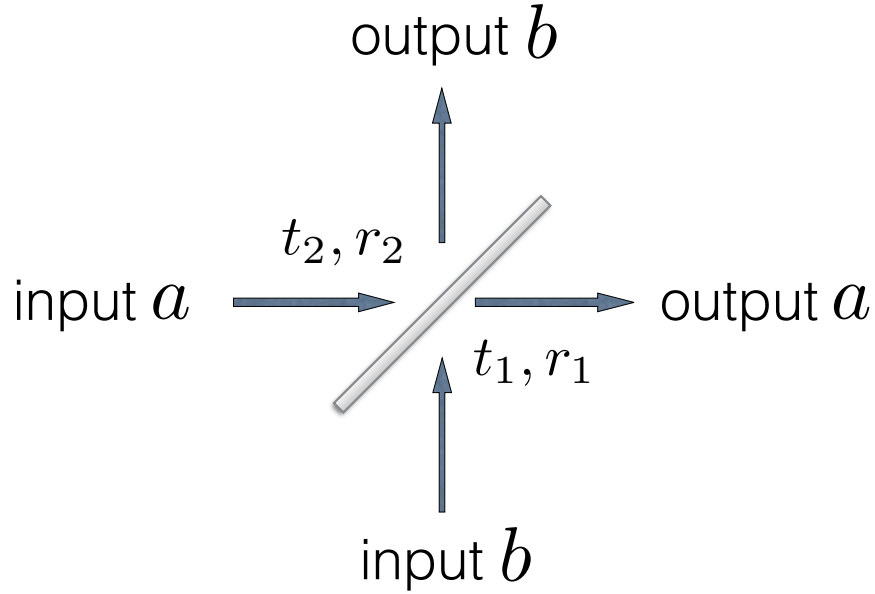
Figure 2.5: Two input modes interfere at a beamsplitter to create two output modes.

For an asymmetric beamsplitter the transmission and reflection from one side of the beamsplitter is different than the transmission and reflection from the other side.

Additionally, it may be useful to express the beamsplitter transformation using the creation operators, therefore from (2.148) we get

$$
\left( \begin{matrix} \hat{a}_{out} \\ \hat{b}_{out} \end{matrix} \right)^\dagger = \left[ \hat{U} \left( \begin{matrix} \hat{a}_{in} \\ \hat{b}_{in} \end{matrix} \right) \right]^\dagger
$$

$$
(\hat{a}_{out}^\dagger, \hat{b}_{out}^\dagger) = (\hat{a}_{in}^\dagger, \hat{b}_{in}^\dagger) \left( \begin{matrix} t_2^* & r_2^* \\ r_1^* & t_1^* \end{matrix} \right) \tag{2.152}
$$

and from (2.151) we get

$$
\left( \begin{matrix} \hat{a}_{in} \\ \hat{b}_{in} \end{matrix} \right)^\dagger = \left[ \hat{U}^\dagger \left( \begin{matrix} \hat{a}_{out} \\ \hat{b}_{out} \end{matrix} \right) \right]^\dagger
$$

$$
(\hat{a}_{in}^\dagger, \hat{b}_{in}^\dagger) = (\hat{a}_{out}^\dagger, \hat{b}_{out}^\dagger) \left( \begin{matrix} t_2 & r_1 \\ r_2 & t_1 \end{matrix} \right). \tag{2.153}
$$

### 2.4.1 Relations among the beamsplitter coefficients

The output and input modes obey the commutation relations

$$
[\hat{a}_{out}, \hat{a}_{out}^\dagger] = [\hat{b}_{out}, \hat{b}_{out}^\dagger] = 1 = [\hat{a}_{in}, \hat{a}_{in}^\dagger] = [\hat{b}_{in}, \hat{b}_{in}^\dagger], \tag{2.154}
$$

$$
[\hat{a}_{out}, \hat{b}_{out}^\dagger] = [\hat{b}_{out}, \hat{a}_{out}^\dagger] = 0 = [\hat{a}_{in}, \hat{b}_{in}^\dagger] = [\hat{b}_{in}, \hat{a}_{in}^\dagger], \tag{2.155}
$$

where equation (2.155) reflects the fact that the two output fields, as well as the two input fields, are assumed to be independent. We expand the commutators in (2.154) and find

$$
\begin{aligned}
[\hat{a}_{out}, \hat{a}_{out}^\dagger] &= (t_2\hat{a}_{in} + r_1\hat{b}_{in})(t_2^*\hat{a}_{in}^\dagger + r_1^*\hat{b}_{in}^\dagger) - (t_2^*\hat{a}_{in}^\dagger + r_1^*\hat{b}_{in}^\dagger)(t_2\hat{a}_{in} + r_1\hat{b}_{in}) \\
&= |t_2|^2 \hat{a}_{in}\hat{a}_{in}^\dagger + t_2 r_1^* \hat{a}_{in}\hat{b}_{in}^\dagger + r_1 t_2^* \hat{b}_{in}\hat{a}_{in}^\dagger + |r_1|^2 \hat{b}_{in}\hat{b}_{in}^\dagger \\
&\quad - |t_2|^2 \hat{a}_{in}^\dagger\hat{a}_{in} - t_2^* r_1 \hat{a}_{in}^\dagger\hat{b}_{in} - r_1^* t_2 \hat{b}_{in}^\dagger\hat{a}_{in} - |r_1|^2 \hat{b}_{in}^\dagger\hat{b}_{in} \\
&= |t_2|^2 [\hat{a}_{in}, \hat{a}_{in}^\dagger] + t_2 r_1^* [\hat{a}_{in}, \hat{b}_{in}^\dagger] + r_1 t_2^* [\hat{b}_{in}, \hat{a}_{in}^\dagger] + |r_1|^2 [\hat{b}_{in}, \hat{b}_{in}^\dagger] \\
&= |t_2|^2 + |r_1|^2,
\end{aligned}
\tag{2.156}
$$

and similarly

$$
[\hat{b}_{out}, \hat{b}_{out}^\dagger] = |r_2|^2 + |t_1|^2,
\tag{2.157}
$$

$$
[\hat{a}_{in}, \hat{a}_{in}^\dagger] = |t_2|^2 + |r_2|^2,
\tag{2.158}
$$

$$
[\hat{b}_{in}, \hat{b}_{in}^\dagger] = |r_1|^2 + |t_1|^2.
\tag{2.159}
$$

We substitute (2.156) – (2.159) into (2.154),

$$
\begin{aligned}
|t_2|^2 + |r_1|^2 &= |r_2|^2 + |t_1|^2 = 1 \\
|t_2|^2 + |r_2|^2 &= |r_1|^2 + |t_1|^2 = 1,
\end{aligned}
\tag{2.160}
$$

and we see that the transmission and reflection coefficients from one side of the beamsplitter are equal in modulus to the corresponding coefficients from the other side,

$$
\begin{aligned}
|t_2| &= |t_1|, \\
|r_2| &= |r_1|.
\end{aligned}
\tag{2.161}
$$

Then we expand the commutators in (2.155) and get

$$
\begin{aligned}
[\hat{a}_{out}, \hat{b}_{out}^\dagger] &= (t_2\hat{a}_{in} + r_1\hat{b}_{in})(r_2^*\hat{a}_{in}^\dagger + t_1^*\hat{b}_{in}^\dagger) - (r_2^*\hat{a}_{in}^\dagger + t_1^*\hat{b}_{in}^\dagger)(t_2\hat{a}_{in} + r_1\hat{b}_{in}) \\
&= t_2 r_2^* \hat{a}_{in}\hat{a}_{in}^\dagger + t_2 t_1^* \hat{a}_{in}\hat{b}_{in}^\dagger + r_1 r_2^* \hat{b}_{in}\hat{a}_{in}^\dagger + r_1 t_1^* \hat{b}_{in}\hat{b}_{in}^\dagger \\
&\quad - r_2^* t_2 \hat{a}_{in}^\dagger\hat{a}_{in} - r_2^* r_1 \hat{a}_{in}^\dagger\hat{b}_{in} - t_1^* t_2 \hat{b}_{in}^\dagger\hat{a}_{in} - t_1^* r_1 \hat{b}_{in}^\dagger\hat{b}_{in} \\
&= t_2 r_2^* [\hat{a}_{in}, \hat{a}_{in}^\dagger] + t_2 t_1^* [\hat{a}_{in}, \hat{b}_{in}^\dagger] + r_1 r_2^* [\hat{b}_{in}, \hat{a}_{in}^\dagger] + r_1 t_1^* [\hat{b}_{in}, \hat{b}_{in}^\dagger] \\
&= t_2 r_2^* + r_1 t_1^*,
\end{aligned}
\tag{2.162}
$$

$$
[\hat{b}_{out}, \hat{a}_{out}^\dagger] = r_2 t_2^* + t_1 r_1^*,
\tag{2.163}
$$

$$
[\hat{a}_{in}, \hat{b}_{in}^\dagger] = t_2^* r_1 + r_2^* t_1,
\tag{2.164}
$$

$$
[\hat{b}_{in}, \hat{a}_{in}^\dagger] = r_1^* t_2 + t_1^* r_2.
\tag{2.165}
$$

A substitution of (2.162) − (2.165) into (2.155) yields the relations

$$t_2 r_2^* + r_1 t_1^* = r_2 t_2^* + t_1 r_1^* = 0$$
$$t_2^* r_1 + r_2^* t_1 = r_1^* t_2 + t_1^* r_2 = 0. \tag{2.166}$$

By writing the explicit form,

$$|t_2| e^{-i\theta_2} |r_1| e^{i\phi_1} + |r_2| e^{-i\phi_2} |t_1| e^{i\theta_1} = 0, \tag{2.167}$$

and rearranging

$$\frac{|r_1|}{|t_1|} = -\frac{|r_2|}{|t_2|} e^{i(\theta_1 + \theta_2 - \phi_1 - \phi_2)}, \tag{2.168}$$

we arrive at the following condition:

$$e^{i(\theta_1 + \theta_2 - \phi_1 - \phi_2)} = -1. \tag{2.169}$$

This equation holds when $(\theta_1 + \theta_2 - \phi_1 - \phi_2)$ is an odd multiple of $\pi$, or as it is more commonly expressed,

$$\theta_1 + \theta_2 = \phi_1 + \phi_2 \pm \pi. \tag{2.170}$$

In summary, for an asymmetric beamsplitter the two transmission coefficients and the two reflection coefficients can be equal in magnitude, (2.161) and the sum of the transmission coefficient phases differs from the sum of the reflection coefficient phases by $\pi$, (2.170).

## 2.4.2   Special cases and conventions

### Real beamsplitter coefficients

We choose to set the sum of the transmission coefficient phases equal to zero,

$$\theta_1 + \theta_2 = 0, \tag{2.171}$$

so that the reflection coefficient phases sum to $\pi$,

$$\phi_2 = \pi - \phi_1 \tag{2.172}$$

(or $\phi_2 = -(\pi + \phi_1)$). If we set $\phi_2 = 0$ then $\phi_1 = \pi$ and the reflection coefficient $r_1$ becomes

$$r_1 = |r_1| e^{i\pi} = -|r_1|. \tag{2.173}$$

In fact, one can set the transmission coefficients to be real too, *i.e.* $\theta_1 = \theta_2 = 0$, so we can have the following beamsplitter transformation matrix,

$$\hat{U} = \begin{pmatrix} t_2 & -r_1 \\ r_2 & t_1 \end{pmatrix}, \tag{2.174}$$

where all coefficients are real.

## Symmetric beamsplitter

We have introduced the *asymmetric* beamsplitter, that is a beamsplitter with different transmission and reflection coefficients from each side, (Figure 2.5). A *symmetric* beamsplitter is one where the two transmission and two reflection coefficients are equal (both in phase and amplitude) from each side of the beamsplitter. Therefore we can drop the subscripts "$1, 2$" from the equations above and have instead

$$\begin{pmatrix} \hat{a}_{out} \\ \hat{b}_{out} \end{pmatrix} = \begin{pmatrix} t & r \\ r & t \end{pmatrix} \begin{pmatrix} \hat{a}_{in} \\ \hat{b}_{in} \end{pmatrix}, \tag{2.175}$$

where the output and input mode commutators yield,

$$|t|^2 + |r|^2 = 1, \tag{2.176}$$
$$tr^* + rt^* = 0. \tag{2.177}$$

From (2.177) we find that the transmission and reflection coefficient phases differ by $\pi/2$,

$$\theta = \phi \pm \frac{\pi}{2}. \tag{2.178}$$

Traditionally, we choose the transmission coefficient to be real ($\theta = 0$) and the reflection coefficient to be imaginary ($\phi = \pm \pi/2$). The beamsplitter transformation matrix then is

$$\hat{U} = \begin{pmatrix} t & ir \\ ir & t \end{pmatrix} \tag{2.179}$$

where $t$ and $r$ are real in this case.

Otherwise, we can get real coefficients by setting $\theta = 0, \phi = 0$. Then for (2.177) to hold, one of the coefficients must be negative. Similarly to (2.174), the beamsplitter transformation matrix is

$$\hat{U} = \begin{pmatrix} t & -r \\ r & t \end{pmatrix}, \tag{2.180}$$

where all coefficients are real. We choose to use (2.180) throughout this thesis. It's convenient to use because all coefficients are real, but we need to remember that there will be a phase change of $\pi$ upon reflection from one side of the beamsplitter only.

## 2.5   Coherent state comparison

The coherent amplitudes behave like classical field amplitudes at a beamsplitter. Consider, for example, two independent coherent states $|\alpha\rangle$ and $|\beta\rangle$, that are input at the modes $a$ and $b$, respectively, of a $50/50$ beamsplitter (Figure 2.6). We take
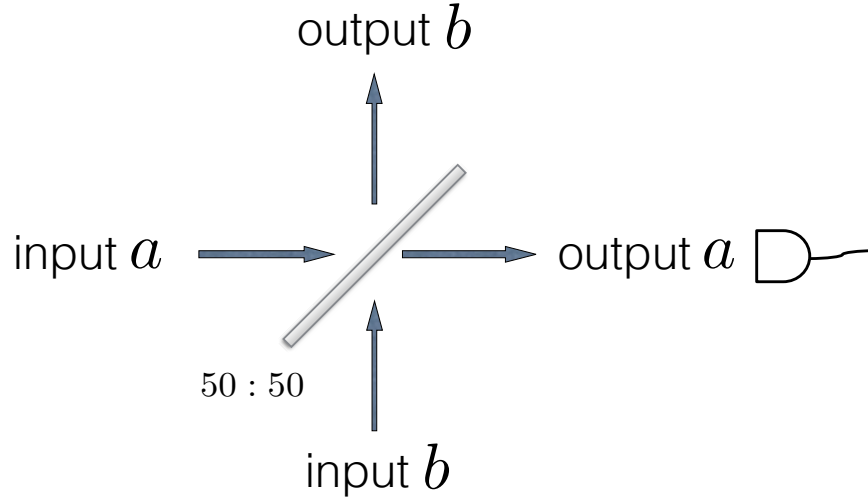


Figure 2.6: The state comparison set-up

It requires only a $50/50$ beamsplitter and a detector.

the beamsplitter transformation matrix to be

$$\hat{U} = \frac{1}{\sqrt{2}} \begin{pmatrix} 1 & -1 \\ 1 & 1 \end{pmatrix}, \tag{2.181}$$

*i.e.* there is a phase change of $\pi$ upon reflection from one arm of the beamsplitter (the lower arm in Figure 2.6). The density operator describing the input states is

$$\hat{\rho}_{in} = \int \mathrm{d}^2\alpha \int \mathrm{d}^2\beta P(\alpha)P(\beta)|\alpha\rangle_a\langle\alpha| \otimes |\beta\rangle_b\langle\beta|, \tag{2.182}$$

where the subscripts $a$ and $b$ indicate the mode that each state is input at, the tensor product indicates that the states are independent from each other and the probability distributions $P(\alpha)$ and $P(\beta)$ are the delta functions

$$P(\alpha) = \delta^2(\alpha - \bar{\alpha})$$
$$P(\beta) = \delta^2(\beta - \bar{\beta}). \tag{2.183}$$

The beamsplitter transformation is

$$\hat{\rho}_{in} \to \hat{U}\hat{\rho}_{out}\hat{U}^\dagger$$
$$= \int \mathrm{d}^2\alpha \int \mathrm{d}^2\beta P(\alpha)P(\beta)\left|\frac{\alpha-\beta}{\sqrt{2}}\right\rangle_a\left\langle\frac{\alpha-\beta}{\sqrt{2}}\right| \otimes \left|\frac{\alpha+\beta}{\sqrt{2}}\right\rangle_b\left\langle\frac{\alpha+\beta}{\sqrt{2}}\right| \tag{2.184}$$

and so the output state is

$$\hat{\rho}_{out} = \left| \frac{\bar{\alpha} - \bar{\beta}}{\sqrt{2}} \right\rangle_a \left\langle \frac{\bar{\alpha} - \bar{\beta}}{\sqrt{2}} \right| \otimes \left| \frac{\bar{\alpha} + \bar{\beta}}{\sqrt{2}} \right\rangle_b \left\langle \frac{\bar{\alpha} + \bar{\beta}}{\sqrt{2}} \right|. \tag{2.185}$$

The states in the output arms remain independent of each other.

Andersson et al. [2006] suggested that in the example above on can tell after a single measurement whether the states $|\alpha\rangle$ and $|\beta\rangle$ are different. One needs to place a photodetector in one of the beamsplitter output ports, say output a (Figure 2.6). The detector indicates whether there are any photons present in that port or not, without resolving them. The probability for the detector to fire, $P(S)$, is given by [Kelley and Kleiner, 1964]

$$\begin{aligned} P(S) &= 1 - P(0) \\ &= 1 - \text{Tr}\{\hat{\rho}_{out}\hat{\pi}_0\} \\ &= 1 - \text{Tr}\{\hat{\rho}_{out} : e^{-\eta \hat{a}^\dagger \hat{a}} :\} \end{aligned} \tag{2.186}$$

where $P(0)$ is the probability of detecting the vacuum state, the colons : : indicate that the operator is normally ordered and $\eta$ is the detector quantum efficiency. If the states are identical then the measured beamsplitter arm contains the vacuum and the detector will not fire. If the states are different in either phase or magnitude then the photodetector fires with probability $P(S)$, which in our example is found to be

$$P(s) = 1 - e^{-(1/2)\eta^2 |\alpha - \beta|^2}. \tag{2.187}$$

The bigger the difference $|\alpha - \beta|$ the higher the success probability of distinguishing the states. In fact, Andersson et al. [2006] show that $P(S)$ approaches 1, while the universal comparison strategy has a probability of success below $1/2$. The technique described above is known as coherent state comparison. It has higher success probability than other comparison methods because it uses the additional knowledge that the states are coherent. It can also be generalised to compare more than two states, but more importantly it can find application in quantum public key distribution schemes (with and without a trusted sender) or in a quantum "lock and key" scheme [Andersson et al., 2006].

## 2.6  Photon subtraction

In this section we show how the beamsplitter transformation, for a beamsplitter with very low reflectivity $r^2 \ll 1$, coupled with detection, provides an approximate photon subtraction.
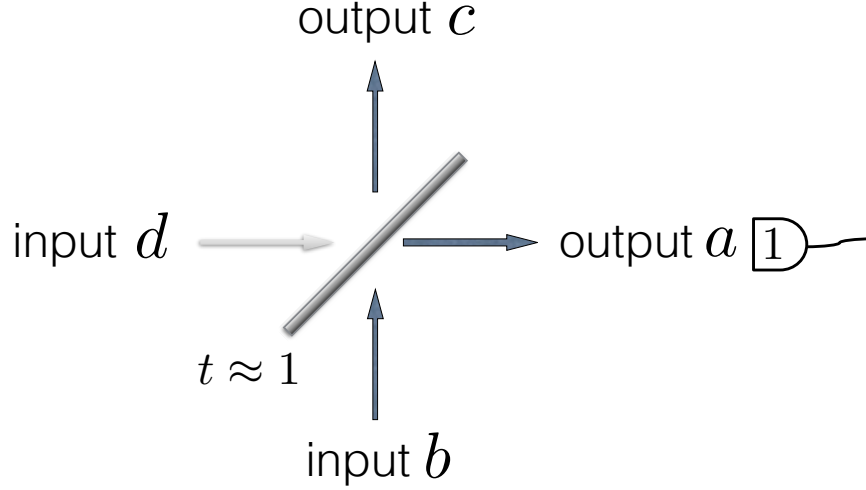


Figure 2.7: A beamsplitter with very high transmissivity coupled with a detector approximates photon subtraction.

We consider a two-mode state incident on the beamsplitter, where one state is as general as possible and the other one is vacuum state,

$$
\hat{\rho}_{\text{in}}^{(2)} = \sum_{m,n=0}^{\infty} \lambda_{m,n} |m\rangle_b \langle n| \otimes |0\rangle_d \langle 0|
$$

$$
= \sum_{m,n=0}^{\infty} \frac{\lambda_{m,n}}{\sqrt{m!n!}} (\hat{b}^\dagger)^m |0,0\rangle \langle 0,0| (\hat{b})^n. \tag{2.188}
$$

We assume that the beamsplitter has a very small reflectivity, $|r| \ll 1$. Such assumption leads us to the following approximation for the two-mode output state,

$$
\hat{\rho}_{\text{out}}^{(2)} = \sum_{m,n=0}^{\infty} \frac{\lambda_{m,n}}{\sqrt{m!n!}} (t\hat{c}^\dagger - r\hat{a}^\dagger)^m |0,0\rangle \langle 0,0| (t^*\hat{c} - r^*\hat{a})^n
$$

$$
= \sum_{m,n=0}^{\infty} \frac{\lambda_{m,n}}{\sqrt{m!n!}} [(t\hat{c}^\dagger)^m - m(t\hat{c}^\dagger)^{m-1} r\hat{a}^\dagger] |0,0\rangle \langle 0,0| [(t^*\hat{c})^n - n(t^*\hat{c})^{n-1} r^*\hat{a}]
$$

$$
+ O(r^2), \tag{2.189}
$$

where we have omitted terms of order $O(r^2)$. By post-selecting on the detection of

a photon in mode $a$ we find that the conditional state in mode $c$ is given by

$$\hat{\rho}_c^{(1)} = \frac{\langle 1_a | \hat{\rho}_{\text{out}}^{(2)} | 1_a \rangle}{\text{Tr}[\langle 1_a | \hat{\rho}_{\text{out}}^{(2)} | 1_a \rangle]}$$

$$= \frac{1}{N} \sum_{m,n=1}^{\infty} \lambda_{m,n} \sqrt{mn} \, t^m (t^*)^n |m-1\rangle\langle n-1| \qquad (2.190)$$

where $N = \sum_{m=1}^{\infty} \lambda_{m,m} m \, |t|^{2m}$.

A photon-subtracted state is given by

$$\hat{\rho}_{\text{subtr}} = \frac{1}{N'} \sum_{m,n=0}^{\infty} \lambda_{m,n} \hat{c} |m\rangle\langle n| \hat{c}^\dagger$$

$$= \frac{1}{N'} \sum_{m,n=1}^{\infty} \lambda_{m,n} \sqrt{mn} |m-1\rangle\langle n-1|, \qquad (2.191)$$

where $N' = \sum_{m=1}^{\infty} \lambda_{m,m} m$. By comparing the two states, (2.190) and (2.191) we see that

$$\lim_{|t| \to 1} \hat{\rho}_c^{(1)} = \hat{\rho}_{\text{subtr}}, \qquad (2.192)$$

which means that a very high transmissivity beamsplitter implements an approximation of the annihilation operator. This technique also applies to coherent states, despite their properties. In the following chapters we will explain how this technique can help to "purify" a mixture of coherent states.

Amplification of quantum optical states

AMPLIFICATION is an integral operation on the transport of information. Amplifiers take a weak input signal and give a strong output signal that it is easier to detect and handle for practical purposes. However, this process is not as straightforward for quantum signals as it is for classical ones. In this chapter we see why this is the case and we overview the techniques that were developed in order to overcome this issue. Finally, we discuss any challenges that remain in order to build a high performance optical amplifier.

## 3.1 Deterministic amplification

### 3.1.1 Conventional linear amplifiers

A classical linear amplifier multiplicatively increases the power of an input signal, $S_i$,

$$S_o = g^2 S_i \tag{3.1}$$

where $S_o$ is the output signal power and $g^2$ is the intensity gain (or photon number gain), $g^2 > 1$. The quality of the output signal is determined by the ratio of the signal power to the noise power,

$$\text{Signal to noise ratio} = S_o/N_o \tag{3.2}$$

and the overall figure of merit is the "noise figure" of the amplifier, which is the signal to noise ratio of the input signal divided by the signal to noise ratio of the output signal,

$$\text{Noise figure} = \frac{(S_i/N_i)}{(S_o/N_o)}. \tag{3.3}$$

The amplifier noise, $N_a$, is additive [Haus and Mullen, 1962],

$$N_o = g^2 N_i + N_a \tag{3.4}$$

and so the noise figure is given by

$$\begin{aligned}
\text{Noise figure} &= \frac{S_i}{N_i} \frac{N_o}{S_o} \\
&= \frac{S_i}{N_i} \frac{(g^2 N_i + N_a)}{g^2 S_i} \\
&= 1 + \frac{N_a}{g^2 N_i}.
\end{aligned} \tag{3.5}$$

It follows that the excess noise caused by the amplifier is

$$\begin{aligned}
\text{Excess noise figure} &= \text{Noise figure} - 1 \\
&= \frac{N_a}{g^2 N_i}.
\end{aligned} \tag{3.6}$$

## 3.1.2 Quantum signal amplification

As with classical signals, we would expect a linear amplifier to increase the amplitude of an arbitrary quantum signal multiplicatively,

$$|\alpha\rangle \rightarrow |g\alpha\rangle, \tag{3.7}$$

where $|g| > 1$ is the amplification gain. However, the above map, (3.7), is not physical. Consider two arbitrary states $|\alpha\rangle$ and $|\beta\rangle$, with overlap

$$|\langle \alpha | \beta \rangle|^2 = e^{-|\alpha - \beta|^2}. \tag{3.8}$$

If an amplifier were to increase the amplitude of both states according to (3.7), then their overlap would be

$$|\langle g\alpha | g\beta \rangle|^2 = e^{-g^2 |\alpha - \beta|^2}. \tag{3.9}$$

In that case, the overlap of the amplified states would be smaller than the overlap of the initial states,

$$e^{-g^2 |\alpha - \beta|^2} < e^{-|\alpha - \beta|^2}; \tag{3.10}$$

in other words, the distinguishability of the two states would have increased (Figure 3.1). The no-cloning theorem clearly forbids this [Wootters and Zurek, 1982].

It follows that the amplification of quantum signals must introduce noise [Caves, 1982],

$$\hat{a}_{\text{out}} = g\hat{a}_{\text{in}} + \hat{L}^\dagger, \tag{3.11}$$

where $\hat{L}^\dagger$ is the added noise operator satisfying $[\hat{L}, \hat{L}^\dagger] = g^2 - 1$. This addition of noise destroys the quantum properties the signal initially had (Figure 3.1).

However, it is possible to implement the transformation (3.7) approximately in a non-deterministic way. We describe such methods in the following section.
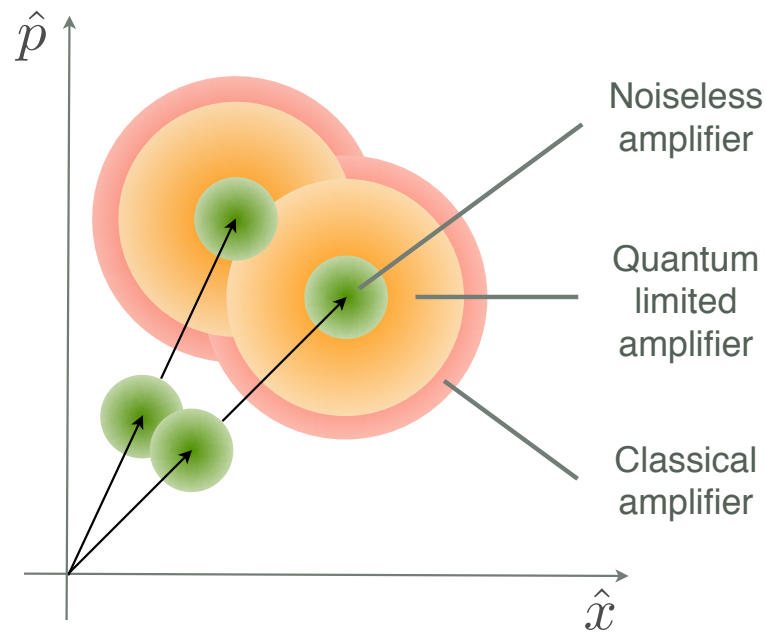
Figure 3.1: Ideally, a noiseless amplifier would not increase the minimum amount of noise in a coherent state. A quantum limited amplifier amplifies the minimum noise and adds some more. A classical amplifier adds even more noise than the quantum amplifier.
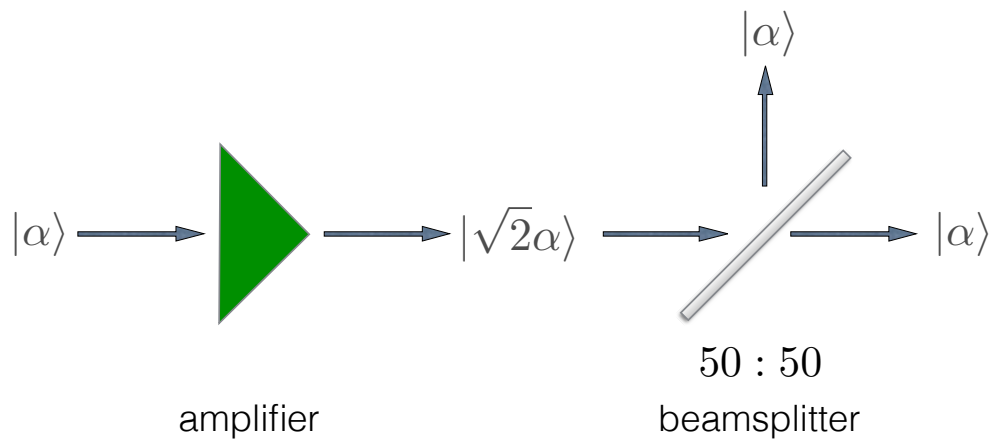


Figure 3.2: A coherent state cloner, *i.e.* a perfect linear amplifier of an arbitrary state followed by a beamsplitter, would violate the no-cloning theorem. It is possible only if the amplifier is implemented non-deterministically.

## 3.2  Probabilistic amplification

The concept of non-deterministic noiseless linear amplification was introduced by Ralph and Lund [2009]. Soon different protocols followed. In this section we review the main techniques of non-deterministic amplification of quantum states.

### 3.2.1  Quantum Scissors-based devices

The first method for non-deterministic amplification was proposed by Ralph and Lund [2009], based on the quantum scissors device of Pegg et al. [1998]. The quantum
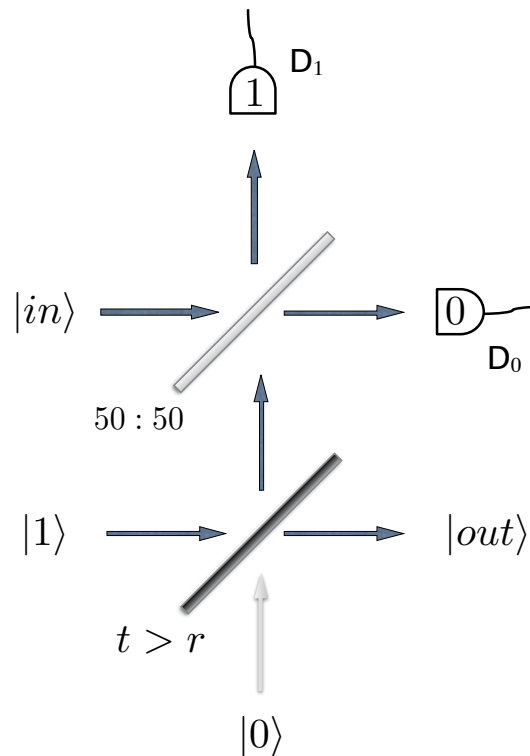


Figure 3.3: In the quantum scissors device a one photon state entangles itself with the vacuum in the lower beamsplitter. One share of this EPR state interferes with a weak coherent state, $|in\rangle = a_0|0\rangle + a_1|1\rangle + a_2|2\rangle + \ldots$, for a Bell state measurement. Post-selection on the measurement results that give one count at detector $D_1$ and zero counts at detector $D_0$, results in an output state that is a truncated version of the input state, $|out\rangle = a_0|0\rangle + a_1|1\rangle$.

In the context of amplification, the gain is defined as $g = t/r > 1$ and so the output state is equal to $|out\rangle = r|0\rangle + t\alpha|1\rangle = |0\rangle + g\alpha|1\rangle \approx |g\alpha\rangle$, for small $\alpha$.

scissors is a device closely related to teleportation [Bennett et al., 1993]: it can teleport a weak coherent state, $|in\rangle = a_0|0\rangle + a_1|1\rangle + a_2|2\rangle + \ldots$, by truncating it to contain only the vacuum and the one photon state, $|out\rangle = a_0|0\rangle + a_1|1\rangle$. As the

contributions of two photons and higher are "cut off", this device was given the name *quantum scissors*.

The quantum scissors device exploits the non-locality of a single photon state after a beamsplitter and uses this state as the EPR pair required for teleportation (Figure 3.3). The quantum scissors device was realised experimentally by Babichev et al. [2003]. They found that the teleportation fidelity is very high, ($99\%$), for small coherent states and that the fidelity drops significantly with increasing input state amplitude.

The proposal of Ralph and Lund [2009] incorporates many quantum scissors devices that run in parallel (Figure 3.4). The input state is split evenly $N$ times and each path becomes the input to a quantum scissors device. When the individual
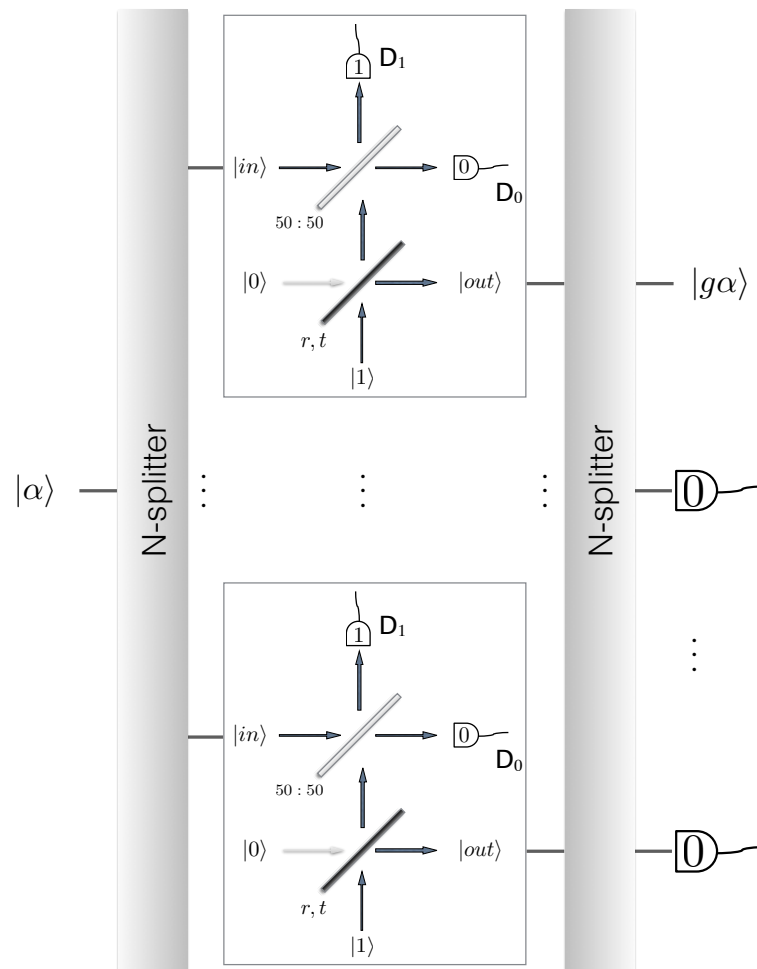


Figure 3.4: The coherent state to be amplified, $|\alpha\rangle$, is split into $N$ paths that become the inputs to the quantum scissors devices, $|in\rangle = |\alpha/\sqrt{N}\rangle$. Given the successful operation of each quantum scissors device, the amplified output states are recombined in an $N$-splitter where all but one paths are measured. If none of the detectors fires, the output state is accepted.

quantum scissors devices work properly, their outputs are recombined in an $N$-splitter. The final output state is accepted if no detector fires in the $N - 1$ measured ports.

This scheme produces an output state that is a very good approximation of the target amplified state, but it has a very low probability of success (Table 3.1). Both the fidelity and the probability of success decrease with gain, $g^2$.

Table 3.1: The (theoretical) fidelity of the output state with the target state is very high for the quantum scissors based device, especially for input states with small mean photon numbers, $|\alpha|^2$. In order to improve the fidelity for higher mean photon numbers, $N$ must increase. However, an increasing number of $N$ reduces the probability of success. This table is for $N = 5$.

| Gain | Fidelity | | Probability of success (%) |
|---|---|---|---|
| | $|\alpha|^2 = 0.2$ | $|\alpha|^2 = 0.5$ | |
| $g^2 \approx 2$ | $> 0.999$ | $\approx 0.99$ | 0.5 |
| $g^2 \approx 6$ | $> 0.999$ | $< 0.97$ | 0.01 |

The quantum scissors based amplifier was realised experimentally by Xiang et al. [2010] and Ferreyrol et al. [2010]. In both experiments the probability that the input state has more than one photons is negligible.

In the Xiang et al. [2010] experiment a spontaneous parametric down conversion (SPDC) source is required to generate the photon pairs; one photon is attenuated to form the input state and the other photon is used as the single photon ancilla in the quantum scissors device. The pair production rate is at $< 2500 s^{-1}$. The probability of success of the device is $\sim 1\%$ and so the success rate is around $25$ counts per second. For very small mean photon numbers, $|\alpha|^2 = 0.02$, the measured visibilities are above $90\%$ for gains smaller than about $g^2 \approx 4$ (Table 3.2).

The quantum scissors based amplifier can be extended to amplify states with two photon numbers [Jeffers, 2010].

Table 3.2: In the experimental implementation of the quantum scissors based amplifier the visibilities for an input state of $|\alpha|^2 = 0.02$ are very high [Xiang et al., 2010].

| Gain | Visibility |
|---|---|
| $g^2 = 2.05$ | 0.929 |
| $g^2 = 2.97$ | 0.910 |
| $g^2 = 3.85$ | 0.936 |

### 3.2.2 Photon addition and photon subtraction devices

Marek and Filip [2010] were the first to proposed that the application of the creation and annihilation operators, $\hat{a}\hat{a}^\dagger$, on a weak coherent state,

$$|\alpha\rangle \approx |0\rangle + \alpha|1\rangle, \tag{3.12}$$

results in the amplified state

$$\hat{a}\hat{a}^\dagger\left(|0\rangle + \alpha|1\rangle\right) \to \hat{a}\left(|1\rangle + \sqrt{2}\alpha|2\rangle\right)$$
$$\to |0\rangle + 2\alpha|1\rangle$$
$$\approx |2\alpha\rangle. \tag{3.13}$$

Kim et al. [2012] studied further the effects of multiple photon addition operations, $\hat{a}^{\dagger m}$, photon subtraction operations, $\hat{a}^m$ and the coherent superposition of the two, $t\hat{a} + r\hat{a}^\dagger$, on weak coherent states of magnitude, $|\alpha| = 0.2$. The target intensity gain was $g^2 = 2$ and they found that the optimum operation in terms of the highest effective gain is given by the photon addition operation. On the other hand the photon subtraction operation gives the highest fidelity. The probability of success decreases approximately exponentially with the number of photon additions and photon subtractions.

In theory, a single photon addition and a photon subtraction give an amplified state that has a fidelity with the target state that exceeds $0.95$ and for two such operations the fidelity is $> 0.986$ [Fiurášek, 2009]. These results correspond to a gain of $g \leq 1.5$ and for a coherent state of $|\alpha| \leq 1$.

Zavatta et al. [2011] realised the single photon addition and photon subtraction operation experimentally. The photon required for the photon addition was produced by stimulated parametric down conversion in a non-linear (LBO) crystal. The single photon is injected to the initial coherent state in another non-linear (BBO) crystal. One part of the resulting beam was measured and the other was subject to photon subtraction. Coincidences between the two detectors herald the amplified output state. They found that the fidelity was $> 90\%$ for states with $|\alpha| \leq 0.65$, for an effective gain of $g_{\text{eff}} \approx 1.6$.

### 3.2.3 Noise addition devices

Marek and Filip [2010] suggested an amplifier that is based on thermal noise addition and photon number resolving detection, also known as phase concentration scheme.

Thermal noise, *i.e.* phase and amplitude modulation, is applied to the input state. The input state is then described by a probabilistic mixture of coherent states which is slightly displaced in the direction of the initial state. Then the state is subject to a photon subtraction measurement which uses a photon number resolving detector. The photon subtraction measurement picks out the higher energy states, thereby displacing the input state towards the higher energies in phase space. The detector heralds the amplified state when a certain threshold number (N=1-4) is surpassed.

The protocol was realised experimentally by Usuga et al. [2010]; Müller et al. [2012]. As the threshold for subtraction increases the gain increases and the probability of success decreases (Table 3.3).

Table 3.3: In the noise addition and photon subtraction amplifier the probability of success decreases with the number of photon subtractions. The gain, on the other hand, increases. This table is for an input state $|\alpha|^2 = 0.186$ [Usuga et al., 2010].

| Subtraction threshold, N | Probability of success | Gain |
|:---:|:---:|:---:|
| 1 | 0.044 | $g^2 \approx 1.25$ |
| 2 | 0.0015 | $g^2 \approx 1.50$ |
| 3 | $4.3 \times 10^{-5}$ | $g^2 \approx 1.72$ |
| 4 | $1.1 \times 10^{-6}$ | $g^2 \approx 2$ |

The fidelity increases as the photon subtraction threshold increases [Müller et al., 2012].

Table 3.4: In the noise addition and photon subtraction amplifier the fidelity decreases with the threshold for photon subtraction increases. This table is for an input state $|\alpha|^2 = 1.0$ [Usuga et al., 2010].

| Subtraction threshold, N | Fidelity |
|:---:|:---:|
| 1 | $\sim 0.875$ |
| 2 | $\sim 0.910$ |
| 3 | $\sim 0.935$ |
| 4 | $\sim 0.950$ |

The noise addition and photon subtraction scheme can be improved slightly if the initial noise is provided by a standard optical amplifier [Jeffers, 2011].

## 3.3   Challenges and problems

In all schemes there is a significant trade-off between the fidelity of the output state with the target state and the probability of success of the device. Furthermore, when the fidelity is high the scheme requires a complex implementation based on quantum resources.

There is a need to find an alternative amplification scheme that balances the performance in fidelity and the probability of success better, while being simple to implement experimentally. Our proposed scheme does not require quantum resources and it amplifies with high gain, high fidelity and high probability of success.

## Quantum Optical State Comparison Amplifier

MOTIVATED BY THE EASE OF GENERATING COHERENT STATES, we propose a scheme for non-deterministic amplification of these states. We explain how a combination of the mature experimental techniques of coherent state comparison and photon subtraction results in a device that can amplify known sets of coherent states with high fidelity and high success probability.

A peer-reviewed version of this work can be found at *Physical Review Letters* **111**, 213601 [Eleftheriadou, Barnett, and Jeffers, 2013].

This chapter is organised as follows,

**Proposed protocol** We divide this section into two parts, a special case and the general case, depending on the gain of amplification and the set of input states.

We start introducing our protocol through a special example, where we consider that the input state is chosen from a binary alphabet and we perform the state comparison technique with a $50:50$ beamsplitter (Subsection 4.1.1). We show that by conditioning the output state on a photon subtraction measurement we get a *perfect* amplified version of the input state. The gain of amplification is $g = t\sqrt{2}$, where $t$ is the transmission coefficient of the photon subtraction beamsplitter. The higher the value of the transmission coefficient, $t$, the less likely the photon subtraction.

In the next subsection, we extend the scheme so that we can achieve a higher gain of amplification (Subsection 4.1.2). This is possible by using a beamsplitter with general coefficients at the state comparison stage, in which case the gain is $g = t_2/r_1$, where $r_1$ is the reflectivity of the state comparison beamsplitter and $t_2$ the transmissivity of the photon subtraction beamsplitter. This allows us to introduce a more intense state in the system, which is the source of the energy that is necessary to achieve higher gain of amplification. The performance of this generalised scheme depends on the set of input states chosen, which we study in detail in its own section.

**Findings** We present the results of the proposed (general) scheme for two sets of input sets: a binary set and a phase symmetric set (Subsections 4.2.1 and 4.2.2, respectively). We calculate the fidelity of the output state with the ideal target state and the probability of success of the amplifier. They both increase with the mean photon number and detector quantum efficiency. A perfect fidelity can be achieved when we reproduce the conditions of the special case example. The probability of success increases with intensity gain but decreases with increasing transmissivity of the photon subtraction beamsplitter, as a successful photon subtraction is less likely. We find that the quantum optical state comparison amplifier outperforms other non-deterministic amplification schemes in terms of fidelity and success probability.

**Discussion** Finally, we summarise the main results and discuss the advantages and limitations of our proposed protocol.

Before we proceed with the introduction of our protocol, let us briefly review the coherent state comparison technique which is central to our amplifier. As we have seen in Chapter 2, section 2.5, when two coherent states, $|\alpha\rangle$ and $|\beta\rangle$, are incident on a $50:50$ beamsplitter, they result in the output state

$$\hat{\rho}_{out} = \left|\frac{\alpha-\beta}{\sqrt{2}}\right\rangle_a \left\langle\frac{\alpha-\beta}{\sqrt{2}}\right| \otimes \left|\frac{\alpha+\beta}{\sqrt{2}}\right\rangle_b \left\langle\frac{\alpha+\beta}{\sqrt{2}}\right|. \tag{4.1}$$

We place a detector at the outport port $a$, (Figure 4.1), and if it registers a count
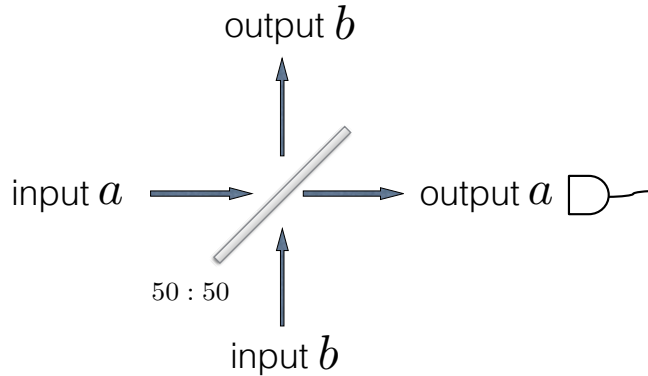


Figure 4.1: The state comparison technique requires only a $(50:50)$ beamsplitter and a detector. A detection event signifies that the input states were different.

we can infer that the input states were different (assuming there are no dark counts) [Andersson et al., 2006]. If the input states are identical, then they interfere such that they create the vacuum state in output $a$ and a state that is twice as big as the input states in output $b$,

$$\hat{\rho}_{out} = \left|\frac{\alpha-\alpha}{\sqrt{2}}\right\rangle_a \left\langle\frac{\alpha-\alpha}{\sqrt{2}}\right| \otimes \left|\frac{\alpha+\alpha}{\sqrt{2}}\right\rangle_b \left\langle\frac{\alpha+\alpha}{\sqrt{2}}\right| = |0\rangle_a\langle 0| \otimes |\sqrt{2}\alpha\rangle_b\langle\sqrt{2}\alpha|. \tag{4.2}$$

If the detector in output $a$ does not fire, then we have an imperfect indication that all the light is in output $b$. We exploit this technique to built an amplifier for coherent states.

## 4.1   Proposed scheme

It is common practice to use the fictional characters Alice and Bob in the description of quantum information protocols. In our protocol, Alice has a set of coherent states that she would like to have amplified. Bob has the device for amplification. Alice selects randomly one of her states and sends it to Bob and based on certain criteria, Bob accepts the output of his device and gives back to Alice the amplified version of her state.

   The key element of Bob's amplifier is a state comparison measurement. We relabel the beamsplitter ports in Figure 4.1 to reflect the role of each port (Figure 4.2). This
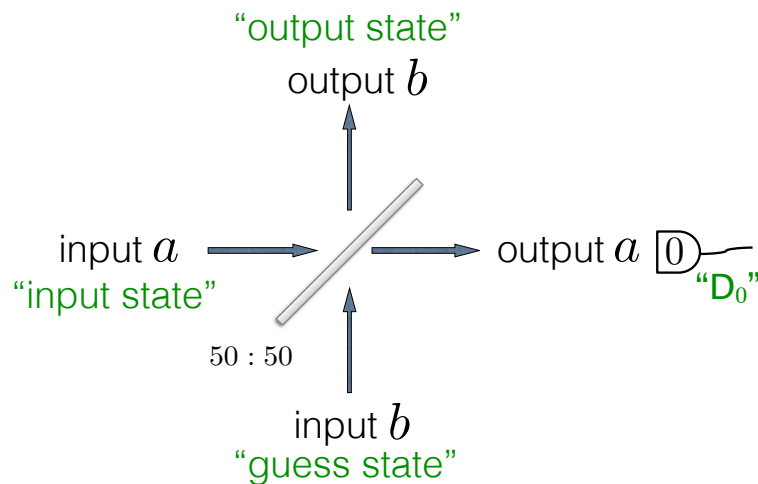


Figure 4.2:   Alice's input state interacts with Bob's guess state at a $50/50$ beamsplitter. The output state is accepted if detector $D_0$ does not fire.

is the nomenclature that we will be using to describe our protocol:

- input state:  is the pure coherent state that Alice wants to have amplified, denoted by $|\alpha\rangle$.

- guess state:  is the pure coherent state that Bob uses in order to achieve amplification of Alice's input state, denoted by $|\beta\rangle$.

- target state:  is the desired amplified version of the input state. For example, for the input state $|\alpha\rangle$ the target state is $|g\alpha\rangle$.

- output state:  is the state that the device produces, $\hat{\rho}_{out}$. In general, this will not be the pure target state, but rather a probabilistic mixture of the target state and some other state (the wrong state).

## 4.1.1 A very special case:
### perfect amplification for a gain of $g = t\sqrt{2}$

Bob does not know what the input state is, but he knows the set that it was chosen from. Let's assume that Alice's set contains only two states: states that are equal in magnitude but are opposite in phase, $\{|\alpha\rangle, |-\alpha\rangle\}$ (Figure 4.3). Alice chooses each
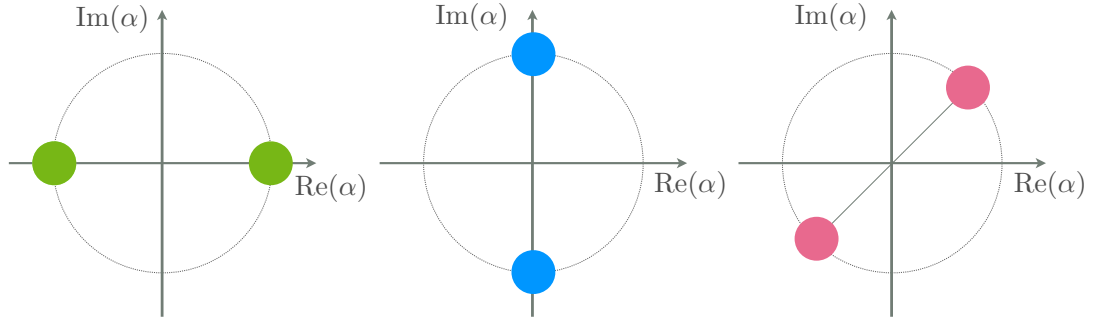


Figure 4.3: Examples of Alice's 2-state sets.

In each set the states have the same magnitude but opposite phase. Bob must know which set Alice chooses, or he must determine this from a prior set of measurements.

state from the set randomly, with equal probability, *i.e.*

$$P(\bar{\alpha}) = \frac{1}{2}\left[\delta^2(\bar{\alpha} - \alpha) + \delta^2(\bar{\alpha} + \alpha)\right]. \tag{4.3}$$

For the amplification to be successful Bob's guess state must be the same as the input state. The best Bob can do, is to choose the guess state from the set $\{|\alpha\rangle, |-\alpha\rangle\}$ too, with the same probability distribution as Alice,

$$P(\bar{\beta}) = \frac{1}{2}\left[\delta^2(\bar{\beta} - \alpha) + \delta^2(\bar{\beta} + \alpha)\right]. \tag{4.4}$$

The system is symmetric: Bob amplifies Alice's input state $|\alpha\rangle$ with his guess state $|\alpha\rangle$ and input state $|-\alpha\rangle$ with his guess state $|-\alpha\rangle$. We will explain only the case where Bob chooses $|\alpha\rangle$, *i.e.*

$$P(\bar{\beta}) = \delta^2(\bar{\beta} - \alpha), \tag{4.5}$$

and a similar approach follows for the other case. For the probability distributions given by (4.3) and (4.5), the two-mode output state from the beamsplitter

$$\hat{\rho}_{out}^{(2)} = \int \mathrm{d}^2\bar{\alpha} \int \mathrm{d}^2\bar{\beta} P(\bar{\alpha})P(\bar{\beta}) \left|\frac{\bar{\alpha} - \bar{\beta}}{\sqrt{2}}\right\rangle_a \left\langle\frac{\bar{\alpha} - \bar{\beta}}{\sqrt{2}}\right| \otimes \left|\frac{\bar{\alpha} + \bar{\beta}}{\sqrt{2}}\right\rangle_b \left\langle\frac{\bar{\alpha} + \bar{\beta}}{\sqrt{2}}\right|, \tag{4.6}$$

becomes

$$\hat{\rho}_{out}^{(2)} = \frac{1}{2} \left| \frac{\alpha - \alpha}{\sqrt{2}} \right\rangle_a \left\langle \frac{\alpha - \alpha}{\sqrt{2}} \right| \otimes \left| \frac{\alpha + \alpha}{\sqrt{2}} \right\rangle_b \left\langle \frac{\alpha + \alpha}{\sqrt{2}} \right|$$
$$+ \frac{1}{2} \left| \frac{-\alpha - \alpha}{\sqrt{2}} \right\rangle_a \left\langle \frac{-\alpha - \alpha}{\sqrt{2}} \right| \otimes \left| \frac{-\alpha + \alpha}{\sqrt{2}} \right\rangle_b \left\langle \frac{-\alpha + \alpha}{\sqrt{2}} \right|$$
$$= \frac{1}{2} |0\rangle_a \langle 0| \otimes |\sqrt{2}\alpha\rangle_b \langle\sqrt{2}\alpha| + \frac{1}{2} |-\sqrt{2}\alpha\rangle_a \langle -\sqrt{2}\alpha| \otimes |0\rangle_b \langle 0|. \qquad (4.7)$$

Half of the times the output port $b$ has the target state, $|\sqrt{2}\alpha\rangle$ and half of the times it has the vacuum. The state comparison measurement changes these proportions.

For a successful coherent state comparison measurement we require that the detector $D_0$ will not fire (Figure 4.2). However, detectors in reality may yield a click without the presence of an actual photon. These events are called dark counts and they might adversely affect the outcome of an experiment. Nevertheless, if the dark count rate is low enough they can be neglected. Such is the case in the scheme that we propose, where gated detection can make the dark count rate insignificant.

The probability that detector $D_0$ does not fire, $P(0)$, is given by [Kelley and Kleiner, 1964]

$$P(0) = \text{Tr}\{\hat{\rho}_{out}^{(2)} : e^{-\eta \hat{a}_a^\dagger \hat{a}_a} :\}, \qquad (4.8)$$

where $0 < \eta \leq 1$ is the quantum efficiency of detector $D_0$, $: e^{-\eta \hat{a}_a^\dagger \hat{a}_a} :$ is a normally ordered operator describing the detection of the vacuum in mode $a$ and $\hat{\rho}_{out}^{(2)}$ is the unconditioned output state of the beamsplitter, (4.6). By inserting (4.7) into the definition (4.8), we find that the probability that detector $D_0$ does not fire is

$$P(0) = \frac{1}{2} + \frac{1}{2} e^{-\eta|-\sqrt{2}\alpha|^2}$$
$$= \frac{1}{2} + \frac{1}{2} e^{-2\eta|\alpha|^2}. \qquad (4.9)$$

Equation (4.9) has two terms: the first is due to the detection of vacuum in mode $a$ and the second, smaller term, is due to the presence of state $|-\sqrt{2}\alpha\rangle$ in mode $a$. Most of the times detector $D_0$ will fire in the presence of $|-\sqrt{2}\alpha\rangle$, in which case we expect Bob to discard the output state as the amplification is not successful. Less frequently though, the detector may "not see" the state $|-\sqrt{2}\alpha\rangle$, not (only) because the detector has a limited quantum efficiency, $\eta < 1$, but because of the nature of coherent states. By expressing coherent states as a linear superposition of number states [Glauber, 1963]

$$|\alpha\rangle = e^{-\frac{1}{2}|\alpha|^2} \sum_{n=0}^{\infty} \frac{\alpha^n}{\sqrt{n!}} |n\rangle, \qquad (4.10)$$

we note that they have a vacuum component; the photon numbers start from $n = 0$. Consequently the detector may project on a coherent state's vacuum component, with probability $e^{-\eta|\alpha|^2}$ for state $|\alpha\rangle$. The bigger the mean photon number, $|\alpha|^2$, the smaller the second term in $P(0)$. The detector is less likely to register an incorrect measurement when a big state is present.

It follows that the output state conditioned on $D_0$ not firing is not a pure state but the mixed state

$$
\hat{\rho}_{\text{output}} = \frac{\text{Tr}_{\text{a}}\{\hat{\rho}_{out}^{(2)} : e^{-\eta \hat{a}_a^\dagger \hat{a}_a} :\}}{\text{Tr}\{\hat{\rho}_{out}^{(2)} : e^{-\eta \hat{a}_a^\dagger \hat{a}_a} :\}}
$$

$$
= \frac{1}{P(0)} \left[ \frac{1}{2} |\sqrt{2}\alpha\rangle_b \langle \sqrt{2}\alpha| + \frac{1}{2} e^{-2\eta|\alpha|^2} |0\rangle_b \langle 0| \right], \tag{4.11}
$$

where $1/P(0)$ acts as the normalisation. In other words, given that detector $D_0$ did not fire, the output state is more likely to be the state $|\sqrt{2}\alpha\rangle$, but there is a small probability that it is the vacuum state.

The output state $\hat{\rho}_{\text{output}}$, (4.11), is a good approximation of the target state $|\sqrt{2}\alpha\rangle$. The fidelity of the output state with the target state is defined as

$$
\text{Fidelity} = \int d^2\bar{\alpha}\, P(\bar{\alpha}) \langle \sqrt{2}\bar{\alpha} | \hat{\rho}_{\text{output}} | \sqrt{2}\bar{\alpha} \rangle. \tag{4.12}
$$

This definition holds for a pure or mixed $\hat{\rho}_{\text{output}}$, while the target state must be pure. Therefore we need to solve (4.12) from Alice's point of view where, instead of the probability distributions (4.3) and (4.5), we have that

$$
P'(\bar{\alpha}) = \delta^2 (\bar{\alpha} - \alpha), \tag{4.13}
$$

$$
Q'(\bar{\beta}) = \frac{1}{2} \left[ \delta^2 (\bar{\beta} - \alpha) + \delta^2 (\bar{\beta} + \alpha) \right]. \tag{4.14}
$$

Therefore Alice finds the two-mode output state to be

$$
\begin{aligned}
\hat{\rho}_{out}^{(2)} &= \int d^2\bar{\alpha} \int d^2\bar{\beta}\, P'(\bar{\alpha}) P'(\bar{\beta}) \left| \frac{\bar{\alpha} - \bar{\beta}}{\sqrt{2}} \right\rangle_a \left\langle \frac{\bar{\alpha} - \bar{\beta}}{\sqrt{2}} \right| \otimes \left| \frac{\bar{\alpha} + \bar{\beta}}{\sqrt{2}} \right\rangle_b \left\langle \frac{\bar{\alpha} + \bar{\beta}}{\sqrt{2}} \right|, \\
&= \frac{1}{2} \left| \frac{\alpha - \alpha}{\sqrt{2}} \right\rangle_a \left\langle \frac{\alpha - \alpha}{\sqrt{2}} \right| \otimes \left| \frac{\alpha + \alpha}{\sqrt{2}} \right\rangle_b \left\langle \frac{\alpha + \alpha}{\sqrt{2}} \right| \\
&\quad + \frac{1}{2} \left| \frac{\alpha + \alpha}{\sqrt{2}} \right\rangle_a \left\langle \frac{\alpha + \alpha}{\sqrt{2}} \right| \otimes \left| \frac{\alpha - \alpha}{\sqrt{2}} \right\rangle_b \left\langle \frac{\alpha - \alpha}{\sqrt{2}} \right| \\
&= \frac{1}{2} |0\rangle_a \langle 0| \otimes |\sqrt{2}\alpha\rangle_b \langle \sqrt{2}\alpha| + \frac{1}{2} |\sqrt{2}\alpha\rangle_a \langle \sqrt{2}\alpha| \otimes |0\rangle_b \langle 0|, \tag{4.15}
\end{aligned}
$$

which, when conditioned on detector $D_0$ not firing, becomes

$$
\hat{\rho}_{\text{output}}^A = \frac{1}{P(0)} \left[ \frac{1}{2} |\sqrt{2}\alpha\rangle_b \langle \sqrt{2}\alpha| + \frac{1}{2} e^{-2\eta|\alpha|^2} |0\rangle_b \langle 0| \right]. \tag{4.16}
$$

In this example, the output state found by Alice, $\hat{\rho}_{\text{output}}^A$, is the same state as the one found by Bob, (4.11), but this is not generally true. By substituting $\hat{\rho}_{\text{output}}^A$ into the

definition (4.12), we find that the fidelity of the output state with the target state is equal to

$$
\begin{aligned}
\text{Fidelity} &= \langle \sqrt{2}\alpha | \hat{\rho}^A_{\text{output}} | \sqrt{2}\alpha \rangle \\
&= \frac{1}{P(0)} \left[ \frac{1}{2} |\langle \sqrt{2}\alpha | \sqrt{2}\alpha \rangle|^2 + \frac{1}{2} e^{-2\eta|\alpha|^2} |\langle \sqrt{2}\alpha | 0 \rangle|^2 \right] \\
&= \frac{1}{P(0)} \left[ \frac{1}{2} + \frac{1}{2} e^{-2\eta|\alpha|^2} e^{-2|\alpha|^2} \right].
\end{aligned}
\tag{4.17}
$$

The second term in the expression reflects the imperfect nature of post-selection.
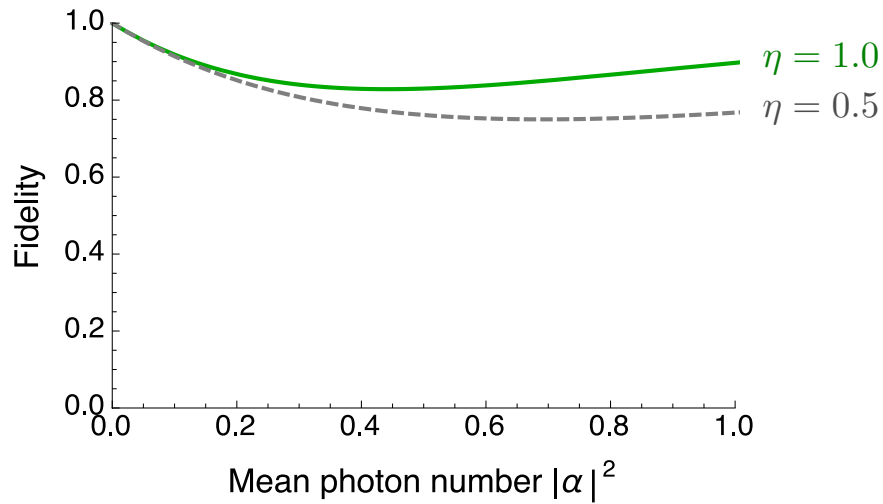


Figure 4.4: The fidelity of the output state with the target state, where the output state is conditioned on the state comparison measurement (only), is very high. It degrades with limited quantum efficiency of the detector involved in the state comparison measurement, $\eta$, as coherent light is not detected and we falsely post-select on this result. The higher the mean photon number, $|\alpha|^2$, the higher the fidelity as it is less likely for the detector to project on the coherent's state vacuum component (this holds for mean photon numbers higher than about $|\alpha|^2 = 0.15$).

The input state is selected randomly from the set $\{|\alpha\rangle, |-\alpha\rangle\}$
and a $50 : 50$ beamsplitter is used for the state comparison technique.

The fidelity depends on the mean photon number of the input state, $|\alpha|^2$ and on the quantum efficiency, $\eta$. For the greatest range of mean photon numbers, the higher mean photon number the smaller the second term in the fidelity measure, so overall the higher the fidelity (Figure 4.4). This is also true for the detector quantum efficiency, $\eta$. The higher it is, the smaller the fraction of incorrectly accepted output states, so the higher the fidelity.

The state comparison stage is the part of our amplifier which determines the strength of amplification. For a higher quality output state we require a photon

subtraction measurement. The photon subtraction stage consists of a beamsplitter with relatively high transmissivity coupled with a detector in the reflected output port and the measurement is considered successful when the detector fires (see Chapter 2, Subsection 2.6). In our particular example the effect of the photon subtraction is to adjust the probabilities in the mixture, (4.11), so that it increases the probability for the target state and decreases the probability for the wrong state. Due to the non-unit transmissivity, $t^2 < 1$ and an imperfect detector, $\eta < 1$, in this measurement, the probability of success of the device reduces.

In this example a photon subtraction measurement following the state comparison measurement results in a pure (final) output state[1], the desired target state . By inspection of the output state $\hat{\rho}_{\text{output}}$, (4.11), which now is incident at the photon subtraction stage,

$$\hat{\rho}_{\text{output}} = \frac{1}{P(0)} \left[ \frac{1}{2} |\sqrt{2}\alpha\rangle_b \langle \sqrt{2}\alpha| + \frac{1}{2} e^{-2\eta|\alpha|^2} |0\rangle_b \langle 0| \right],$$

we notice that a count at the detector could not have been caused by the vacuum state. Therefore, the resulting output state is the pure state $\hat{\rho}_{\text{output}} = |t\sqrt{2}\alpha\rangle_b \langle t\sqrt{2}\alpha|$. In fact, in this particular example it suffices to condition the output state on the photon subtraction measurement only. If the input state was chosen from a set that included more than two states, then by conditioning the output on the state comparison and photon subtraction measurements improves the fidelity of the output state with the target state.

In summary, we propose that a state comparison measurement involving a $50 : 50$ beamsplitter followed by a photon subtraction measurement can achieve perfect amplification of a coherent state chosen at random from the set $\{|\alpha\rangle, |-\alpha\rangle\}$, (Figure 4.5). The three-mode input state is

$$\hat{\rho}_{in}^{(3)} = \int \mathrm{d}^2\bar{\alpha} \int \mathrm{d}^2\bar{\beta} \ P(\bar{\alpha}) \ P(\bar{\beta}) \ |\bar{\alpha}\rangle_a \langle \bar{\alpha}| \otimes |\bar{\beta}\rangle_b \langle \bar{\beta}| \otimes |0\rangle_c \langle 0|, \tag{4.18}$$

which transforms to the three-mode output state

$$\begin{aligned}
\hat{\rho}_{out}^{(3)} = \int \mathrm{d}^2\bar{\alpha} \int \mathrm{d}^2\bar{\beta} \ P(\bar{\alpha}) \ P(\bar{\beta}) \left| \frac{\bar{\alpha} - \bar{\beta}}{\sqrt{2}} \right\rangle_a \left\langle \frac{\bar{\alpha} - \bar{\beta}}{\sqrt{2}} \right| \\
\otimes \left| \frac{t(\bar{\alpha} + \bar{\beta})}{\sqrt{2}} \right\rangle_b \left\langle \frac{t(\bar{\alpha} + \bar{\beta})}{\sqrt{2}} \right| \otimes \left| \frac{-r(\bar{\alpha} + \bar{\beta})}{\sqrt{2}} \right\rangle_c \left\langle \frac{-r(\bar{\alpha} + \bar{\beta})}{\sqrt{2}} \right|,
\end{aligned} \tag{4.19}$$

when we consider a $50 : 50$ beamsplitter at the state comparison stage, (Figure 4.5). For the probability distributions

$$\begin{aligned}
P(\bar{\alpha}) &= \frac{1}{2} \left[ \delta^2(\bar{\alpha} - \alpha) + \delta^2(\bar{\alpha} + \alpha) \right], \\
P(\bar{\beta}) &= \delta^2(\bar{\beta} - \alpha),
\end{aligned} \tag{4.20}$$

---

[1]From now on we call "output state" the final state that exits the device and was conditioned on both the state comparison and photon subtraction measurements (Figure 4.5).
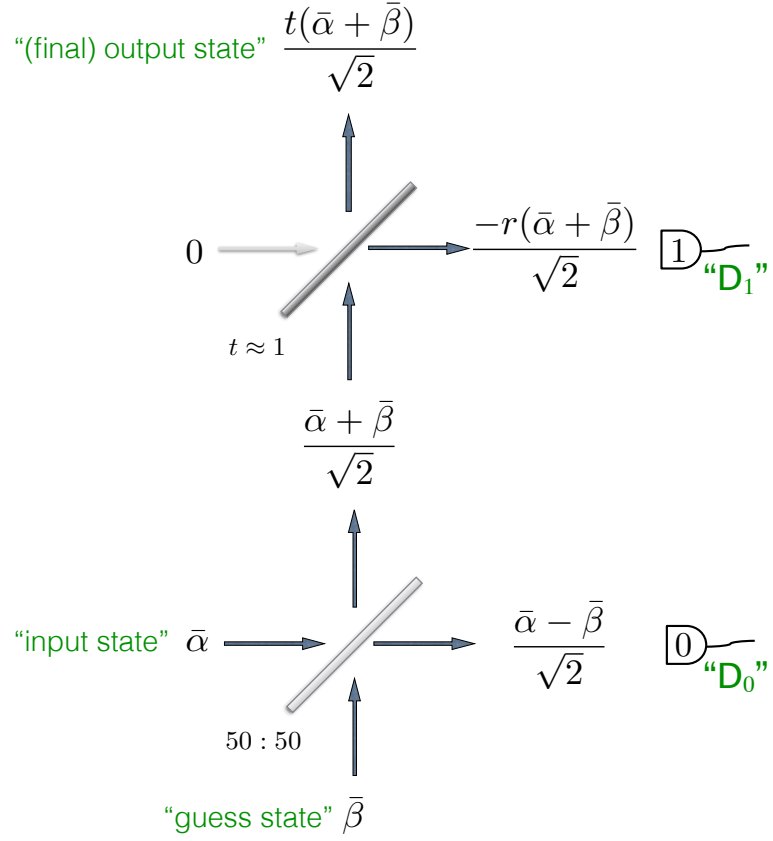
Figure 4.5: Coherent amplitude transformation at the $(50 : 50)$ state comparison beamsplitter and photon subtraction beamsplitter.

The output state is accepted when $D_0$ does not fire and $D_1$ does.

the three-mode output state is

$$
\hat{\rho}_{out}^{(3)} = \frac{1}{2} |0\rangle_a \langle 0| \otimes \left| t\sqrt{2}\alpha \right\rangle_b \left\langle t\sqrt{2}\alpha \right| \otimes \left| -r\sqrt{2}\alpha \right\rangle_c \left\langle -r\sqrt{2}\alpha \right|
$$
$$
+ \frac{1}{2} \left| -\sqrt{2}\alpha \right\rangle_a \left\langle -\sqrt{2}\alpha \right| \otimes |0\rangle_b \langle 0| \otimes |0\rangle_c \langle 0|. \tag{4.21}
$$

## Probability of success

The device operates successfully when the detector at the state comparison stage does not fire and the detector at the photon subtraction stage does. We define the probability of success, $P(S)$, as the joint probability of these two successful measurements,

$$
\begin{aligned}
P(S) &= P(0_{D_0}, 1_{D_1}) \\
&= P(0_{D_0}) \, P(1_{D_1} | 0_{D_0}),
\end{aligned} \tag{4.22}
$$

where $D_i$ denotes the detector involved in the measurement (as in Figure 4.5). It is equal to

$$P(S) = \text{Tr} \left\{ \hat{\rho}_{out}^{(3)} : \exp\left\{ -\eta_0 \hat{a}_a^\dagger \hat{a}_a \right\} \left( 1 - \exp\left\{ -\eta_1 \hat{a}_c^\dagger \hat{a}_c \right\} \right) : \right\}, \qquad (4.23)$$

where $\eta_i$ is the quantum efficiency of detector $D_i$ and $\hat{\rho}_{out}^{(3)}$ is the three-mode output state given in (4.19),

$$P(S) = \text{Tr} \left\{ \hat{\rho}_{out}^{(3)} : \exp\left\{ -\eta_0 \hat{a}_a^\dagger \hat{a}_a \right\} \left( 1 - \exp\left\{ -\eta_1 \hat{a}_c^\dagger \hat{a}_c \right\} \right) : \right\},$$
$$= \int \mathrm{d}^2 \bar{\alpha} \int \mathrm{d}^2 \bar{\beta} \; P(\bar{\alpha}) \; P(\bar{\beta}) \; \exp\left\{ -\eta_0 \left| \frac{\bar{\alpha} - \bar{\beta}}{\sqrt{2}} \right|^2 \right\}$$
$$\times \left( 1 - \exp\left\{ -\eta_1 \left| \frac{-r(\bar{\alpha} + \bar{\beta})}{\sqrt{2}} \right|^2 \right\} \right). \qquad (4.24)$$

By substituting the probability distributions given in (4.20) we find that the probability of success is

$$P(S) = \frac{1}{2} \left( 1 - \exp\left\{ -2\eta_1 r^2 |\alpha|^2 \right\} \right) + \frac{1}{2} \exp\left\{ -2\eta_0 |\alpha|^2 \right\} \times (1 - 1)$$
$$= \frac{1}{2} \left( 1 - \exp\left\{ -2\eta_1 r^2 |\alpha|^2 \right\} \right). \qquad (4.25)$$

It depends on the subtraction beamsplitter transmissivity $t^2$, $(r^2 = 1 - t^2)$, on the photon subtraction detector quantum efficiency $\eta_1$ and on the mean photon number $|\alpha|^2$ (Figure 4.6). As the transmissivity decreases, the probability of success increases. As we would like to have a gain as close to $\sqrt{2}$ as possible and a high probability of success, we suggest that a value of $t^2 = 0.9$ compensates well between the two. The higher the quantum efficiency of the detector involved in the photon subtraction measurement and the higher the mean photon number, the higher the probability of success as the probability for subtraction and to herald a successful photon subtraction increases.

## Conditional output state

The output state conditioned on the state comparison detector not firing and the photon subtraction detector firing, is given by

$$\hat{\rho}_{\text{output}} = \frac{\text{Tr}_{a,c} \left\{ \hat{\rho}_{out}^{(3)} : \exp\left\{ -\eta_0 \hat{a}_a^\dagger \hat{a}_a \right\} \left( 1 - \exp\left\{ -\eta_1 \hat{a}_c^\dagger \hat{a}_c \right\} \right) : \right\}}{\text{Tr} \left\{ \hat{\rho}_{out}^{(3)} : \exp\left\{ -\eta_0 \hat{a}_a^\dagger \hat{a}_a \right\} \left( 1 - \exp\left\{ -\eta_1 \hat{a}_c^\dagger \hat{a}_c \right\} \right) : \right\}},$$

$$= \frac{\text{Tr}_{a,c} \left\{ \hat{\rho}_{out}^{(3)} : \exp\left\{ -\eta_0 \hat{a}_a^\dagger \hat{a}_a \right\} \left( 1 - \exp\left\{ -\eta_1 \hat{a}_c^\dagger \hat{a}_c \right\} \right) : \right\}}{P(S)}. \qquad (4.26)$$

Figure 4.6: The probability of success, which is about $10\%$, $(> 0.09)$, for a state of mean photon number $|\alpha|^2 = 1$ and an intensity gain of $g^2 = 1.8$, is high for non-deterministic amplification. It increases with the mean photon number, $|\alpha|^2$ and detector quantum efficiency, $\eta$, as the probability for successful photon subtraction increases.

The input state is selected randomly from the set $\{|\alpha\rangle, |-\alpha\rangle\}$
and a $50:50$ beamsplitter is used for the state comparison technique.
This plot is for photon subtraction beamsplitter transmissivity $t^2 = 0.9$.

In our example this is equal to

$$\hat{\rho}_{\text{output}} = \frac{1}{P(S)} \int d^2\bar{\alpha} \int d^2\bar{\beta} \, P(\bar{\alpha}) \, P(\bar{\beta}) \left| \frac{t(\bar{\alpha} + \bar{\beta})}{\sqrt{2}} \right\rangle_b \left\langle \frac{t(\bar{\alpha} + \bar{\beta})}{\sqrt{2}} \right|$$
$$\times \exp\left\{ -\eta_0 \left| \frac{\bar{\alpha} - \bar{\beta}}{\sqrt{2}} \right|^2 \right\} \left( 1 - \exp\left\{ -\eta_1 \left| \frac{-r(\bar{\alpha} + \bar{\beta})}{\sqrt{2}} \right|^2 \right\} \right), \qquad (4.27)$$

$$\hat{\rho}_{\text{output}} = \frac{1}{P(S)} \frac{1}{2} \left( 1 - e^{-2\eta_1 r^2 |\alpha|^2} \right) |t\sqrt{2}\alpha\rangle_b \langle t\sqrt{2}\alpha|$$
$$= |t\sqrt{2}\alpha\rangle_b \langle t\sqrt{2}\alpha|. \qquad (4.28)$$

This is indeed the target state (Figure 4.7). In this particular example we would get the same result without the conditioning on the state comparison measurement.

The gain of amplification is $g = t\sqrt{2}$. The higher the transmission coefficient of the photon subtraction beamsplitter, the higher the gain. However, the higher the transmission coefficient the less likely the photon subtraction, (4.25). So there is a trade-off between the highest gain and a non-zero success probability of the device. In our graphs we use a transmissivity of $t^2 = 0.9$ which gives a reasonably high success probability and a gain of $g^2 = 1.8$.
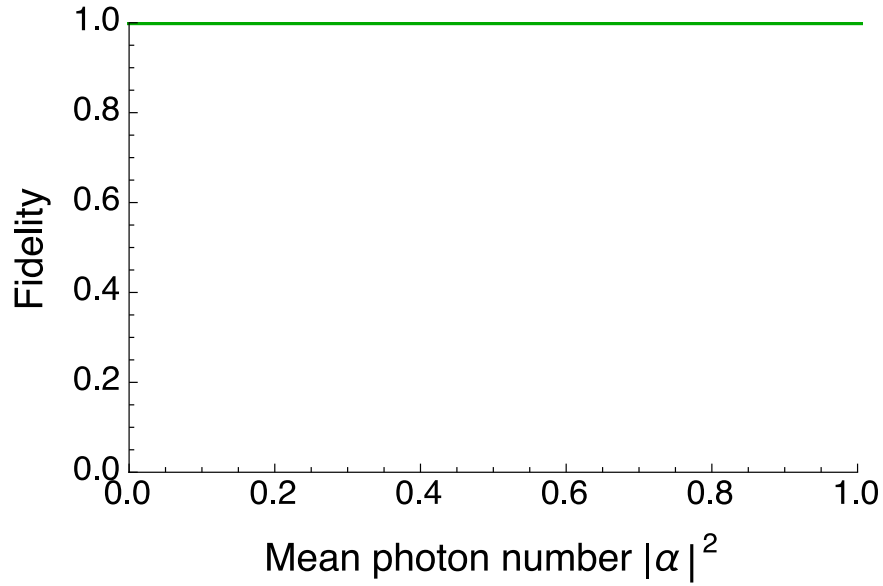
Figure 4.7: The fidelity of the output state with the target state, where the output is conditioned on the photon subtraction measurement, is 1. It is independent of the mean photon number, $|\alpha|^2$, the detector quantum efficiency, $\eta$ and the subtraction beamsplitter transmissivity, $t^2$. The gain of amplification is $g = t\sqrt{2}$. For a realistic photon subtraction we take $t^2 = 0.9$ and so the gain is $g^2 = 1.8$.

The input state is selected randomly from the set $\{|\alpha\rangle, |-\alpha\rangle\}$
and a $50:50$ beamsplitter is used for the state comparison technique.

The gain does not depend only on the transmission coefficient of the photon subtraction beamsplitter. The $\sqrt{2}$ term is a result of our choice to use a $50:50$ beamsplitter at the state comparison measurement (Figure 4.5). We explain how we can extend this scheme to get a much higher amplification gain in the following section.

### 4.1.2   General scheme

The system we proposed is easily extensible to higher gains: we replace the $50:50$ state comparison beamsplitter with a beamsplitter with the general beamsplitter coefficients $t_1, r_1$ (Figure 4.8). Then the three-mode output state is transformed as follows:

$$\hat{\rho}_{out}^{(3)} = \int \mathrm{d}^2\bar{\alpha} \int \mathrm{d}^2\bar{\beta} \; P(\bar{\alpha}) \; P(\bar{\beta}) \; |t_1\bar{\alpha} - r_1\bar{\beta}\rangle_a \langle t_1\bar{\alpha} - r_1\bar{\beta}|$$
$$\otimes |t_2(r_1\bar{\alpha} + t_1\bar{\beta})\rangle_b \langle t_2(r_1\bar{\alpha} + t_1\bar{\beta})| \otimes |-r_2(r_1\bar{\alpha} + t_1\bar{\beta})\rangle_c \langle -r_2(r_1\bar{\alpha} + t_1\bar{\beta})|,$$
$$(4.29)$$

where $t_2, r_2$ are the beamsplitter coefficients for the photon subtraction beamsplitter (Figure 4.8). For the input state $\bar{\alpha} \to \alpha$ and the guess state $\bar{\beta} \to t_1/r_1\alpha$, the target

"output state" $\qquad t_2(r_1\bar{\alpha} + t_1\bar{\beta})$

$0 \longrightarrow \qquad \longrightarrow -r_2(r_1\bar{\alpha} + t_1\bar{\beta})\ \boxed{1}\ \text{“D}_1\text{”}$

$t_2 \approx 1$

$r_1\bar{\alpha} + t_1\bar{\beta}$

"input state" $\bar{\alpha} \longrightarrow \qquad \longrightarrow t_1\bar{\alpha} - r_1\bar{\beta}\ \ \boxed{0}\ \text{“D}_0\text{”}$

$t_1, r_1$

"guess state" $\bar{\beta}$
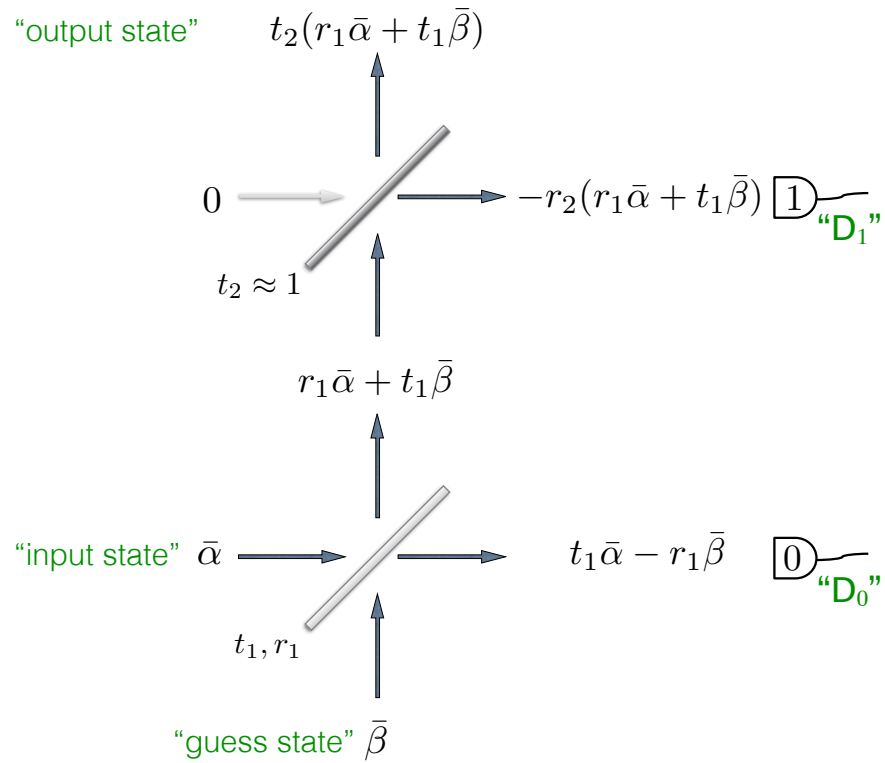
Figure 4.8: The quantum optical state comparison amplifier.

The output is accepted on no detection events at the state comparison measurement $(D_0)$ and a detection event at the photon subtraction measurement $(D_1)$.

state is

$$t_2\left(r_1\bar{\alpha} + t_1\bar{\beta}\right) \rightarrow t_2\left(r_1\alpha + \frac{t_1^2}{r_1}\alpha\right)$$
$$= \frac{t_2}{r_1}\left(r_1^2\alpha + t_1^2\alpha\right) = \frac{t_2}{r_1}\alpha \tag{4.30}$$

Therefore the nominal gain is $g = t_2/r_1$.

## Probability of success

The probability of success is the joint probability that the state comparison measurement gives no counts at $D_0$ and the photon subtraction measurement gives a count at $D_1$. It is given by

$$P(S) = \text{Tr}\left\{\hat{\rho}_{out}^{(3)} : \exp\left\{-\eta_0 \hat{a}_a^\dagger \hat{a}_a\right\}\left(1 - \exp\left\{-\eta_1 \hat{a}_c^\dagger \hat{a}_c\right\}\right) :\right\},$$

$$= \int d^2\bar{\alpha} \int d^2\bar{\beta}\, P(\bar{\alpha})\, P(\bar{\beta})\, \exp\left\{-\eta_0 \left|t_1\bar{\alpha} - r_1\bar{\beta}\right|^2\right\}$$

$$\times \left(1 - \exp\left\{-\eta_1\left| - r_2(r_1\bar{\alpha} + t_1\bar{\beta})\right|^2\right\}\right). \tag{4.31}$$

where we used the three-mode output state $\hat{\rho}_{out}^{(3)}$ defined in (4.29) and $\eta_i$ is the quantum efficiency of detector $D_i$.

## Conditional output state

The output state conditioned on the state comparison detector not firing and the photon subtraction detector firing, is given by

$$\hat{\rho}_{\text{output}} = \frac{\text{Tr}_{a,c}\left\{\hat{\rho}_{out}^{(3)} : \exp\left\{-\eta_0 \hat{a}_a^\dagger \hat{a}_a\right\}\left(1 - \exp\left\{-\eta_1 \hat{a}_c^\dagger \hat{a}_c\right\}\right) :\right\}}{\text{Tr}\left\{\hat{\rho}_{out}^{(3)} : \exp\left\{-\eta_0 \hat{a}_a^\dagger \hat{a}_a\right\}\left(1 - \exp\left\{-\eta_1 \hat{a}_c^\dagger \hat{a}_c\right\}\right) :\right\}},$$

$$= \frac{\text{Tr}_{a,c}\left\{\hat{\rho}_{out}^{(3)} : \exp\left\{-\eta_0 \hat{a}_a^\dagger \hat{a}_a\right\}\left(1 - \exp\left\{-\eta_1 \hat{a}_c^\dagger \hat{a}_c\right\}\right) :\right\}}{P(S)}. \tag{4.32}$$

## Fidelity

We introduced the definition of the fidelity of the output state with the target state as (4.12)

$$\text{Fidelity} = \int d^2\bar{\alpha} P(\bar{\alpha})\langle g\bar{\alpha}|\hat{\rho}_{\text{output}}|g\bar{\alpha}\rangle,$$

where $g = t_2/r_1$ in general, which holds for a pure target state $|g\bar{\alpha}\rangle$. Alice knows what the input state is (4.13), so from her point of view the target state is pure.

Another way of defining the fidelity, that can be evaluated by either Alice or Bob, is the following: the fidelity of the output state with the target state is the probability of passing a measurement test, $T$, given that the device operated successfully, $S$,

$$\text{Fidelity} = P(T|S)$$
$$= \frac{P(T,S)}{P(S)}$$
$$= \frac{\int d^2\bar{\alpha} \int d^2\bar{\beta}\, P(\bar{\alpha})\, P(\bar{\beta})\, P(T|S,\bar{\alpha},\bar{\beta})\, P(S|\bar{\alpha},\bar{\beta})}{\int d^2\bar{\alpha} \int d^2\bar{\beta}\, P(\bar{\alpha})\, P(\bar{\beta})\, P(S|\bar{\alpha},\bar{\beta})}, \tag{4.33}$$

where we define $P(S|\bar{\alpha},\bar{\beta})$ as

$$P(S|\bar{\alpha},\bar{\beta}) \equiv \exp\left\{-\eta_0|t_1\bar{\alpha} - r_1\bar{\beta}|^2\right\} \times \left(1 - \exp\left\{-\eta_1 r_2^2|r_1\bar{\alpha} + t_1\bar{\beta}|^2\right\}\right) \tag{4.34}$$

and

$$P(T|S, \bar{\alpha}, \bar{\beta}) = P(T|\bar{\alpha}, \bar{\beta}) \equiv |\langle g\bar{\alpha}|t_2(r_1\bar{\alpha} + t_1\bar{\beta})\rangle|^2 \tag{4.35}$$

is the overlap of the output state with the target state given that Alice's state was $\bar{\alpha}$ and Bob's state was $\bar{\beta}$. Therefore $P(T, S)$ is equal to

$$P(T, S) = \int \mathrm{d}^2\bar{\alpha} \int \mathrm{d}^2\bar{\beta} \; P(\bar{\alpha}) \; P(\bar{\beta}) \; |\langle g\bar{\alpha}|t_2(r_1\bar{\alpha} + t_1\bar{\beta})\rangle|^2 \; P(S|\bar{\alpha}, \bar{\beta}). \tag{4.36}$$

In this section we introduced the quantum optical state comparison amplifier, which is based on the techniques of coherent state comparison and photon subtraction. The output state is accepted conditioned on no counts from the state comparison measurement and a count from the photon subtraction measurement. The nominal gain is $g = t_2/r_1$. We defined the conditional output state and the measures of the probability of success and the fidelity of the output state with the target state $|t_2/r_1\alpha\rangle$.

In the following section we present the results of these measures for two particular sets on input states. Furthermore, we compare the performance of the quantum optical state comparison amplifier to other schemes of non-deterministic amplification.

## 4.2 Findings

In this section we present the results for the figures of merit of our device. We group them in two sections based on the set of states from which Alice chooses the input state. Of particular interest are the following two sets (Figure 4.9):

- 2-state set: contains two states of equal magnitude that are positioned opposite on the phase space, for example $\{\alpha, -\alpha\}$,

- Phase symmetric set: contains states of equal magnitude but unknown phase on the phase space, for example $\{|\alpha|e^{i\theta}\}$, $0 \leq \theta < 2\pi$.

We assume that Alice selects the input state randomly from her set of states, with equal probability for each state. The probability distributions associated with the two sets are

$$P(\bar{\alpha}) = \frac{1}{2}\left[\delta^2(\bar{\alpha} - \alpha) + \delta^2(\bar{\alpha} + \alpha)\right] \tag{4.37}$$

for the 2-state set and

$$P(\bar{\alpha}) = \frac{1}{2\pi|\alpha|}\delta(|\bar{\alpha}| - |\alpha|) \tag{4.38}$$

for the state symmetric set. Bob chooses his set of states based on Alice's set. In all scenarios we assume that Bob can measure the magnitude of Alice's input states but not their phase. We demonstrate the scheme for Bob's choice $(t_1/r_1)\alpha$,

$$P(\bar{\beta}) = \delta^2\left(\bar{\beta} - \frac{t_1}{r_1}\alpha\right). \tag{4.39}$$
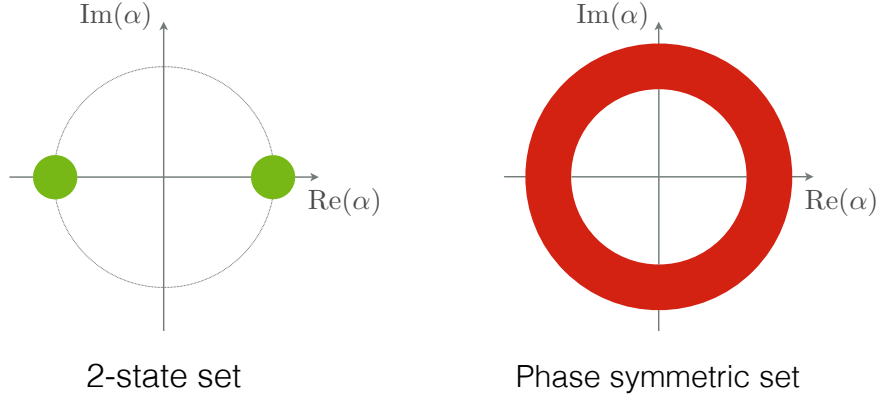
Figure 4.9: We consider two examples of sets from which Alice chooses the input state: the 2-state set and the phase symmetric set.

### 4.2.1 Amplification for a set of 2 coherent states

#### Probability of success

By using the probability distributions for the 2-state system, (4.37) and (4.39), into (4.31), we find that the probability of success is equal to

$$
\begin{aligned}
P(S) = &\frac{1}{2}\left[1 - \exp\left\{-\eta_1 g^2|\alpha|^2\left(1/t_2^2 - 1\right)\right\}\right] \\
&+ \frac{1}{2}\exp\left\{-4\eta_0|\alpha|^2\left(1 - t_2^2/g^2\right)\right\} \\
&\times\left[1 - \exp\left\{-\eta_1 g^2|\alpha|^2\left(1/t_2^2 - 1\right)\left(1 - 2t_2^2/g^2\right)^2\right\}\right].
\end{aligned}
\tag{4.40}
$$

The first part of (4.40) corresponds to Bob having made the correct guess (the input state was $\alpha$) and the second part corresponds to the incorrect guess (input state $-\alpha$). The probability of success increases with intensity gain (Figure 4.10), as well as with input state amplitude, as photon subtraction is more probable. Furthermore, higher quantum efficiency, $\eta$, ensures that successful photon subtractions are less likely to be missed.

#### Conditional output state

Having calculated the probability of success, we calculate the normalised density operator for the output state, (4.32):

$$
\begin{aligned}
\hat{\rho}_{\text{output}} = \frac{1}{P(S)}\Bigg(&\frac{1}{2}\left[1 - \exp\left\{-\eta_1 g^2|\alpha|^2\left(1/t_2^2 - 1\right)\right\}\right]|g\alpha\rangle\langle g\alpha| \\
&+ \frac{1}{2}\left[1 - \exp\left\{-\eta_1 g^2|\alpha|^2\left(1/t_2^2 - 1\right)\left(1 - 2t_2^2/g^2\right)^2\right\}\right] \\
&\times\exp\left\{-4\eta_0|\alpha|^2\left(1 - t_2^2/g^2\right)\right\}|g\alpha\left[1 - 2\left(t_2^2/g^2\right)\right]\rangle\langle g\alpha\left[1 - 2\left(t_2^2/g^2\right)\right]|\Bigg).
\end{aligned}
\tag{4.41}
$$
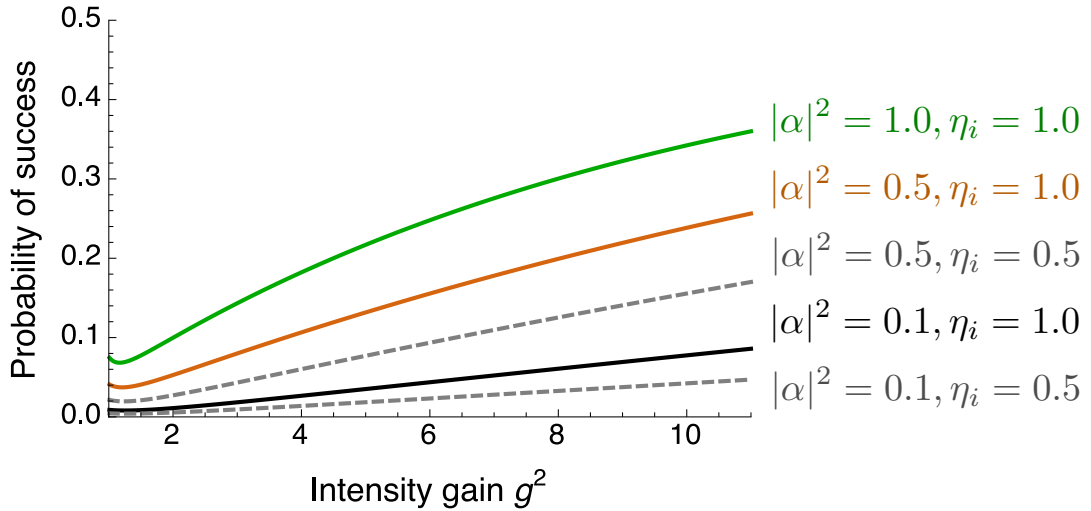
Figure 4.10: The probability of success is not limited by the mean photon number, $|\alpha|^2$, or the intensity gain, $g^2$, but in fact increases with these two parameters. Higher detector quantum efficiencies, $\eta_i$, result in higher probability of success. (Not shown: the plots for $|\alpha|^2 = 1, \eta_i = 0.5$ and $|\alpha|^2 = 0.5, \eta_i = 1$ are identical.)

The input state is selected randomly from the set $\{|\alpha\rangle, |-\alpha\rangle\}$.
This plot is for photon subtraction beamsplitter transmissivity $t_2^2 = 0.9$.

## Fidelity

We find that the numerator of the fidelity is

$$
\begin{aligned}
P(T,S) = \ & \frac{1}{2}\left[1 - \exp\left\{-\eta_1 g^2 |\alpha|^2 \left(1/t_2^2 - 1\right)\right\}\right] \\
& + \frac{1}{2}\exp\left\{-4\eta_0 |\alpha|^2 \left(1 - t_2^2/2\right)\right\} \\
& \times \left[1 - \exp\left\{-\eta_1 g^2 |\alpha|^2 \left(1/t_2^2 - 1\right)\left(1 - 2t_2^2/g^2\right)^2\right\}\right] \\
& \times \exp\left\{-4g^2 |\alpha|^2 \left(1 - t_2^2/g^2\right)^2\right\}.
\end{aligned}
\tag{4.42}
$$

The state comparison amplifier performs better, in terms of the fidelity of the output state with the target state, as the mean photon number increases (Figure 4.11). The fidelity decreases with intensity gain, apart from a region between $1 < g^2 \leq 2$, where it increases until it reaches unity at $g = t_2\sqrt{2}$.

Decreasing detector quantum efficiency, $\eta_i$ degrades the fidelity, as it corresponds to accepting incorrectly identified zero counts at $D_0$ (Figure 4.11). It also corresponds to fewer recorded events of successful photon subtraction at $D_1$, although this is a determining factor in the probability of success rather than the fidelity directly (Figure 4.12). Higher quantum efficiency improves the fidelity more significantly for states with higher mean photon numbers, *e.g.* $|\alpha|^2 = 1.0$, compared to states with smaller
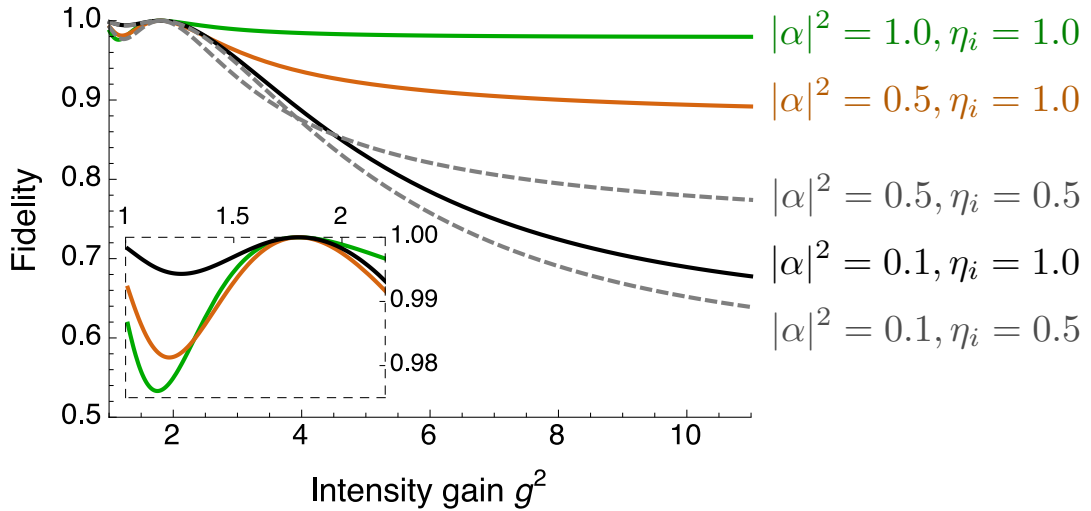
Figure 4.11: The fidelity of the output state with the target state increases with higher mean photon numbers, $|\alpha|^2$ and higher detector quantum efficiencies, $\eta_i$. (Not shown: the plots for $|\alpha|^2 = 1, \eta_i = 0.5$ and $|\alpha|^2 = 0.5, \eta_i = 1$ are identical.)

The output state is identical to the target state for a gain of $g = t_2\sqrt{2}$, *i.e.* when a $50:50$ beamsplitter is used at the state comparison stage.

The input state is selected randomly from the set $\{|\alpha\rangle, |-\alpha\rangle\}$. This plot is for photon subtraction beamsplitter transmissivity $t_2^2 = 0.9$.

mean photon numbers, *e.g.* $|\alpha|^2 = 0.1$ (Figure 4.12). When a $50:50$ beamsplitter is used at the state comparison stage, the fidelity is independent of the detector quantum efficiency (subsection 4.1.1, Figure 4.7).

The fidelity and probability of success would degrade if we took into account any dark counts present in the system. Darks counts have the opposite effect compared to detector quantum efficiency: we would throw away any correctly amplified states when the state comparison detector fires and we would mistakenly accept any unamplified states when the photon subtraction detector fires. Recent experiments have very low dark count rates and we can assume that they are not present in our system [Clarke et al., 2012].

## Noise figure

As an additional figure of merit for the performance of our amplifier, we calculate the noise figure which we define as the signal to noise ratio of the output signal to the signal to noise ratio of the input,

$$\text{Noise figure} = \frac{\text{SNR}_{\text{output}}}{\text{SNR}_{\text{input}}}. \tag{4.43}$$
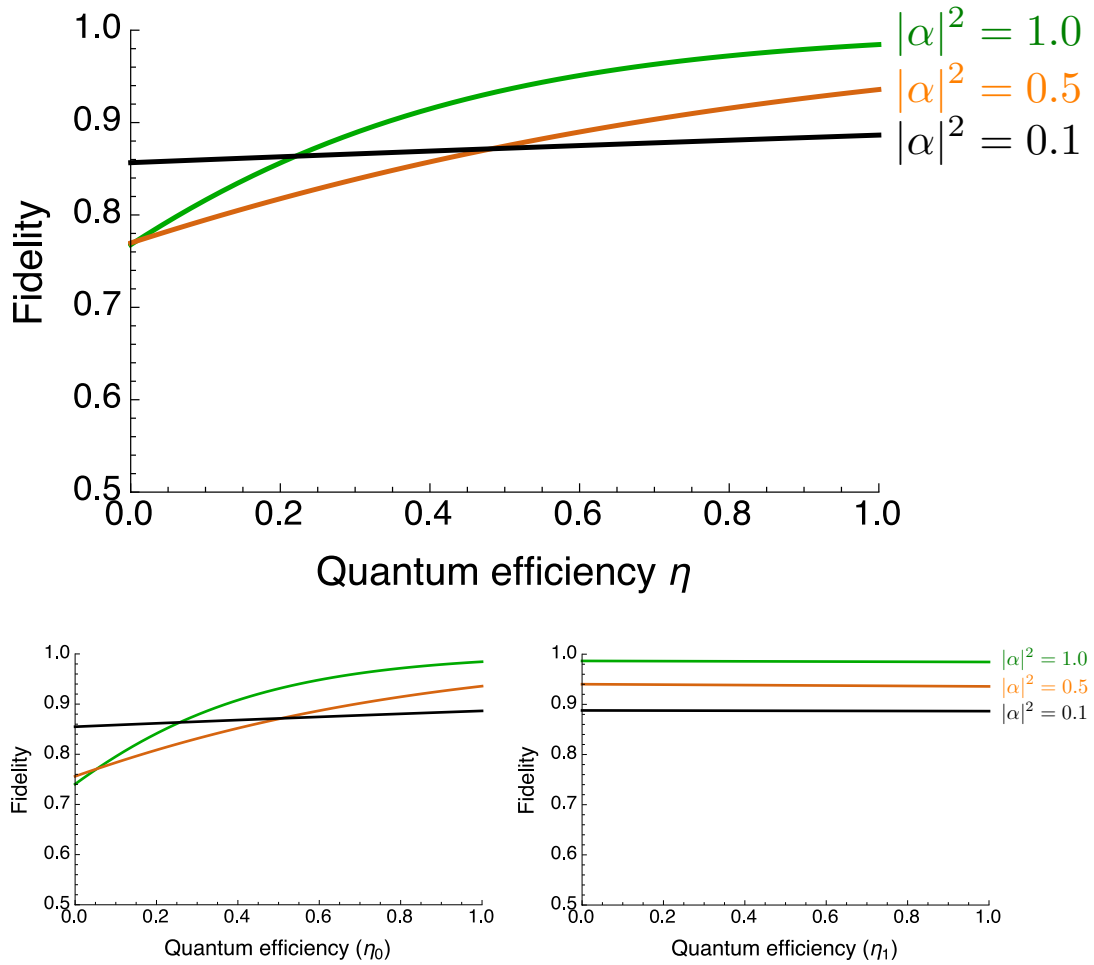
Figure 4.12: The fidelity of the output state with the target state increases with detector quantum efficiency, $\eta$ and with mean photon number, $|\alpha|^2$.

The quality of the detector at the state comparison stage, $\eta_0$, is the determining factor in the fidelity, rather than the efficiency of the detector at the photon subtraction stage, $\eta_1$. (The top plot is for $\eta = \eta_0 = \eta_1$.)

The input state is selected randomly from the set $\{|\alpha\rangle, |-\alpha\rangle\}$.
All plots are for $t_2^2 = 0.9$ and intensity gain $g^2 = 4$.

We take the signal to noise ratio, SNR, to be the ratio of the mean to the standard deviation for the $\hat{X}$ quadrature,

$$\text{SNR} = \frac{\langle \hat{X} \rangle}{\sqrt{\langle (\Delta X)^2 \rangle}} \tag{4.44}$$

where $\hat{X} = (\hat{a}^\dagger + \hat{a})/2$. For the output state $\hat{\rho}_{\text{output}}$, (4.41), the mean is equal to

$$
\begin{aligned}
\langle \hat{X} \rangle_{\text{output}} &= \mathrm{Tr}\{\hat{\rho}_{\text{output}} \hat{X}\} \\
&= \mathrm{Tr}\left\{ \frac{1}{2}(\hat{a}^\dagger + \hat{a}) \times \frac{1}{P(S)} \right. \\
&\quad \left. \times \left( P(\alpha|S)|g\alpha\rangle\langle g\alpha| + P(-\alpha|S)\big|g\alpha \left[1 - 2\left(t_2^2/g^2\right)\right]\big\rangle\big\langle g\alpha \left[1 - 2\left(t_2^2/g^2\right)\right]\big| \right) \right\} \\
&= \frac{1}{2P(S)}\left\{ P(\alpha|S)(g\alpha^* + g\alpha) \right. \\
&\quad \left. + P(-\alpha|S)\left(g\alpha^* \left[1 - 2\left(t_2^2/g^2\right)\right] + g\alpha \left[1 - 2\left(t_2^2/g^2\right)\right]\right) \right\} \\
&= \frac{1}{2P(S)}g\alpha^* \left\{ P(\alpha|S) + P(-\alpha|S)\left[1 - 2\left(t_2^2/g^2\right)\right] \right\} \\
&\quad + \frac{1}{2P(S)}g\alpha \left\{ P(\alpha|S) + P(-\alpha|S)\left[1 - 2\left(t_2^2/g^2\right)\right] \right\} \\
&= \frac{1}{P(S)}g|\alpha| \left\{ P(\alpha|S) + P(-\alpha|S)\left[1 - 2\left(t_2^2/g^2\right)\right] \right\},
\end{aligned}
\tag{4.45}
$$

where $P(\pm\alpha|S)$ is the conditional probability that the input state was $\pm\alpha$ given that the device operated successfully:

$$
\begin{aligned}
P(\alpha|S) &= \frac{1}{2}\left[1 - \exp\left\{-\eta_1 g^2 |\alpha|^2 \left(1/t_2^2 - 1\right)\right\}\right] \\
P(-\alpha|S) &= \frac{1}{2}\left[1 - \exp\left\{-\eta_1 g^2 |\alpha|^2 \left(1/t_2^2 - 1\right)\left(1 - 2t_2^2/g^2\right)^2\right\}\right] \\
&\quad \times \exp\left\{-4\eta_0 |\alpha|^2 \left(1 - t_2^2/g^2\right)\right\}.
\end{aligned}
\tag{4.46}
$$

Therefore

$$
\langle \hat{X} \rangle_{\text{output}}^2 = \frac{1}{P(S)^2}g^2|\alpha|^2 \left\{ P(\alpha|S) + P(-\alpha|S)\left[1 - 2\left(t_2^2/g^2\right)\right] \right\}^2.
\tag{4.47}
$$

Next, we calculate $\langle \hat{X}^2 \rangle_{\text{output}}$,

$$
\begin{aligned}
\langle \hat{X}^2 \rangle_{\text{output}} &= \mathrm{Tr}\{\hat{\rho}_{\text{output}} \hat{X}^2\} \\
&= \mathrm{Tr}\left\{ \frac{1}{4}\left(\hat{a}^{\dagger 2} + \hat{a}^2 + 2\hat{a}^\dagger\hat{a} + 1\right) \times \frac{1}{P(S)} \right. \\
&\quad \left. \times \left( P(\alpha|S)|g\alpha\rangle\langle g\alpha| + P(-\alpha|S)\big|g\alpha \left[1 - 2\left(t_2^2/g^2\right)\right]\big\rangle\big\langle g\alpha \left[1 - 2\left(t_2^2/g^2\right)\right]\big| \right) \right\} \\
&= \frac{1}{4P(S)}\left\{ P(\alpha|S)(g^2\alpha^{*2} + g^2\alpha^2 + 2g^2|\alpha|^2 + 1) \right. \\
&\quad + P(-\alpha|S)\left(g^2\alpha^{*2}\left[1 - 2\left(t_2^2/g^2\right)\right]^2 + g^2\alpha^2\left[1 - 2\left(t_2^2/g^2\right)\right]^2 \right. \\
&\quad \left.\left. + 2g^2|\alpha|^2\left[1 - 2\left(t_2^2/g^2\right)\right]^2 + 1\right) \right\}
\end{aligned}
\tag{4.48}
$$

$$\langle \hat{X}^2 \rangle_{\text{output}} = \frac{1}{4P(S)} g^2 \alpha^{*2} \left\{ P(\alpha|S) + P(-\alpha|S) \left[ 1 - 2 \left( t_2^2/g^2 \right) \right]^2 \right\}$$

$$+ \frac{1}{4P(S)} g^2 \alpha^2 \left\{ P(\alpha|S) + P(-\alpha|S) \left[ 1 - 2 \left( t_2^2/g^2 \right) \right]^2 \right\}$$

$$+ \frac{1}{4P(S)} 2g^2 |\alpha|^2 \left\{ P(\alpha|S) + P(-\alpha|S) \left[ 1 - 2 \left( t_2^2/g^2 \right) \right]^2 \right\}$$

$$+ \frac{P(\alpha|S) + P(-\alpha|S)}{4P(S)}$$

$$= \frac{1}{4P(S)} g^2 \left\{ P(\alpha|S) + P(-\alpha|S) \left[ 1 - 2 \left( t_2^2/g^2 \right) \right]^2 \right\} \left( \alpha^{*2} + \alpha^2 + 2|\alpha|^2 \right)$$

$$+ \frac{1}{4}$$

$$= \frac{1}{P(S)} g^2 |\alpha|^2 \left\{ P(\alpha|S) + P(-\alpha|S) \left[ 1 - 2 \left( t_2^2/g^2 \right) \right]^2 \right\} + \frac{1}{4}, \qquad (4.49)$$

and so we find that the variance is equal to

$$(\Delta X)^2_{\text{output}} = \langle \hat{X}^2 \rangle_{\text{output}} - \langle \hat{X} \rangle^2_{\text{output}}$$

$$= \frac{1}{P(S)} g^2 |\alpha|^2 \left\{ P(\alpha|S) + P(-\alpha|S) \left[ 1 - 2 \left( t_2^2/g^2 \right) \right]^2 \right\} + \frac{1}{4}$$

$$- \frac{1}{P(S)^2} g^2 |\alpha|^2 \left\{ P(\alpha|S) + P(-\alpha|S) \left[ 1 - 2 \left( t_2^2/g^2 \right) \right] \right\}^2. \qquad (4.50)$$

Therefore the signal to noise ratio for the output state is

$$\text{SNR}_{\text{output}} = \frac{1}{P(S)} g|\alpha| \left\{ P(\alpha|S) + P(-\alpha|S) \left[ 1 - 2 \left( t_2^2/g^2 \right) \right] \right\}$$

$$\times \left[ \frac{1}{P(S)} g^2 |\alpha|^2 \left\{ P(\alpha|S) + P(-\alpha|S) \left[ 1 - 2 \left( t_2^2/g^2 \right) \right]^2 \right\} + \frac{1}{4} \right.$$

$$\left. - \frac{1}{P(S)^2} g^2 |\alpha|^2 \left\{ P(\alpha|S) + P(-\alpha|S) \left[ 1 - 2 \left( t_2^2/g^2 \right) \right] \right\}^2 \right]^{-1/2}. \qquad (4.51)$$

For the input state $\hat{\rho}_{\text{input}} = |\alpha\rangle\langle\alpha|$ the signal to noise ratio is $\text{SNR}_{\text{input}} = 2|\alpha|$, as

$$\begin{aligned}
\langle\hat{X}\rangle_{\text{input}} &= \text{Tr}\{\hat{\rho}_{\text{input}}\hat{X}\} \\
&= \text{Tr}\left\{\frac{1}{2}|\alpha\rangle\langle\alpha|(\hat{a}^\dagger + \hat{a})\right\} \\
&= \frac{1}{2}(\alpha^* + \alpha) \\
&= |\alpha|
\end{aligned}$$

$$\begin{aligned}
\langle\hat{X}^2\rangle_{\text{input}} &= \text{Tr}\{\hat{\rho}_{\text{input}}\hat{X}^2\} \\
&= \text{Tr}\left\{\frac{1}{4}|\alpha\rangle\langle\alpha|\left(\hat{a}^{\dagger 2} + \hat{a}^2 + 2\hat{a}^\dagger\hat{a} + 1\right)\right\} \\
&= \frac{1}{4}\left(\alpha^{*2} + \alpha^2 + 2|\alpha|^2 + 1\right) \\
&= \frac{1}{4}\left[(\alpha^* + \alpha)^2 + 1\right] \\
&= \frac{1}{4}\left[(2|\alpha|)^2 + 1\right] \\
&= |\alpha|^2 + \frac{1}{4}
\end{aligned}$$

$$\begin{aligned}
(\Delta X)^2_{\text{input}} &= \langle\hat{X}^2\rangle_{\text{input}} - \langle\hat{X}\rangle^2_{\text{input}} \\
&= |\alpha|^2 + \frac{1}{4} - |\alpha|^2 = \frac{1}{4}.
\end{aligned}$$

Therefore the noise figure reads

$$\begin{aligned}
\text{Noise figure} &= \frac{\text{SNR}_{\text{output}}}{\text{SNR}_{\text{input}}} \\
&= \frac{1}{2|\alpha|} \times \frac{1}{P(S)}g|\alpha|\left\{P(\alpha|S) + P(-\alpha|S)\left[1 - 2\left(t_2^2/g^2\right)\right]\right\} \\
&\quad \times \left[\frac{1}{P(S)}g^2|\alpha|^2\left\{P(\alpha|S) + P(-\alpha|S)\left[1 - 2\left(t_2^2/g^2\right)\right]^2\right\} + \frac{1}{4}\right. \\
&\quad \left. - \frac{1}{P(S)^2}g^2|\alpha|^2\left\{P(\alpha|S) + P(-\alpha|S)\left[1 - 2\left(t_2^2/g^2\right)\right]\right\}^2\right]^{-1/2}. \quad (4.52)
\end{aligned}$$

The noise figure is higher than one (for gains $> g^2 = 1.5$), as expected, and there is a clear improvement with increasing gain, (Figure 4.13). It is relatively insensitive to the mean photon number, $|\alpha|^2$ and detector quantum efficiency, $\eta_i$.
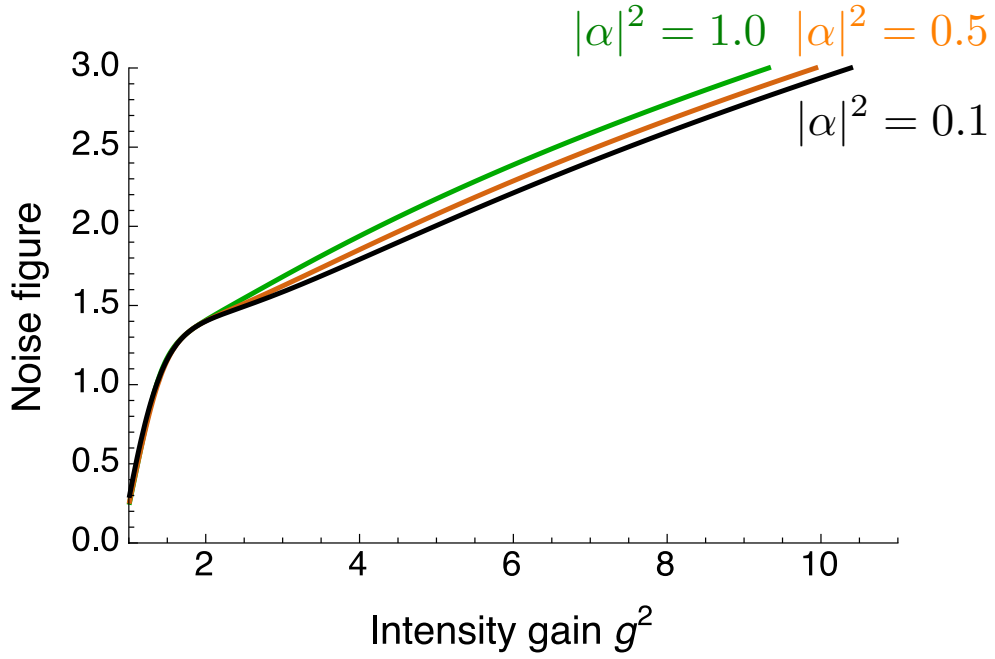
Figure 4.13: The noise figure increases with intensity gain, $g^2$, for gains greater than about $g^2 > 1.8$. It increases slightly with the mean photon number, $|\alpha|^2$. (Not shown: the noise figure is relatively insensitive to detector quantum efficiency, $\eta_i$. This plot is for $\eta_i = 1$.)

The input state is selected randomly from the set $\{|\alpha\rangle, |-\alpha\rangle\}$. This plot is for photon subtraction beamsplitter transmissivity $t_2^2 = 0.9$.

## 4.2.2   Amplification for a phase symmetric set of states

It may be the case that Alice can choose the input state from a set where there are many states, all equal in magnitude but with different phase, $\{|\alpha|e^{i\theta}\}$, for all $0 \leq \theta < 2\pi$ (as in Figure 4.9). We assume that the states are equally distributed around the phase space and Alice chooses her state at random. The probability distribution associated with Alice's input state is given by equation (4.38) and we demonstrate the scheme for Bob's choice given by (4.39).

In this subsection we study the performance of our amplifier for an input state chosen from the phase symmetric set of states. We verify that the detector quantum efficiency, $\eta_i$ and the photon subtraction beamsplitter transmissivity, $t_2^2$, play the same role (for the same reasons) as in the case where the input state is selected from a binary alphabet (Subsection 4.2.1).

The dependence of the fidelity and the probability of success with the mean photon number shows more clearly the competing nature between these two measures: the higher the mean photon number the higher the probability of success but the lower the fidelity.

## Probability of success

The probability of success, (4.31), becomes

$$
\begin{aligned}
P(S) &= \int d^2\bar{\alpha} \int d^2\bar{\beta}\; P(\bar{\alpha})\; Q(\bar{\beta})\; P(S|\bar{\alpha},\bar{\beta}) \\
&= \int |\bar{\alpha}|\mathrm{d}|\bar{\alpha}| \int_0^{2\pi} \mathrm{d}\theta \int \mathrm{d}^2\bar{\beta}\; \frac{1}{2\pi|\alpha|}\delta\left(|\bar{\alpha}| - |\alpha|\right)\; \delta^2\left(\bar{\beta} - \frac{t_1}{r_1}\alpha\right) \\
&\quad \times \exp\left\{-\eta_0 \left| t_1\bar{\alpha} - r_1\bar{\beta} \right|^2\right\} \times \left(1 - \exp\left\{-\eta_1 \left| - r_2(r_1\bar{\alpha} + t_1\bar{\beta}) \right|^2\right\}\right) \\
&= \frac{1}{2\pi}\int_0^{2\pi} \mathrm{d}\theta\; \exp\left\{-\eta_0 \left| t_1|\alpha|e^{i\theta} - t_1\alpha \right|^2\right\} \\
&\quad \times \left(1 - \exp\left\{-\eta_1 \left| - r_2\left(r_1|\alpha|e^{i\theta} + t_1^2/r_1\alpha\right) \right|^2\right\}\right). \tag{4.53}
\end{aligned}
$$

We note that, in general, the phase of Bob's state is different from the phase of Alice's state, therefore

$$
t_1|\alpha|e^{i\theta} - t_1\alpha = t_1|\alpha|e^{i\theta} - t_1|\alpha|e^{i\phi} \neq 0. \tag{4.54}
$$

For simplicity, we assume that Bob's state is on the positive real axis and the relative phase between Alice's and Bob's states is given by $\theta$. Then the probability of success is equal to

$$
\begin{aligned}
P(S) &= \frac{1}{2\pi}\int_0^{2\pi} \mathrm{d}\theta\; \exp\left\{-\eta_0 \left| t_1|\alpha|e^{i\theta} - t_1|\alpha| \right|^2\right\} \\
&\quad \times \left(1 - \exp\left\{-\eta_1 \left| - r_2\left(r_1|\alpha|e^{i\theta} + t_1^2/r_1|\alpha|\right) \right|^2\right\}\right) \\[2mm]
&= \frac{1}{2\pi}\int_0^{2\pi} \mathrm{d}\theta \exp\left\{-2\eta_0|\alpha|^2 t_1^2\left(1 - \cos\theta\right)\right\} \\
&\quad \times \left(1 - \exp\left\{-\eta_1|\alpha|^2\left(r_2^2/r_1^2\right)\left[1 - 2r_1^2\left(1 - r_1^2\right)\left(1 - \cos\theta\right)\right]\right\}\right),
\end{aligned}
$$

$$
\begin{aligned}
P(S) &= \exp\left\{-2\eta_0|\alpha|^2\left(1 - t_2^2/g^2\right)\right\} I_0\left[2\eta_0|\alpha|^2\left(1 - t_2^2/g^2\right)\right] \\
&\quad - \exp\left\{-2\eta_0|\alpha|^2\left(1 - t_2^2/g^2\right)\right\} \\
&\quad \times \exp\left\{2\eta_1|\alpha|^2\left(1 - t_2^2\right)\left(1 - t_2^2/g^2\right) - \eta_1|\alpha|^2 g^2\left(1/t_2^2 - 1\right)\right\} \\
&\quad \times I_0\left[2\eta_0\alpha^2\left(1 - t_2^2/g^2\right) - 2\eta_1|\alpha|^2\left(1 - t_2^2\right)\left(1 - t_2^2/g^2\right)\right], \tag{4.55}
\end{aligned}
$$

where $I_0$ is a modified Bessel Function of the zeroth order [Watson, 1995]. The probability of success has the same trend as for the 2-state system: it increases with intensity gain and increasing mean photon number, because the photon subtraction probability becomes higher (Figure 4.14). Decreasing quantum efficiency, $\eta_i$, lowers the probability of success, as the probability for successful photon subtraction decreases.
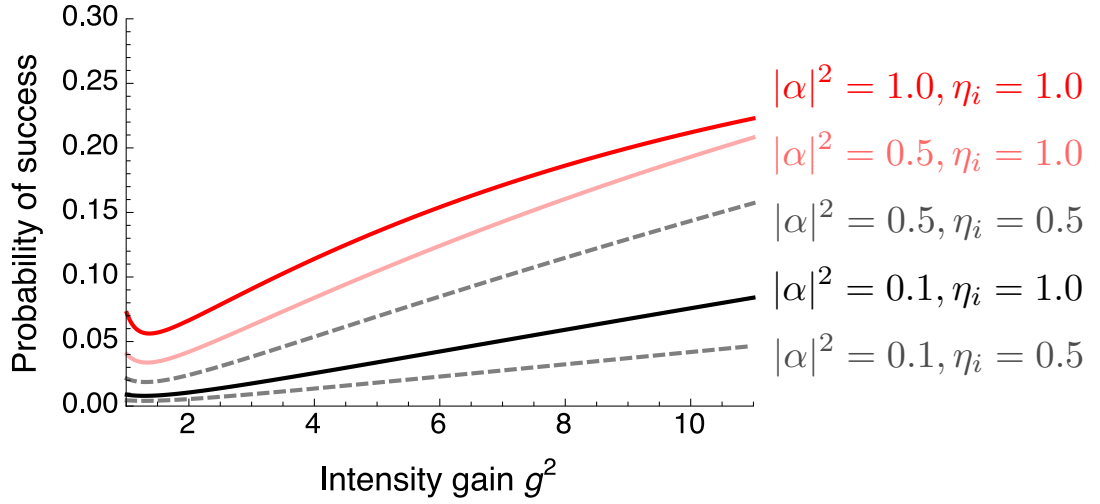
Figure 4.14: The probability of success increases with mean photon number, $|\alpha|^2$, detector quantum efficiency, $\eta_i$ and intensity gain, $g^2$.
(Not shown: the plots for $|\alpha|^2 = 1, \eta_i = 0.5$ and $|\alpha|^2 = 0.5, \eta_i = 1$ are identical.)

The input state is selected randomly from the phase symmetric set.
This plot is for photon subtraction beamsplitter transmissivity $t_2^2 = 0.9$.

## Fidelity

The numerator of the fidelity, $P(T, S)$, (defined in (4.33)), for the phase symmetric system is equal to

$$
P(T, S) = \int \mathrm{d}^2\bar{\alpha} \int \mathrm{d}^2\bar{\beta}\; P(\bar{\alpha})\; P(\bar{\beta})\; \left|\left\langle g\bar{\alpha}\middle| t_2\left(r_1\bar{\alpha} + t_1\bar{\beta}\right)\right\rangle\right|^2
$$

$$
\times \exp\left\{-\eta_0\left|t_1\bar{\alpha} - r_1\bar{\beta}\right|^2\right\} \times \left(1 - \exp\left\{-\eta_1\left|-r_2(r_1\bar{\alpha} + t_1\bar{\beta})\right|^2\right\}\right)
$$

$$
= \int |\bar{\alpha}|\mathrm{d}|\bar{\alpha}| \int_0^{2\pi} \mathrm{d}\theta \int \mathrm{d}^2\bar{\beta}\; \frac{1}{2\pi|\alpha|}\delta\left(|\bar{\alpha}| - |\alpha|\right)\; \delta^2\left(\bar{\beta} - \frac{t_1}{r_1}\alpha\right)
$$

$$
\times \left|\left\langle g\bar{\alpha}\middle| t_2\left(r_1\bar{\alpha} + t_1\bar{\beta}\right)\right\rangle\right|^2
$$

$$
\times \exp\left\{-\eta_0\left|t_1\bar{\alpha} - r_1\bar{\beta}\right|^2\right\} \times \left(1 - \exp\left\{-\eta_1\left|-r_2(r_1\bar{\alpha} + t_1\bar{\beta})\right|^2\right\}\right),
$$

$$
(4.56)
$$
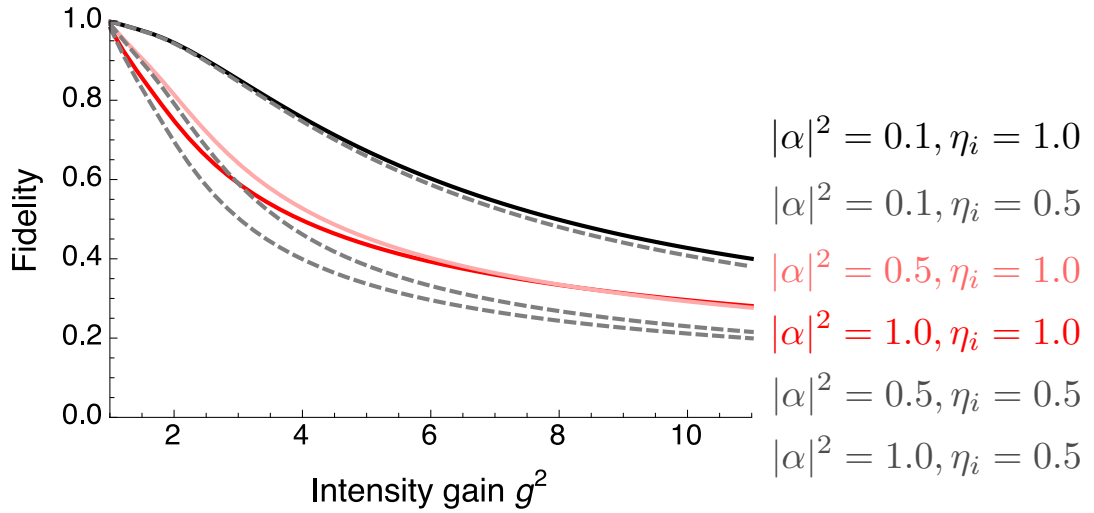
Figure 4.15: The state comparison amplifier produces a better version of the target state for states with smaller mean photon numbers. The fidelity is higher for higher detector quantum efficiencies, $\eta_i$.

The input state is selected randomly from the phase symmetric set.
This plot is for photon subtraction beamsplitter transmissivity $t_2^2 = 0.9$.

$$P(T,S) = \frac{1}{2\pi} \int_0^{2\pi} \mathrm{d}\theta \; \left| \langle g|\alpha|e^{i\theta} | t_2 \left( r_1|\alpha|e^{i\theta} + t_1^2/r_1\alpha \right) \rangle \right|^2$$

$$\times \exp\left\{ -\eta_0 \left| t_1|\alpha|e^{i\theta} - t_1\alpha \right|^2 \right\}$$

$$\times \left( 1 - \exp\left\{ -\eta_1 \left| - r_2 \left( r_1|\alpha|e^{i\theta} + t_1^2/r_1\alpha \right) \right|^2 \right\} \right). \qquad (4.57)$$

We assume that the relative phase between Alice's and Bob's states is $\theta$, therefore

$$P(T,S) = \frac{1}{2\pi} \int_0^{2\pi} \mathrm{d}\theta \; \left| \langle g|\alpha|e^{i\theta} | t_2 \left( r_1|\alpha|e^{i\theta} + t_1^2/r_1|\alpha| \right) \rangle \right|^2$$

$$\times \exp\left\{ -\eta_0 \left| t_1|\alpha|e^{i\theta} - t_1|\alpha| \right|^2 \right\}$$

$$\times \left( 1 - \exp\left\{ -\eta_1 \left| - r_2 \left( r_1|\alpha|e^{i\theta} + t_1^2/r_1|\alpha| \right) \right|^2 \right\} \right), \qquad (4.58)$$

which is equal to
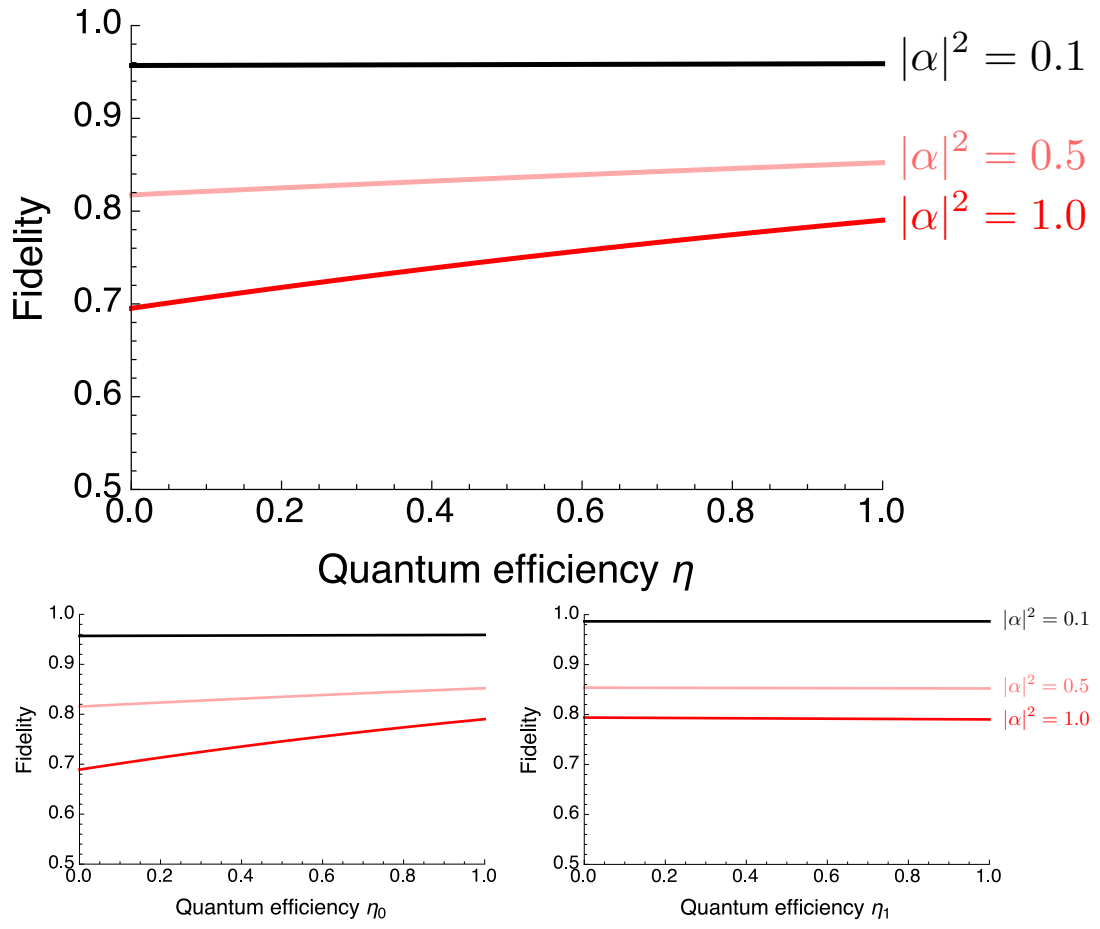
Figure 4.16: The fidelity of the output state with the target state is relatively insensitive to detector quantum efficiency, $\eta$, especially for small mean photon numbers, $|\alpha|^2$. The quantum efficiency of the detector at the photon subtraction stage, $\eta_1$, has almost no effect on the fidelity.

The input state is selected randomly from the phase symmetric set.
All plots are for $t_2^2 = 0.9$ and intensity gain $g^2 = 1.8$.

$$
\begin{aligned}
P(T,S) = {} & \exp\left\{-2\eta_0|\alpha|^2\left(1 - t_2^2/g^2\right) - 2|\alpha|^2 g^2\left(1 - t_2^2/g^2\right)^2\right\} \\
& \times I_0\left[2\eta_0|\alpha|^2\left(1 - t_2^2/g^2\right) + 2|\alpha|^2 g^2\left(1 - t_2^2/g^2\right)^2\right] \\
& - \exp\left\{-2|\alpha|^2\left(1 - t_2^2/g^2\right)\left(\eta_0 - \eta_1\left(1 - t_2^2\right)\right) - 2|\alpha|^2 g^2\left(1 - t_2^2/g^2\right)^2\right\} \\
& \times \exp\left\{-\eta_1|\alpha|^2 g^2\left(1/t_2^2 - 1\right)\right\} \\
& \times I_0\left[2|\alpha|^2\left(1 - t_2^2/g^2\right)\left(\eta_0 - \eta_1\left(1 - t_2^2\right)\right) + 2|\alpha|^2 g^2\left(1 - t_2^2/g^2\right)^2\right].
\end{aligned}
$$

$$(4.59)$$

The phase symmetric system performs better, in terms of the fidelity of the output state with the target state, for states with small mean photon numbers (Figure 4.15). The fidelity is almost insensitive to the detector quantum efficiency (Figure 4.16). A limited detector quantum efficiency will have the greater effect in decreasing the fidelity for higher mean photon numbers. A state with a high mean photon number (around $|\alpha|^2 = 1.0$) in the measured beamsplitter arm ought to be detected and not pass for a zero result at the state comparison measurement.

### 4.2.3 Comparison with other schemes

Every amplification scheme proposed works well for the purpose that it was built to serve. Some were built to work with single photons as input, others with coherent states. Some care about the quality of the output state, for others a "working" probability of success is more important. For some the gain is a crucial factor, others emphasise on the range of states to amplify. However, it is instructive to compare different schemes. There is no right measure in order to make comparisons; inevitably some schemes are more or less favoured depending one's priorities.

In this subsection we compare the fidelity of the quantum optical state comparison amplifier with the noise addition [Marek and Filip, 2010; Usuga et al., 2010] and quantum scissors protocols [Ralph and Lund, 2009; Xiang et al., 2010; Ferreyrol et al., 2010]. We amplify an input coherent state of mean photon number $|\alpha|^2 = 0.5$
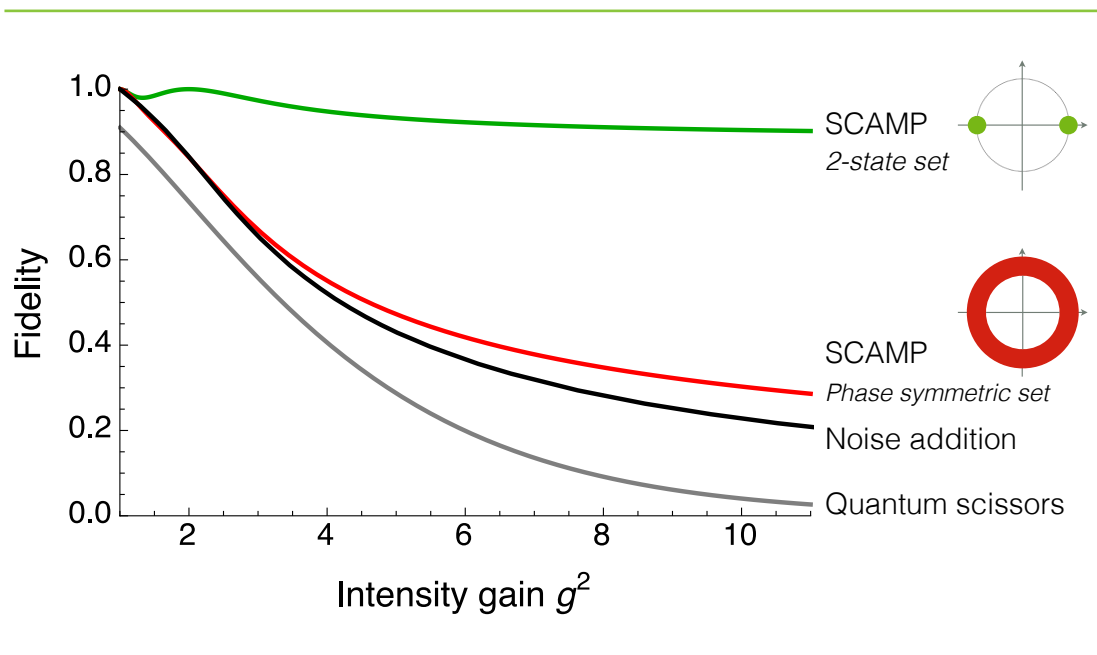


Figure 4.17: The state comparison amplifier (SCAMP) produces a higher quality output state compared to other non-deterministic amplification schemes over a wide range of amplifier gains.

This plot is for an input state of mean photon number $|\alpha|^2 = 0.5$ and for an ideal photon subtraction (i.e. transmissivity $t_2^2 = 0.99$).

(Figure 4.17). The quantum scissors device has a high fidelity for small amplitude states; for a state with mean photon number $|\alpha|^2 = 0.5$ the fidelity quickly degrades as the gain increases. The noise addition scheme and the phase symmetric set of the quantum optical state comparison amplifier have a very similar behaviour. In our plot we consider an ideal photon subtraction for both schemes and one photon subtraction for the noise addition scheme. When we consider an input chosen from the 2-state set, the quantum optical state comparison amplifier has a clear advantage over the other methods, as it achieves a fidelity equal to one at a gain of two and it maintains a high fidelity, ($> 0.9$), for all other gains.

## 4.3   Discussion of results

In this chapter we proposed a method for non-deterministic amplification of coherent states. Our method is based on coherent state comparison followed by photon subtraction (Figure 4.8). The device operates successfully when there are no detection events at the state comparison measurement and a detection event at the photon subtraction measurement.

The gain of amplification is determined at the state comparison measurement, mainly. Alice's "weak" coherent state interferes with Bob's "stronger" state such that when their phases are matched appropriately, the output at this stage is an amplified version of Alice's input state. (We assume that Bob knows/can measure the magnitude of Alice's state. The phase, on the other hand, is completely unknown.) It follows that given a successful state comparison measurement, the gain of amplification is inversely proportional to the beamsplitter reflection coefficient, $r_1$.

Post-selection after the state comparison measurement results in a mixed output state. The photon subtraction measurement "purifies" the output from incorrect guesses. A successful photon subtraction reinforces the probability that we have the desired target state in our output. Under certain circumstances, we can be $100\%$ certain that we have the desired target state (Figure 4.7).

The transmissivity of the beamsplitter used in the photon subtraction measurement needs to be high so that it won't degrade the gain significantly. The nominal gain, therefore, is equal to $g = t_2/r_1$, where $t_2$ is the transmission coefficient of the beamsplitter at the photon subtraction measurement and $r_1$ is the reflection coefficient of the beamsplitter at the state comparison measurement.

On the other hand, the higher the transmission coefficient of the beamsplitter involved in the photon subtraction technique, the lower the probability for a successful photon subtraction. However, the less likely the photon subtraction the higher fidelity of the output state with the target state. For a realistic photon subtraction, a transmission intensity of $t_2^2 = 0.9$ compensates well between the two.

We found that the successful operation of our device increases with intensity gain, $g^2$ and mean photon number, $|a|^2$. This is because the probability for photon subtraction approaches one, $P(1|0) \to 1$, in the high gain limit.

Our most striking result, is the perfect fidelity our device can achieve for an intensity gain of $g^2 = 1.8$ when the input state is chosen from a binary alphabet (Figure 4.7). Otherwise, the general trend is that the fidelity of the output state

compared with the target state increases with the mean photon number, $|\alpha|^2$ and decreases with intensity gain, $g^2$.

The quantum efficiency of the two detectors causes imperfections in the scheme, but the "opposite" roles of the two detectors in our conditioning seem to counterbalance the effect. A limited quantum efficiency of the detector involved in the state comparison measurement would mean accepting more incorrect states, thus degrading the fidelity of the output state with the target state and increasing the probability of success. On the other hand a limited quantum efficiency of the detector at the photon subtraction measurement does not affect the fidelity of the output state; the detector is less likely to herald a correctly amplified state, thereby decreasing the probability of success.

We assume that there are no dark counts present in our system. This is the major assumption for successful coherent state comparison [Andersson et al., 2006]. Clearly this is not the case in practice, but gated dark count rates can be very low. We shall see that this is a reasonable assumption for our experiment.

In order to put our amplifier into context, we compare the fidelity of the output state with the target state to other non-deterministic amplification schemes (Figure 4.17, for a mean photon number of $|\alpha|^2 = 0.5$) [Ralph and Lund, 2009; Xiang et al., 2010; Ferreyrol et al., 2010; Marek and Filip, 2010; Usuga et al., 2010]. For an input state chosen from a binary set our amplifier has a very high fidelity ranging between 1 to 0.9 for all gains. For an input state chosen from a phase symmetric set of states our amplifier has higher fidelity than the noise addition and quantum scissors schemes, though it's performance is very similar to the noise addition scheme.

The gain of our amplifier does not depend on the mean photon number of the input state and in fact the fidelity and probability of success increase with the mean photon number, in contrast to the other schemes. Furthermore, our scheme does not require any complex equipment for its implementation (like parametric down conversion as in scissors-based devices, or the photon number resolving detectors that are used in the noise addition scheme) and it is straightforward to realise experimentally. In the next chapter we show the results of the practical implementation of our proposed protocol.

The key result is the perfect fidelity we can achieve with the quantum optical state comparison amplifier. This means that the device has the potential to find application as an optical repeater in a quantum communications scheme. Furthermore, in situations where Alice and Bob do not share a phase reference, they can use the state comparison amplifier to establish one [Bartlett et al., 2007].

# Experimental implementation of the Quantum Optical State Comparison Amplifier

P RACTICAL TESTS PROVIDE QUANTITATIVE DATA that shed light on the suitability of a theoretical protocol for real life implementation. This chapter is dedicated on the experimental implementation of the quantum optical state comparison amplifier. We describe the experimental set-up and analyse the results for sets of two, four and eight input states.

The analysis of the experimental data presented in this chapter is my work. The experimental implementation was assembled and operated by Ross. J. Donaldson, Robert J. Collins and Gerald S. Buller at Heriot-Watt University, Edinburgh, U.K.

A peer-reviewed version of this work has been accepted for publication in *Physical Review Letters*

This chapter is organised as follows,

**Implementation** This section describes the experimental set-up and the methods used to collect the experimental data for an input state chosen from a set of two, four and eight coherent states.

**Findings** We group the results of analysing the data in three subsections: the 2-state, 4-state and 8-state system (Subsections 5.2.1, 5.2.2 and 5.2.3, respectively). We calculate the success rate of the amplifier and the fidelity of the output state with the ideal target state. We find that, despite experimental imperfections, both measures are very high for all sets. Furthermore, we show that the quantum optical state comparison amplifier increases significantly the fraction of the target state in the output when it works properly. Additionally, we find a very high interferometric visibility and we show that the amplifier does not add any significant noise to the signal, when the input is chosen from a binary alphabet of coherent states.

**Discussion** Finally, we summarise the main results and compare the experimental performance of our protocol with others from the literature.

## 5.1 Implementation

We test the quantum optical state comparison amplifier for a fixed gain and a varying magnitude of the input states. We use a $50:50$ beamsplitter for the state comparison measurement and a $90:10$ beamsplitter for the photon subtraction measurement, which provide a nominal gain of amplification of $g^2 = 1.8$. In this configuration the *input* states and the *guess* states have the same magnitude, $|\alpha|$.

We test the device for different sets of input states*, equally spaced around the phase space (Figure 5.1):

- 2-state set: $\{|\alpha|, -|\alpha|\}$,

- 4-state set: $\{|\alpha|, |\alpha|e^{i\pi/2}, -|\alpha|, |\alpha|e^{i3\pi/2}\}$,

- 8-state set: $\{|\alpha|, |\alpha|e^{i\pi/4}, |\alpha|e^{i\pi/2}, |\alpha|e^{i3\pi/4}, -|\alpha|, |\alpha|e^{i5\pi/4}, |\alpha|e^{i3\pi/2}, |\alpha|e^{i7\pi/4}\}$.



|  2-state set  |  4-state set  |  8-state set  |
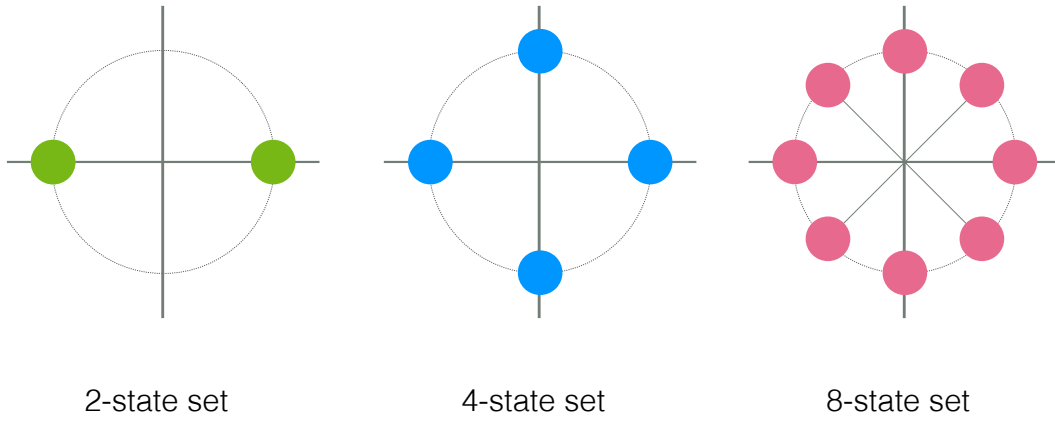
Figure 5.1: The input state is selected from a set that contains either two, four or eight coherent states equally spaced around the phase space. In each set the states have the same magnitude and they are selected at random with equal probability.

**\*Notice**: Strictly speaking and according to the nomenclature we introduced in the previous chapter, we test the state comparison amplifier from Alice's point of view: *i.e.* the *input* state is always $|\alpha\rangle$, and the *guess* state is chosen at random from either the 2-state, 4-state or 8-state set. We use this implementation as we are restricted to engineer only the target state $|g\alpha\rangle$ for the analysis measurement.

The protocol yields the same results whether we test it from Bob's point of view (as in the theory chapter) or Alice's point of view (as in this chapter). Due to this equivalence, in the following sections we do not emphasise again that Bob chooses at random the *guess* state but instead we refer to this guess state with the general term "the input state" to the amplifier.

### 5.1.1 Experimental set-up

Figure 5.2 shows the experimental set-up for the state comparison amplifier. Subsection 5.1.2 has the detailed characteristics of the components.

For the purposes of the experimental implementation, the input and guess states originate from the same source and they are split at a $50 : 50$ beamsplitter before they are input into the quantum optical state comparison amplifier.

The guess state encounters the phase modulator in its path, which induces a phase change on the guess state. The phase modulator produces a known repeated sequence of phase shifts, with duration $1$ $\mu$s for each phase. The sequence of the phase shifts is:

- 2-state set: $(0, \pi)$

- 4-state set: $(0, \pi, \pi/2, 3\pi/2)$

- 8-state set: $(0, \pi, \pi/2, 3\pi/2, \pi/4, 5\pi/4, 3\pi/4, 7\pi/4)$.

An air-gap in the path of the input state establishes the highest mean fringe visibility of the interference between the input and guess states. For the 2-state system, for example, the counts at detector $D_0$ are minimised when the phase modulator produces the phase $\theta = 0$ (say) and are maximised for $\theta = \pi$. For the 4- and 8-state systems we can also test the symmetry of the device: the air-gap is adjusted so that additional opposite states, say with phases $\theta = \pi/2$ and $\theta = 3\pi/2$, give the maximum and the minimum of counts at detector $D_0$. (In the analysis of the data in Section 5.2 we present the average of all results, *i.e.* we average over the two possible ways to test the 4-state system and the four possible ways to test the 8-state system.) The state comparison measurement is crucial in order to determine the relative phase between the input and guess states and set in this way a phase reference.

An outer interferometer is set up in order to analyse the output state of the quantum optical state comparison amplifier. Two $50 : 50$ beamsplitters are used: one to separate the target amplified state with the one that will be split into the input and guess states later and another that combines the target and output states for the analysis measurement at $D_A$ and $D_B$. The target state has the same phase as the input state. A computer controlled air-gap is used to ensure the highest mean fringe visibility between the target and output states, by minimising and maximising the counts at $D_A$ and $D_B$ in a similar manner as it is used in the inner interferometer.

### 5.1.2 Technical Methods

In this subsection we provide the technical details of the experimental implementation.

The interferometric visibilities in our set-up are:

- Inner interferometer: $92.41\%$

- Outer interferometer: $92.24\%$          (before conditional filtering [see below])
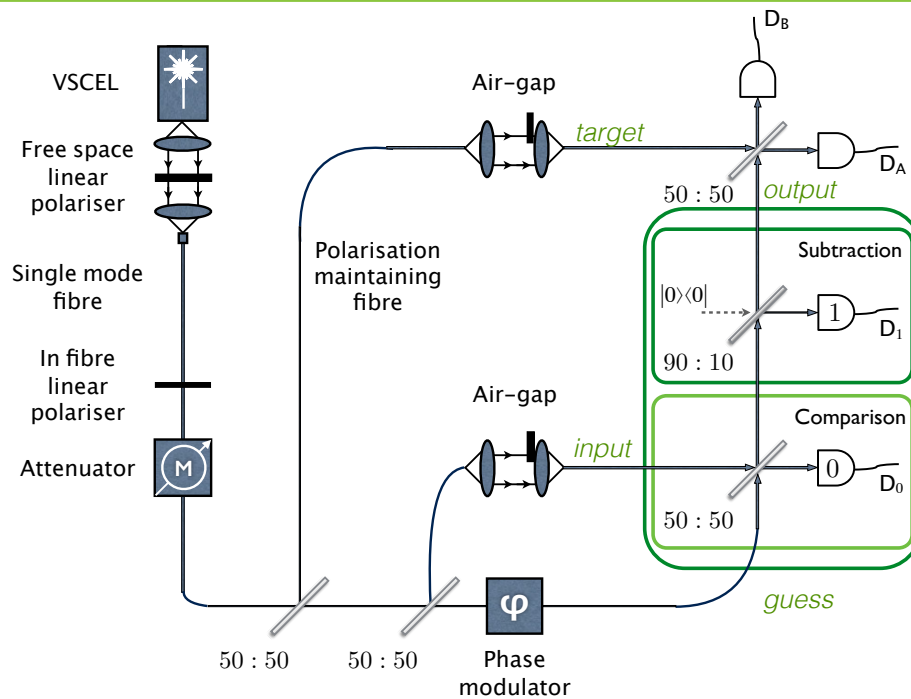
Figure 5.2: For the experimental set-up we require:

- Vertical Cavity Surface Emitting Laser (VCSEL)    *launches coherent states*

- Free-space linear polariser    *polarises signal*

- Single-mode fibre    *couples signal to fibre*

- In-fibre linear polariser    *polarises signal*

- Polarisation maintaining fibre    *transfers signal to destination*

- Computer controlled attenuator    *sets the mean photon number per pulse*

- Computer controlled air-gaps    *adjust relative path lengths of interferometers*

- Lithium niobate (LiNbO3) phase modulator    *establishes phase encoding*

- Beamsplitters
    - $50 : 50$ beamsplitters $(\times 4)$    *input/guess, state comparison, analysis $(\times 2)$*
    - $90 : 10$ beamsplitter    *for photon subtraction*

- Detectors $(\times 4)$    *for state comparison, photon subtraction, analysis $(\times 2)$*

## Key features of components and operation

- Vertical Cavity Surface Emitting Laser (VCSEL)

    - temperature stabilised
    - central wavelength: $850.38$ nm
    - spectral bandwidth: $0.37$ nm
    - central wavelength stability: $\pm 0.8$ pm
    - pulse repetition frequency: $1$ MHz

- Single-mode fibre: core diameter $5$ $\mu$m

- Polarisation maintaining fibre [Kumar and Ghatak, 2011]

    - "panda eye" polarisation maintaining fibre
    - core diameter: $5$ $\mu$m
    - final polarisation extinction ratio: $1200 : 1$

- Computer-controlled attenuator

    - based on stepper motor controlled knife-edge      *spatially intercepts beam*

- Computer-controlled adjustable length air-gaps

    - contain manual knife-edge attenuators      *balance optical loss in fibres*
    - can adjust path lengths at $\sim 15$ nm steps over a $1.5$ $\mu$m range

- Lithium niobate (LiNbO3) phase modulator

    - clocked at $1$ MHz
    - phase-locked to the laser
    - requires $6$ V to cause a phase change of $\pi$ rad
    - variance with the desired state: $\pm 1.6 \times 10^{-3}$ rad

- Detectors

    - commercially available
    - free-running
    - thick-junction [Clarke et al., 2011]
    - Geiger mode Silicon single photon avalanche diodes (Si-SPADs) [Spinelli et al., 1996; Buller and Collins, 2010]
    - mean[1] quantum efficiency: $40.5\%$ (at a wavelength of $850$ nm) [Collins et al., 2010]

---

[1]This is the mean of all four detectors. The quantum efficiency of each detector is: $D_0 = 41\%$, $D_1 = 0.38\%$, $D_A = 0.43\%$, and $D_B = 0.40\%$.

- mean raw dark count rate: 296 counts per second
- mean gated dark count rate: 8 counts per second

- Computer-controlled time-stamping electronics [Wahl et al., 2008]

  - phase-locked to the laser: rubidium (Rb) reference clock
    *(common to laser driver, phase modulator driver and time-stamping electronics)*

  - recording with time intervals of $1\ \mathrm{ps}$

  - maximum event rate recording: $\sim 4\ \mathrm{MHz}$
    *(combination of computer, custom software and time-stamping electronics)*

  - receive all events caused by an individual laser pulse simultaneously: electrical delays were used on the outputs of the detectors

- Custom software [by Robert J. Collins]

  - Gating process:
    - event filtering: $\pm 2\ \mathrm{ns}$ window of expected arrival time
    - mean event retention: $96.5\%$ of events
    - non-time-correlated background events (laser disabled): discarded $97\%$

  - Conditional filtering (for output state analysis)
    *(Condition: no detection events at $D_0$ and a detection event at $D_1$)*
    - $\pm 2\ \mathrm{ns}$ window of event expected arrival time
    - accounts for detector temporal response with varying photon flux [Gordon et al., 2005]
    - non-time-correlated background events (laser disabled): 0 (zero)
      *($600$ individual $1\ \mathrm{s}$ duration measurements)*

## 5.2 Findings

In this section we present the results of analysing the experimental data that were obtained using the set-up described in the previous section (Section 5.1). The analysis of the data is my work.

### 5.2.1 Amplification for a set of 2 coherent states

IN this subsection we present the results for the amplification of an input chosen at random from a set of two coherent states (Figure 5.1).

For the analysis measurement, we interfere the output state of the quantum optical state comparison amplifier with the target state at a $50 : 50$ beamsplitter with a detector in each output arm, $D_A$ and $D_B$, (Figure 5.2). We assume that the quantum optical state comparison amplifier produces one of the following output states: either $|g\alpha\rangle$ when it works correctly or $|0\rangle$ when it does not work, both *a priori* equally likely (Figure 5.3). We expect to see the following trends:
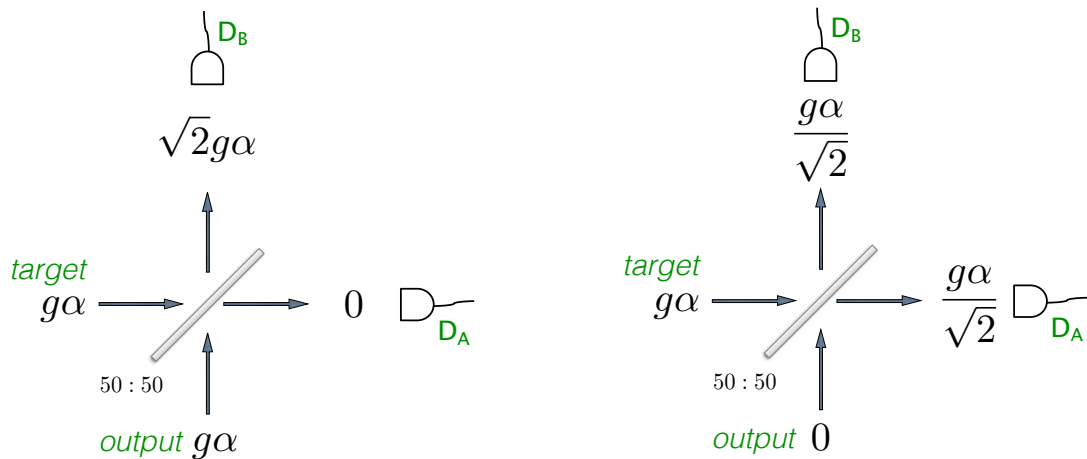


Figure 5.3: We assume that the quantum optical state comparison amplifier produces either state $|g\alpha\rangle$ or $|0\rangle$. The output state is interfered with the target state, $|g\alpha\rangle$, for an analysis measurement.

- When the quantum optical state comparison amplifier works, the output state $|g\alpha\rangle$ interferes with the target state $|g\alpha\rangle$, creating the vacuum state in the beamsplitter arm where $D_A$ is placed and the state $|\sqrt{2}g\alpha\rangle$ in the other arm. Therefore $D_B$ fires and $D_A$ does not.

- When the quantum optical state comparison amplifier does not work, *i.e.* produces the output state $|0\rangle$, the target state $|g\alpha\rangle$ is halved at the $50 : 50$ beamsplitter. We expect $D_A$ and $D_B$ to register the same number of counts.

In other words, as the phase of the guess state alternates between $0$ and $\pi$, the events recorded at each detector will accumulate into two peaks:

- for detector $D_A$, one peak will be of intensity $0$ and the other of intensity $1/2|g\alpha|^2$, whereas

- for detector $D_B$, one peak will be of intensity $2|g\alpha|^2$ and the other of intensity $1/2|g\alpha|^2$.

## Visibility

In order to determine how close the output state is to the ideal target state, we can do a visibility calculation. We define the visibility as the difference between the two
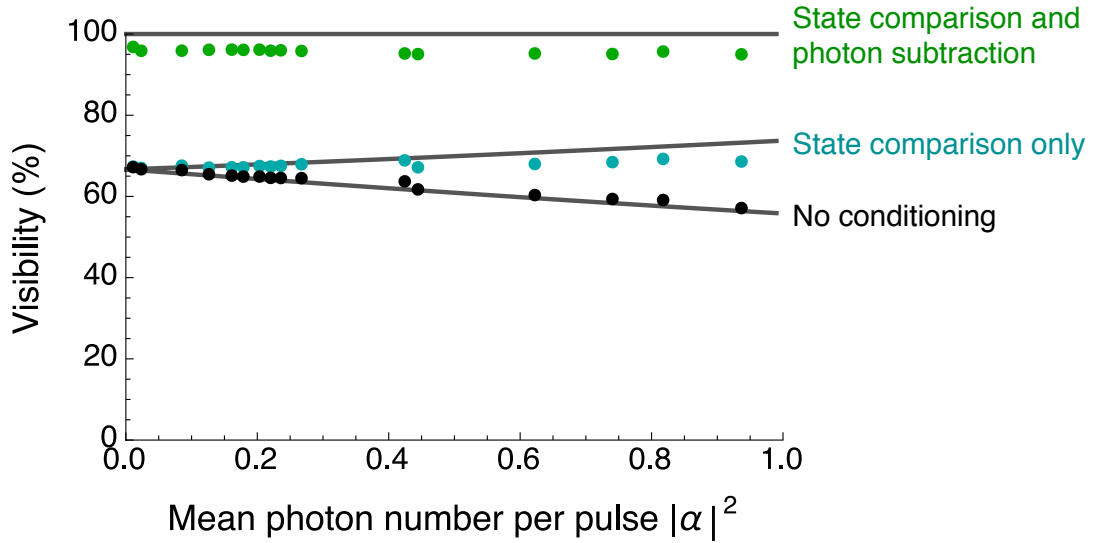


Figure 5.4: The visibility at the outer interferometer is progressively increased as the output state is not conditioned on any measurement result, it is conditioned on the state comparison measurement only, and then it is conditioned on both the state comparison and photon subtraction measurements, in which case it is almost $100\%$ ($\sim 96\%$). The average standard error is $\pm0.05$. The solid lines are theoretical predictions based on experimental parameters.

Note that in this and any other occurrences of "standard error", we mean the root mean square (RMS) error, which gives an indication of the quality of the average value of the corresponding quantity.

intensities in each detector divided by their sum,

$$\text{Visibility}^A = \frac{|I^A_{\text{max}} - I^A_{\text{min}}|}{I^A_{\text{max}} + I^A_{\text{min}}}. \tag{5.1}$$

where for example $I^A_{\text{max}}$ corresponds to the highest intensity in detector $D_A$, and $I^A_{\text{min}}$ to the lowest intensity, and in the same way we can define it for detector $D_B$.

Alternatively, we can define a visibility across both detectors, as

$$\text{Visibility} = \frac{|I_{\text{max}}^B - I_{\text{min}}^A|}{I_{\text{max}}^B + I_{\text{min}}^A + I_{\text{max}}^A + I_{\text{min}}^B}, \tag{5.2}$$

where the numerator gives the maximum difference in intensity between the four peaks and the denominator takes into account all the intensities.

Theoretically, the visibility is given by the trace of the state in the output arms of the beamsplitter used for the analysis measurement, $\hat{U}|g\alpha\rangle\langle g\alpha| \otimes \hat{\rho}_{output}\hat{U}^\dagger$, with the number operator $\hat{n} = \hat{a}^\dagger\hat{a}$,

$$\text{Visibility}^{Th} = \text{Tr}\left\{\left(\hat{U}|g\alpha\rangle\langle g\alpha| \otimes \hat{\rho}_{output}\hat{U}^\dagger\right)\hat{a}^\dagger\hat{a}\right\}, \tag{5.3}$$

where $\hat{U}$ represents the beamsplitter transformation, $|g\alpha\rangle$ is the target state and $\rho_{output}$ is the output of the state comparison amplifier. The detectors in our experiment do not resolve the number of photons, but simply indicate that there some photons present. Therefore the detection is described by the operator $\hat{\pi} = 1 - \hat{\pi}_0$, where $\hat{\pi}_0$ is the projection on the vacuum, $\hat{\pi}_0 = |0\rangle\langle 0|$. We want to account for the limited quantum efficiency at the detector, $\eta_j$, therefore we take $\hat{\pi}_0 =: e^{-\eta_j\hat{a}^\dagger\hat{a}} :$, and so the visibility for the theoretical prediction is given by

$$\text{Visibility}^{Th} = \text{Tr}\left\{\left(\hat{U}|g\alpha\rangle\langle g\alpha| \otimes \hat{\rho}_{output}\hat{U}^\dagger\right)\left(1 - : e^{-\eta_j\hat{a}^\dagger\hat{a}} :\right)\right\}. \tag{5.4}$$

We find that the visibility at the outer interferometer is very close to $100\%$ ($\sim 96\%$ on average) when the device operates successfully (Figure 5.4). If we relax the conditioning, for example post-selecting the output on the state comparison measurement result only, the visibility degrades ($\sim 68\%$). However, the experiment confirms the theoretical prediction: for an input chosen from the 2-state set and for a fixed gain of $g^2 = 1.8$, by conditioning the output state on the photon subtraction measurement, guarantees a(n almost) perfect visibility which implies an (almost) ideal output state.

## Estimation of the output state density operator

For an input state chosen from a binary alphabet of states, the density operator for the output state has the following form

$$\hat{\rho}_{output} = P_{g\alpha}|g\alpha\rangle\langle g\alpha| + P_0|0\rangle\langle 0|, \tag{5.5}$$

where $P_{g\alpha}$ is the normalised probability that the output state is $|g\alpha\rangle$ and $P_0$ is the normalised probability that the output state is the vacuum.

We calculate these probabilities given the photo counts at detectors $D_A$ and $D_B$ from the analysis measurement (Figure 5.3). We assume that the state comparison amplifier produces either $|g\alpha\rangle$ or $|0\rangle$, that *a priori* are equally likely. We take into account the possibility that the output and the target state may not be identical due to experimental set-up imperfections, by introducing the quantities $\delta$ and $\epsilon$ (Figure 5.5). Later we find that these quantities are not necessary for the fidelity estimation.

Furthermore, we take into account a loss factor, $\ell$, before the detectors. We determine the loss by comparing the counts at detector $D_0$ with the theoretical prediction when the input state is $|-\alpha\rangle$ and the counts at detector $D_1$ with the theoretical prediction when the input state is $|\alpha\rangle$. For an $\ell$ varying from $0$ to $1$, where $1$ means that there is no loss, we found that the loss in this system was $0.33$.
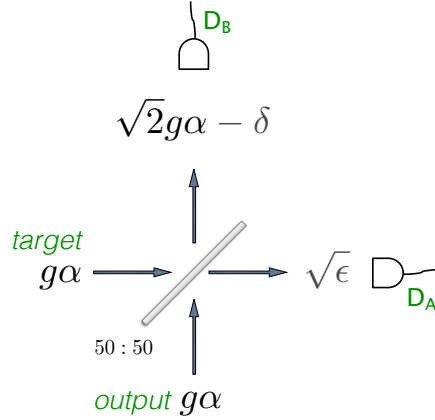


Figure 5.5: We introduce the quantities $\delta$ and $\epsilon$ to take into account interferometric misalignments.

The probability that detector $D_B$ fires and detector $D_A$ does not fire, given that the output of the state comparison amplifier is state $|g\alpha\rangle$, is given by

$$
\begin{aligned}
P(1,0|g\alpha) &= \left(1 - e^{-\eta\ell|\sqrt{2}g\alpha-\delta|^2}\right) e^{-\eta\ell|\sqrt{\epsilon}|^2} \\
&= e^{-\eta\ell\epsilon} - e^{-\eta\ell\left(|\sqrt{2}g\alpha-\delta|^2+|\sqrt{\epsilon}|^2\right)} \\
&= e^{-\eta\ell\epsilon} - e^{-\eta\ell 2g^2|\alpha|^2} \\
&\approx 1 - e^{-2\eta\ell g^2|\alpha|^2} - \eta\ell\epsilon,
\end{aligned}
\tag{5.6}
$$

which holds to the first order approximation in $\epsilon$ and where we used the relation we obtain by equating the input and output photon numbers (Figure 5.5):

$$
g^2|\alpha|^2 + g^2|\alpha|^2 = |\sqrt{2}g\alpha - \delta|^2 + |\sqrt{\epsilon}|^2.
\tag{5.7}
$$

Similarly, we find that the probability that detector $D_B$ does not fire and detector $D_A$ does, given that the output of the state comparison amplifier is state $|g\alpha\rangle$, is given by

$$
\begin{aligned}
P(0,1|g\alpha) &= \left(1 - e^{-\eta\ell\epsilon}\right) e^{-\eta\ell|\sqrt{2}g\alpha-\delta|^2} \\
&= \left(e^{\eta\ell\epsilon} - 1\right) e^{-\eta\ell|\sqrt{2}g\alpha-\delta|^2} e^{-\eta\ell\epsilon} \\
&\approx \eta\ell\epsilon \, e^{-2\eta\ell g^2|\alpha|^2}.
\end{aligned}
\tag{5.8}
$$

The probability that both detectors fire, given that the output state is $|g\alpha\rangle$, is

$$
\begin{aligned}
P(1,1|g\alpha) &= \left(1 - e^{-\eta\ell|\sqrt{2}g\alpha - \delta|^2}\right)\left(1 - e^{-\eta\ell\epsilon}\right) \\
&= 1 - e^{-\eta\ell\epsilon} - e^{-\eta\ell|\sqrt{2}g\alpha - \delta|^2} + e^{-2\eta\ell g^2|\alpha|^2} \\
&= 1 - e^{-\eta\ell\epsilon} - e^{+\eta\ell\epsilon}e^{-2\eta\ell g^2|\alpha|^2} + e^{-2\eta\ell g^2|\alpha|^2} \\
&= 1 - e^{-\eta\ell\epsilon} + e^{-2\eta\ell g^2|\alpha|^2}\left(1 - e^{+\eta\ell\epsilon}\right) \\
&\approx 1 - (1 - \eta\ell\epsilon) + e^{-2\eta\ell g^2|\alpha|^2}\left(1 - 1 - \eta\ell\epsilon\right) \\
&= \eta\ell\epsilon + e^{-2\eta\ell g^2|\alpha|^2}\left(-\eta\ell\epsilon\right) \\
&= \eta\ell\epsilon\left(1 - e^{-2\eta\ell g^2|\alpha|^2}\right).
\end{aligned} \tag{5.9}
$$

We use the notation $n_A^{g\alpha}$ and $n_B^{g\alpha}$ to indicate the number of counts at $D_A$ and $D_B$, respectively, when the output is $|g\alpha\rangle$. We want to find the number of pulses, $N_{g\alpha}$, that generated these counts. The number of pulses is related to the number of counts in the following way:

$$
\begin{aligned}
n_A^{g\alpha} &= [P(0,1|g\alpha) + P(1,1|g\alpha)]\,N_{g\alpha} \\
&= \left[\eta\ell\epsilon\,e^{-2\eta\ell g^2|\alpha|^2} + \eta\ell\epsilon\left(1 - e^{-2\eta\ell g^2|\alpha|^2}\right)\right]N_{g\alpha} \\
&= \eta\ell\epsilon N_{g\alpha}
\end{aligned} \tag{5.10}
$$

and similarly for the number of pulses that generated the counts at $D_B$:

$$
\begin{aligned}
n_B^{g\alpha} &= [P(1,0|g\alpha) + P(1,1|g\alpha)]\,N_{g\alpha} \\
&= \left[1 - e^{-2\eta\ell g^2|\alpha|^2} - \eta\ell\epsilon + \eta\ell\epsilon\left(1 - e^{-2\eta\ell g^2|\alpha|^2}\right)\right]N_{g\alpha} \\
&= \left[1 - e^{-2\eta\ell g^2|\alpha|^2} - \eta\ell\epsilon e^{-2\eta\ell g^2|\alpha|^2}\right]N_{g\alpha} \\
&= \left[1 - e^{-2\eta\ell g^2|\alpha|^2}\right]N_{g\alpha} - n_A^{g\alpha}e^{-2\eta\ell g^2|\alpha|^2}.
\end{aligned} \tag{5.11}
$$

Therefore the number of pulses that generated the counts at $D_A$ and $D_B$ when the output state is $|g\alpha\rangle$, is given by

$$
N_{g\alpha} = \frac{n_A^{g\alpha}e^{-2\eta\ell g^2|\alpha|^2} + n_B^{g\alpha}}{1 - e^{-2\eta\ell g^2|\alpha|^2}}. \tag{5.12}
$$

We follow the same procedure to find the pulses, $N_0$, that generated the counts at the detectors $D_A$ and $D_B$ when the output state is the vacuum. The probability that detector $D_B$ does not fire and detector $D_A$ does is equal to probability that detector $D_B$ fires and detector $D_A$ does not (Figure 5.3), and it is given by

$$
P(1,0|0) = P(0,1|0) = e^{-\frac{1}{2}\eta\ell g^2|\alpha|^2}\left(1 - e^{-\frac{1}{2}\eta\ell g^2|\alpha|^2}\right). \tag{5.13}
$$

The probability that both detectors fire when the output is the vacuum, is equal to

$$
P(1,1|0) = \left(1 - e^{-\frac{1}{2}\eta\ell g^2|\alpha|^2}\right)^2. \tag{5.14}
$$

$n_A^0$ and $n_B^0$ indicate the number of counts at $D_A$ and $D_B$, respectively, when the output is the vacuum. It follows that

$$n_A^0 = n_B^0 = \left(1 - e^{-\frac{1}{2}\eta \ell g^2 |\alpha|^2}\right) N_0$$

and by solving for $N_0$ and taking the average of both equalities we have that

$$N_0 = \frac{n_A^0 + n_B^0}{2\left(1 - e^{-\frac{1}{2}\eta \ell g^2 |\alpha|^2}\right)}. \tag{5.15}$$

We express the probabilities $P_{g\alpha}$ and $P_0$ of the density operator, (5.5), in terms of the number of pulses, as

$$P_{g\alpha} = \frac{N_{g\alpha}}{N_{g\alpha} + N_0},$$

$$P_0 = \frac{N_0}{N_{g\alpha} + N_0}. \tag{5.16}$$

Therefore the output state operator is equal to

$$\hat{\rho}_{output} = \frac{N_{g\alpha}}{N_{g\alpha} + N_0}|g\alpha\rangle\langle g\alpha| + \frac{N_0}{N_{g\alpha} + N_0}|0\rangle\langle 0|. \tag{5.17}$$

## Success rate

We define the success rate of our amplifier as the probability of success, $P(S)$, multiplied by the frequency of operation of the laser,

$$\text{Success rate} = P(S) \times \text{clock-rate}_{\text{laser}} \tag{5.18}$$

where the clock-rate in our experiment is at $1$ MHz. The probability of success is the joint probability that the state comparison measurement gives no counts and the photon subtraction measurement results in a detection event,

$$P(S) = P(0_{D_0}, 1_{D_1}) = P(0)_{D_0} \; P(1|0)_{D_1}. \tag{5.19}$$

We evaluate the success rate by adding the actual counts collected at detector $D_1$, given that $D_0$ had not fired, when the input state was either $|\alpha\rangle$ or $|-\alpha\rangle$,

$$\text{Success rate} = n_1^\alpha + n_1^{-\alpha}. \tag{5.20}$$

Due to the straightforward relation between the success rate and the probability of success, (5.18), the success rate has the same dependance with the input state magnitude, $|\alpha|$, as the probability of success, $P(S)$: the higher the input state magnitude is, the more probable a successful photon subtraction and thus a higher probability of success (Figure 5.6). The simple way we use to generate our input states, *i.e.* through a laser, is a determining factor to the success rate: a higher pulse repetition frequency of the laser will result in an even higher success rate. We selected a pulse repetition frequency of $1$ MHz to avoid any damage to the detectors due to too high energy at large mean photon numbers. At $1$ MHz we get more than $26000$ successfully amplified states of mean photon per pulse $|\alpha|^2 = 1.0$, (Figure 5.6).
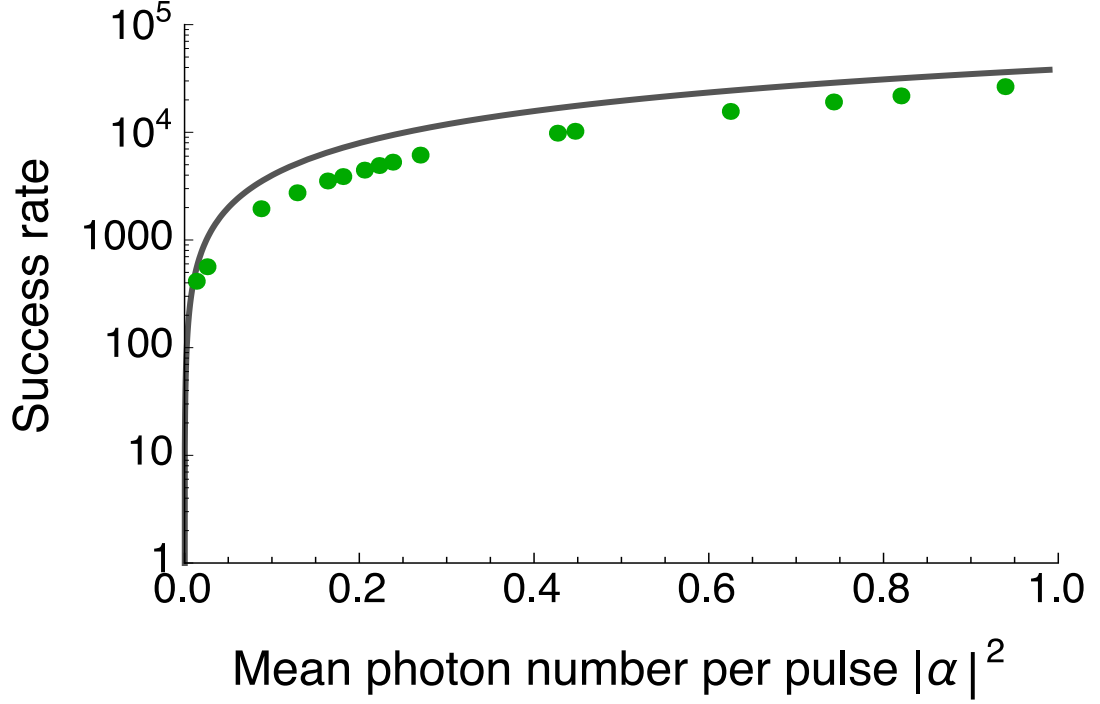
Figure 5.6: The success rate is very high (up to $26544$ s$^{-1}$ at $|\alpha|^2 = 1.0$, by a 1 MHz laser) and it increases with the mean photon number per pulse, $|\alpha|^2$, as photon subtraction becomes more likely. The solid line is the theoretical prediction based on experimental parameters. A higher pulse repetition frequency increases the success rate multiplicatively.

## Fidelity

The quality of the output state is determined by its overlap with the target state, or in other words, the fidelity of the output state with the target state,

$$\text{Fidelity} = \langle g\alpha | \hat{\rho}_{output} | g\alpha \rangle, \tag{5.21}$$

where $|g\alpha\rangle$ is the target state and $\hat{\rho}_{output}$ is the output state given in (5.33). Therefore the fidelity of the output state with the target state is equal to

$$\begin{aligned}
\text{Fidelity} &= \langle g\alpha | \left( \frac{N_{g\alpha}}{N_{g\alpha} + N_0} |g\alpha\rangle\langle g\alpha| + \frac{N_0}{N_{g\alpha} + N_0} |0\rangle\langle 0| \right) |g\alpha\rangle \\
&= \frac{N_{g\alpha}}{N_{g\alpha} + N_0} + \frac{N_0}{N_{g\alpha} + N_0} e^{-g^2|\alpha|^2}.
\end{aligned} \tag{5.22}$$

The state produced by the quantum optical state comparison amplifier has a high fidelity with the target state (Figure 5.7). The fidelity decreases slightly with higher mean photon numbers because of the detectors used: the SPAD detectors operate in Geiger mode, *i.e.* they give a standard output electrical signal that is unrelated to the intensity of the incident optical field.
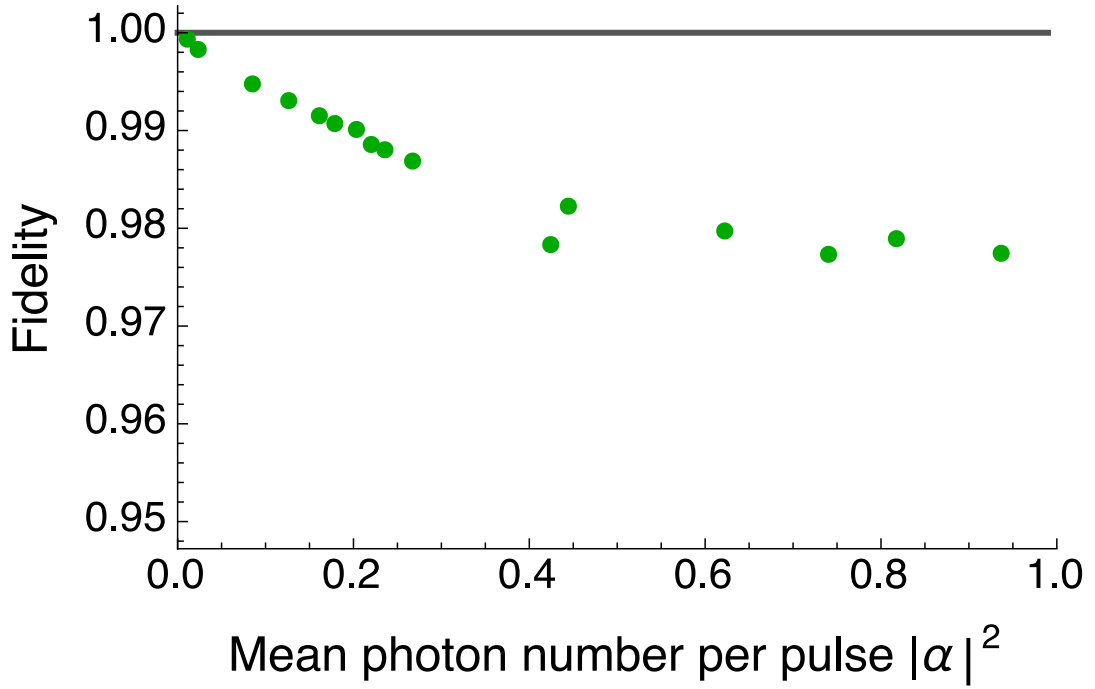
Figure 5.7: The state produced by the quantum optical state comparison amplifier has a very high fidelity with the target state. The average standard error is $\pm 0.0003$. In theory the fidelity is perfect (solid line).

## Target State Fraction

The output of the quantum optical state comparison amplifier is the mixed state

$$\hat{\rho}_{output} = \frac{N_{g\alpha}}{N_{g\alpha} + N_0}|g\alpha\rangle\langle g\alpha| + \frac{N_0}{N_{g\alpha} + N_0}|0\rangle\langle 0|,$$

although in theory for this particular gain, $g^2 = 1.8$, $N_0 = 0$ and the output is the pure target state $|g\alpha\rangle$, given that the amplifier worked, (Chapter 4, Subsection 4.1.1)). However, from the fidelity and visibility calculations we find that this mixed state is very close to the desired target state.

It follows that the output state is mainly the target plus a small fraction of the wrong (*i.e.* vacuum) state. In order to appreciate the proportion of the target state in the mixture, we plot the "target state fraction", where

$$\text{Target state fraction} = \frac{N_{g\alpha}}{N_{g\alpha} + N_0}. \tag{5.23}$$

The target state was produced over $96\%$ of times, (Figure 5.8). This means that conditioning the output state on the successful operation of the device, *i.e.* no counts at the state comparison measurement and a count at the photon subtraction
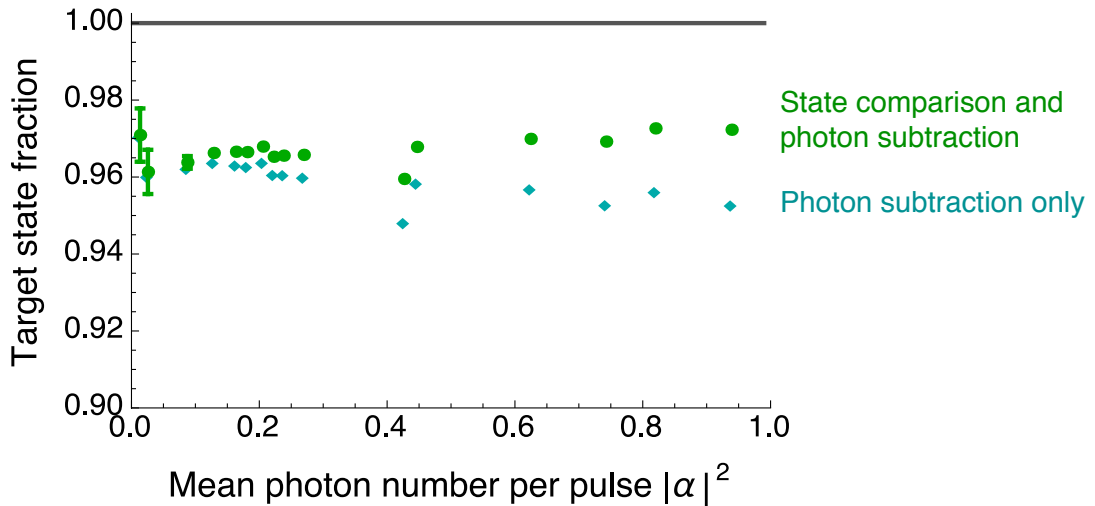
Figure 5.8: The quantum optical state comparison amplifier produced the desired amplified state about $97\%$ of times, when it was conditioned on both the state comparison and photon subtraction measurements; without the conditioning on photon subtraction this percentage would be $50\%$. Post-selecting on the photon subtraction measurement only results in a very high target state fraction also ($\sim 96\%$), however the conditioning on coherent state comparison is important for high mean photon numbers per pulse. The solid lines are theoretical predictions based on experimental parameters.

The standard errors on the first three points are $\pm 0.0069$, $\pm 0.0058$, and $\pm 0.0016$, respectively, and the errors progressively decrease so that the average standard error is $\pm 0.0007$.

measurement, increases the probability to have the desired target state in the output from $50\%$ to almost $100\%$. For small mean photon numbers per pulse we can relax the conditioning on the state comparison measurement, but for higher mean photon numbers the conditioning on the state comparison measurement is necessary in order to detect and discard not amplified states.

## Equivalent input noise

We calculate the equivalent input noise, which determines the amount of noise that must be added to the input signal in order to get the same output noise, if the amplifier were noiseless. It is defined as [Ferreyrol et al., 2010]

$$N_{eq} = \frac{(\Delta \hat{X})^2_{output}}{g^2} - (\Delta \hat{X})^2_{input}, \qquad (5.24)$$

where the $\hat{X}_i$ quadrature is $\hat{X}_i = (\hat{a}^\dagger + \hat{a})/2$, and the variance is $(\Delta \hat{X}_i)^2 = \langle \hat{X}_i^2 \rangle - \langle \hat{X}_i \rangle^2$.

The equivalent input noise is positive for deterministic amplifiers but it can be negative for non-deterministic ones. For example for the input state $|\alpha\rangle$ which has a variance $(\Delta \hat{X})^2_{input} = 1/4$, a perfect amplifier would produce the output state $|g\alpha\rangle$ with the same variance. Therefore the equivalent input noise for an intensity gain of $g^2 = 1.8$ is equal to $N_{eq} = -1/9$.

In our case, we need to define an effective gain,

$$g_{eff} = \frac{\langle \hat{X} \rangle_{output}}{\langle \hat{X} \rangle_{input}}, \tag{5.25}$$

because of the vacuum state in the *output* state, $\hat{\rho}_{output}$,

$$\hat{\rho}_{output} = P_{g\alpha}|g\alpha\rangle\langle g\alpha| + P_0|0\rangle\langle 0|.$$

Therefore the definition for the equivalent input noise, (5.24), becomes

$$N_{eq} = \frac{(\Delta \hat{X})^2_{output}}{g^2_{eff}} - (\Delta \hat{X})^2_{input},$$

$$= \frac{(\Delta \hat{X})^2_{output}\langle \hat{X} \rangle^2_{input}}{\langle \hat{X} \rangle^2_{output}} - (\Delta \hat{X})^2_{input}. \tag{5.26}$$

For our output state we find,

$$\langle \hat{X} \rangle_{output} = \mathrm{Tr}\{\hat{\rho}_{output}\hat{X}_{output}\}$$

$$= \frac{1}{2}\mathrm{Tr}\{(P_{g\alpha}|g\alpha\rangle\langle g\alpha| + P_0|0\rangle\langle 0|)\left(\hat{a}^\dagger + \hat{a}\right)\}$$

$$= \frac{1}{2}P_{g\alpha}\left(g\alpha^* + g\alpha\right) = P_{g\alpha}\,g|\alpha|, \tag{5.27}$$

thus

$$\langle \hat{X} \rangle^2_{output} = P^2_{g\alpha}\,g^2|\alpha|^2, \tag{5.28}$$

and

$$\langle \hat{X}^2 \rangle_{output} = \mathrm{Tr}\{\hat{\rho}_{output}\hat{X}^2_{output}\}$$

$$= \frac{1}{4}\mathrm{Tr}\{(P_{g\alpha}|g\alpha\rangle\langle g\alpha| + P_0|0\rangle\langle 0|)\left(\hat{a}^{\dagger 2}_i + \hat{a}^2_i + 2\hat{a}^\dagger_i\hat{a}_i + 1\right)\}$$

$$= \frac{1}{4}\left[P_{g\alpha}\left(g^2\alpha^{*2} + g^2\alpha^2 + 2g^2|\alpha|^2 + 1\right) + P_0\,(1)\right]$$

$$= \frac{1}{4}\left[P_{g\alpha}\left(4g^2|\alpha|^2 + 1\right) + 1 - P_{g\alpha}\right]$$

$$= P_{g\alpha}\,g^2|\alpha|^2 + \frac{1}{4}. \tag{5.29}$$

Therefore the variance is equal to

$$(\Delta \hat{X})^2_{output} = P_{g\alpha}\,g^2|\alpha|^2 + \frac{1}{4} - P^2_{g\alpha}\,g^2|\alpha|^2$$

$$= P_{g\alpha}\,g^2|\alpha|^2(1 - P_{g\alpha}) + \frac{1}{4}. \tag{5.30}$$
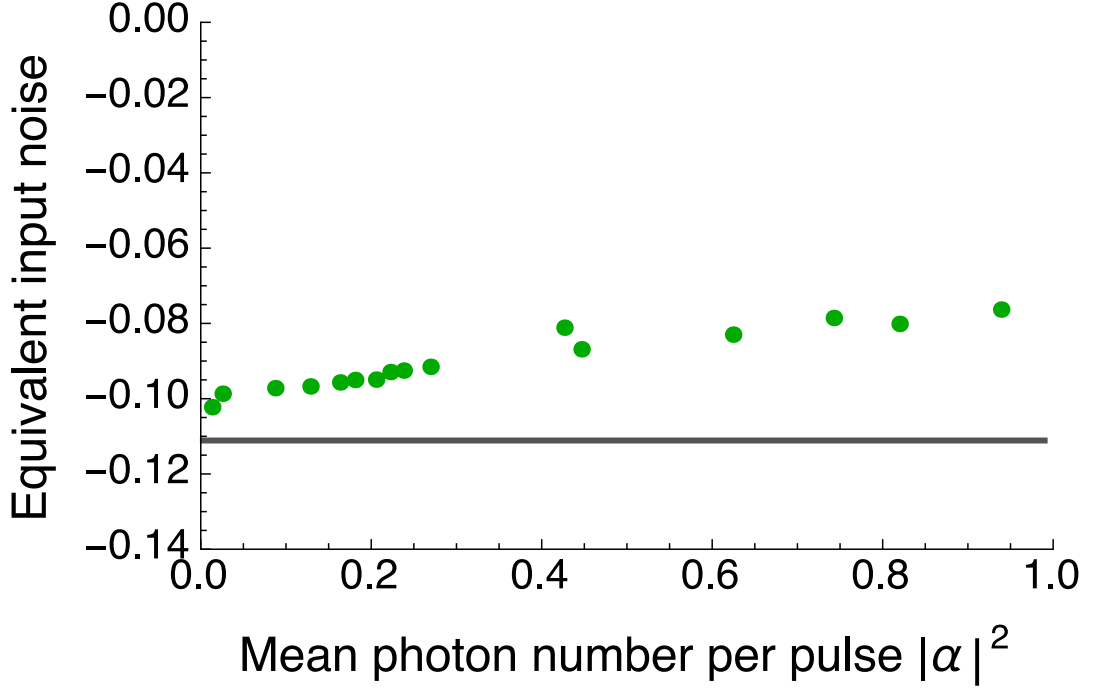
Figure 5.9: The equivalent input noise for the quantum optical state comparison amplifier is negative and compares very well with the ideal value $-1/9$ (solid line) when the intensity gain is $g^2 = 1.8$.

Then the equivalent input noise is equal to

$$N_{eq} = \frac{(\Delta \hat{X})^2_{output} \langle \hat{X} \rangle^2_{input}}{\langle \hat{X} \rangle^2_{output}} - (\Delta \hat{X})^2_{input}$$

$$= \frac{\left(g^2 |\alpha|^2 P_{g\alpha}(1 - P_{g\alpha}) + \frac{1}{4}\right) |\alpha|^2}{P^2_{g\alpha} \, g^2 |\alpha|^2} - \frac{1}{4}$$

$$= \frac{4g^2 |\alpha|^2 P_{g\alpha}(1 - P_{g\alpha}) + 1 - P^2_{g\alpha} g^2}{4 P^2_{g\alpha} \, g^2}. \qquad (5.31)$$

The equivalent input noise increases slightly with the mean photon number per pulse, but remains negative and very close to the ideal value $-1/9$ for all mean photon numbers (Figure 5.9). This means that the quantum optical amplifier does not add any significant noise to the signal.

### 5.2.2 Amplification for a set of 4 coherent states

IN this subsection we show the results for amplifying an input chosen at random from a set of four coherent states (Figure 5.1). Technical limitations restricted the maximum mean photon number per pulse to be around $|\alpha|^2 = 0.6$. We found the loss factor $\ell$ to be $0.19$.

#### Estimation of the output state density operator

For an input state chosen at random from a set of four coherent states, the density operator for the output state has the following form

$$
\begin{aligned}
\hat{\rho}_{output} = {} & P_{g\alpha}|g\alpha\rangle\langle g\alpha| + P_0|0\rangle\langle 0| \\
& + P_{\frac{1}{2}g\alpha(1+i)}\left|\frac{1}{2}g\alpha(1+i)\right\rangle\left\langle\frac{1}{2}g\alpha(1+i)\right| \\
& + P_{\frac{1}{2}g\alpha(1-i)}\left|\frac{1}{2}g\alpha(1-i)\right\rangle\left\langle\frac{1}{2}g\alpha(1-i)\right|,
\end{aligned} \tag{5.32}
$$

where all the probabilities are normalised. The probabilities to have the states $|\frac{1}{2}g\alpha(1\pm i)\rangle$ in the output are equal, $P_{\frac{1}{2}g\alpha(1+i)} = P_{\frac{1}{2}g\alpha(1-i)}$. These probabilities are greater than the probability to have the vacuum state in the output and smaller than the probability to have the target state, $P_0 < P_{\frac{1}{2}g\alpha(1\pm i)} < P_{g\alpha}$.

We calculate these probabilities following a similar procedure to the one we used for an input chosen from a set of two coherent states (Subsection 5.2.1). Appendix 5.A.1 shows explicitly the derivation of the output state density operator, which in terms of the numbers of pulses we find to be equal to

$$
\begin{aligned}
\hat{\rho}_{output} = {} & \frac{N_{g\alpha}}{N_{g\alpha} + N_0 + 2N_{g\alpha(1+\pm i)/2}}|g\alpha\rangle\langle g\alpha| \\
& + \frac{N_0}{N_{g\alpha} + N_0 + 2N_{g\alpha(1+\pm i)/2}}|0\rangle\langle 0| \\
& + \frac{N_{g\alpha(1+\pm i)/2}}{N_{g\alpha} + N_0 + 2N_{g\alpha(1+\pm i)/2}}\left|\frac{1}{2}g\alpha(1+i)\right\rangle\left\langle\frac{1}{2}g\alpha(1+i)\right| \\
& + \frac{N_{g\alpha(1+\pm i)/2}}{N_{g\alpha} + N_0 + 2N_{g\alpha(1+\pm i)/2}}\left|\frac{1}{2}g\alpha(1-i)\right\rangle\left\langle\frac{1}{2}g\alpha(1-i)\right|.
\end{aligned} \tag{5.33}
$$

#### Success rate

We evaluate the success rate by adding the counts registered at detector $D_1$, given that detector $D_0$ did not fire,

$$
\text{Success rate} = n_1^{\alpha} + n_1^{-\alpha} + n_1^{i\alpha} + n_1^{-i\alpha}. \tag{5.34}
$$

We find that the success rate is very high, $14211$ s$^{-1}$ at around $|\alpha|^2 = 0.6$. A higher pulse repetition frequency of the laser would increase this further. The success rate increases with higher mean photon numbers per pulse as the probability for photon subtraction increases.
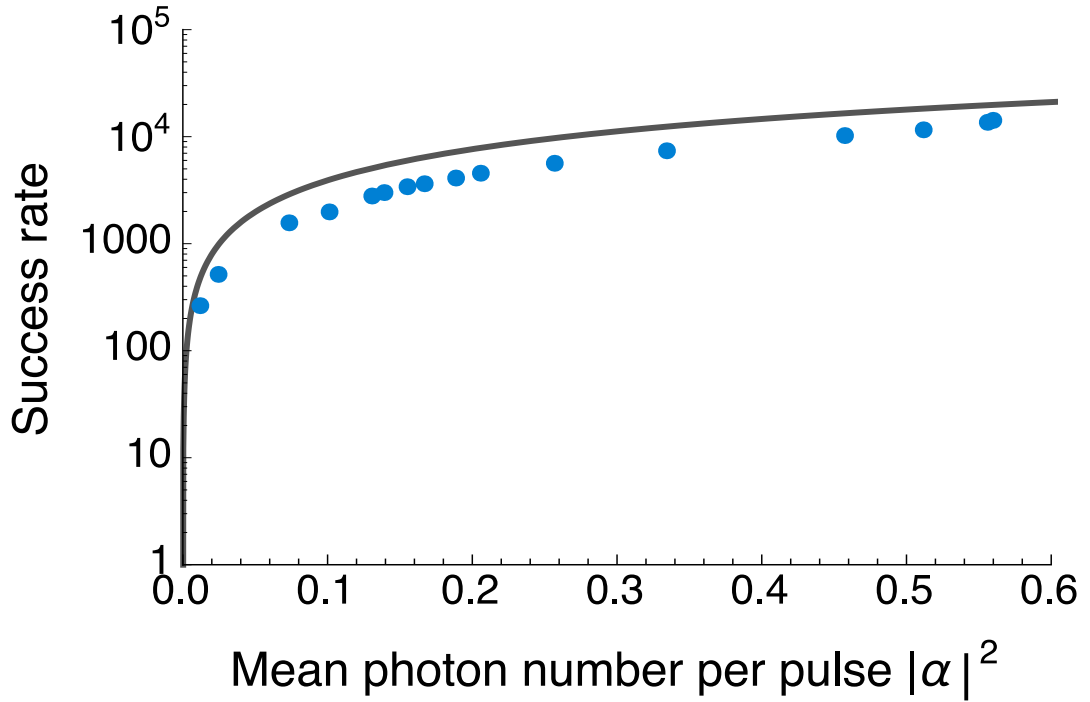
Figure 5.10: The success rate is very high ($14211 \text{ s}^{-1}$ at around $|\alpha|^2 = 0.6$ and 1 MHz pulse repetition frequency) and it increases with the mean photon number per pulse, $|\alpha|^2$, as photon subtraction becomes more likely. The solid line is the theoretical prediction based on experimental parameters.

### Fidelity

The fidelity of the output state with the target state is equal to

$$
\begin{aligned}
\text{Fidelity} = \langle g\alpha | \Bigg( &\frac{N_{g\alpha}}{N_{g\alpha} + N_0 + 2N_{g\alpha(1+\pm i)/2}} |g\alpha\rangle\langle g\alpha| \\
+ &\frac{N_0}{N_{g\alpha} + N_0 + 2N_{g\alpha(1+\pm i)/2}} |0\rangle\langle 0| \\
+ &\frac{N_{g\alpha(1+\pm i)/2}}{N_{g\alpha} + N_0 + 2N_{g\alpha(1+\pm i)/2}} |1/2 g\alpha(1+i)\rangle\langle 1/2 g\alpha(1+i)| \\
+ &\frac{N_{g\alpha(1+\pm i)/2}}{N_{g\alpha} + N_0 + 2N_{g\alpha(1+\pm i)/2}} |1/2 g\alpha(1-i)\rangle\langle 1/2 g\alpha(1-i)| \Bigg) |g\alpha\rangle. \quad (5.35)
\end{aligned}
$$
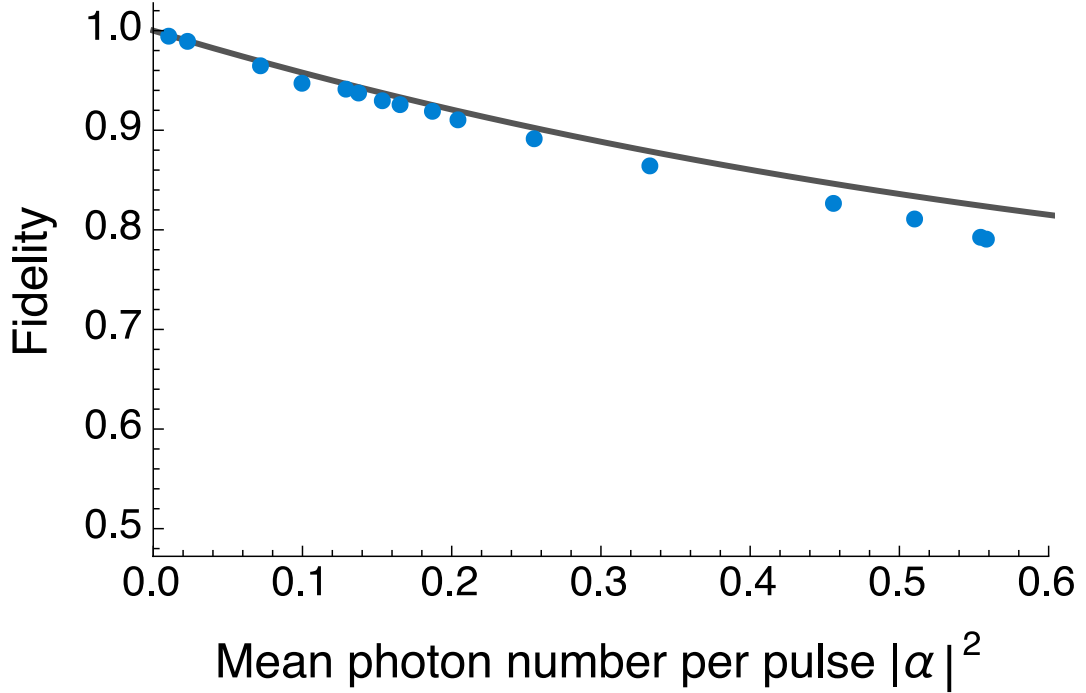
Figure 5.11: The state produced by the quantum optical state comparison amplifier has a high fidelity with the target state. The average standard error is $\pm 0.0022$. The solid line is the theoretical prediction based on experimental parameters.

$$
\begin{aligned}
\text{Fidelity} =\; & \frac{N_{g\alpha}}{N_{g\alpha} + N_0 + 2N_{g\alpha(1+\pm i)/2}} \\
& + \frac{N_0}{N_{g\alpha} + N_0 + 2N_{g\alpha(1+\pm i)/2}} e^{-g^2|\alpha|^2} \\
& + 2\frac{N_{g\alpha(1+\pm i)/2}}{N_{g\alpha} + N_0 + 2N_{g\alpha(1+\pm i)/2}} e^{-\frac{1}{2}g^2|\alpha|^2}.
\end{aligned}
\tag{5.36}
$$

The state produced by the quantum optical state comparison amplifier has a high fidelity with the target state (Figure 5.11). The fidelity drops (to the lowest value $0.8$) with higher mean photon numbers.

## Target State Fraction

The target state fraction is equal to

$$
\text{Target state fraction} = \frac{N_{g\alpha}}{N_{g\alpha} + N_0 + 2N_{g\alpha(1+\pm i)/2}}.
\tag{5.37}
$$

Post selecting on the photon subtraction measurement increases the probability to have the target state in the output from $25\%$ to $48\%$ (Figure 5.12).
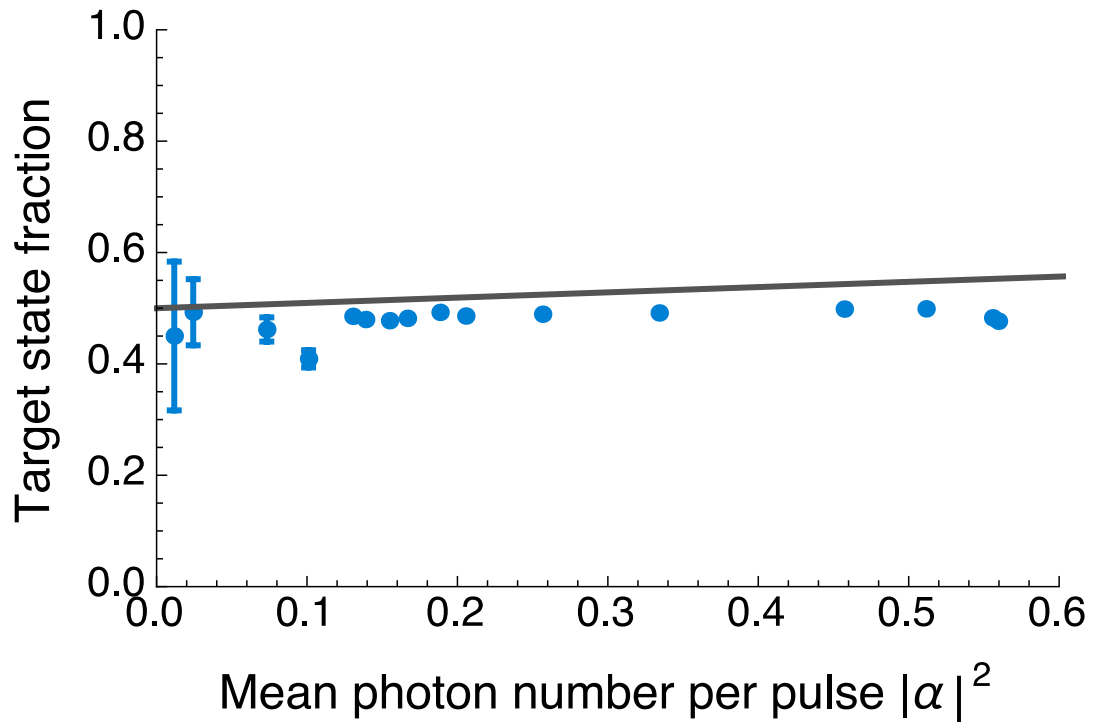
Figure 5.12: The quantum optical state comparison amplifier produced the desired amplified state about $50\%$ of times, which is twice as many times compared to the case where the conditioning on the photon subtraction measurement is not taken into account. The solid line is the theoretical prediction based on experimental parameters.

The standard errors on the first four points are $\pm 0.1336$, $\pm 0.0594$, $\pm 0.0217$ and $\pm 0.0154$, respectively, and the errors progressively decrease so that the average standard error is $\pm 0.0201$.

### 5.2.3 Amplification for a set of 8 coherent states

IN this subsection we show the results for amplifying an input chosen at random from a set of eight coherent states (Figure 5.1). Technical limitations restricted the maximum mean photon number per pulse to be $|\alpha|^2 = 0.21$. The loss factor $\ell$ is equal to $0.07$.

### Estimation of the output state density operator

For an input state chosen at random from a set of eight coherent states, the density operator for the output state has the following form:

$$\hat{\rho}_{output} = P_{g\alpha}|g\alpha\rangle\langle g\alpha| + P_0|0\rangle\langle 0|$$

$$+ P_{\frac{1}{2}g\alpha(1\pm i)}\left|\frac{1}{2}g\alpha(1+i)\right\rangle\left\langle\frac{1}{2}g\alpha(1+i)\right|$$

$$+ P_{\frac{1}{2}g\alpha(1\pm i)}\left|\frac{1}{2}g\alpha(1-i)\right\rangle\left\langle\frac{1}{2}g\alpha(1-i)\right|$$

$$+ P_{\frac{1}{2}g\alpha\left(\frac{\sqrt{2}}{2}(1+i)+1\right)}\left|\frac{1}{2}g\alpha\left(\frac{\sqrt{2}}{2}(1+i)+1\right)\right\rangle\left\langle\frac{1}{2}g\alpha\left(\frac{\sqrt{2}}{2}(1+i)+1\right)\right|$$

$$+ P_{\frac{1}{2}g\alpha\left(\frac{\sqrt{2}}{2}(1-i)+1\right)}\left|\frac{1}{2}g\alpha\left(\frac{\sqrt{2}}{2}(1-i)+1\right)\right\rangle\left\langle\frac{1}{2}g\alpha\left(\frac{\sqrt{2}}{2}(1-i)+1\right)\right|$$

$$+ P_{\frac{1}{2}g\alpha\left(\frac{\sqrt{2}}{2}(-1+i)+1\right)}\left|\frac{1}{2}g\alpha\left(\frac{\sqrt{2}}{2}(-1+i)+1\right)\right\rangle\left\langle\frac{1}{2}g\alpha\left(\frac{\sqrt{2}}{2}(-1+i)+1\right)\right|$$

$$+ P_{\frac{1}{2}g\alpha\left(\frac{\sqrt{2}}{2}(-1-i)+1\right)}\left|\frac{1}{2}g\alpha\left(\frac{\sqrt{2}}{2}(-1-i)+1\right)\right\rangle\left\langle\frac{1}{2}g\alpha\left(\frac{\sqrt{2}}{2}(-1-i)+1\right)\right|,$$

$$(5.38)$$

where the last four states are due to the input states $|\frac{\sqrt{2}}{2}\alpha(1\pm i)\rangle$ and $|\frac{\sqrt{2}}{2}\alpha(-1\pm i)\rangle$. It follows that

$$P_{\frac{1}{2}g\alpha\left(\frac{\sqrt{2}}{2}(1+i)+1\right)} = P_{\frac{1}{2}g\alpha\left(\frac{\sqrt{2}}{2}(1-i)+1\right)},$$

$$P_{\frac{1}{2}g\alpha\left(\frac{\sqrt{2}}{2}(-1+i)+1\right)} = P_{\frac{1}{2}g\alpha\left(\frac{\sqrt{2}}{2}(-1-i)+1\right)},$$

$$(5.39)$$

and

$$P_0 < P_{\frac{1}{2}g\alpha\left(\frac{\sqrt{2}}{2}(-1\pm i)+1\right)} < P_{\frac{1}{2}g\alpha(1\pm i)} < P_{\frac{1}{2}g\alpha\left(\frac{\sqrt{2}}{2}(1\pm i)+1\right)} < P_{g\alpha}. \qquad (5.40)$$

We follow the same procedure as in the previous subsections (see Subsection 5.2.1) to find these probabilities in terms of the numbers of pulses that generated the counts in our detectors:

$$P_{g\alpha} = \frac{1}{P(S)}N_{g\alpha}$$

$$P_0 = \frac{1}{P(S)}N_0$$

$$P_{\frac{1}{2}g\alpha(1\pm i)} = \frac{1}{P(S)}N_{g\alpha(1+\pm i)/2}$$

$$P_{\frac{1}{2}g\alpha\left(\frac{\sqrt{2}}{2}(1\pm i)+1\right)} = \frac{1}{P(S)}N_{\frac{1}{2}g\alpha\left(\frac{\sqrt{2}}{2}(1\pm i)+1\right)}$$

$$P_{\frac{1}{2}g\alpha\left(\frac{\sqrt{2}}{2}(-1\pm i)+1\right)} = \frac{1}{P(S)}N_{\frac{1}{2}g\alpha\left(\frac{\sqrt{2}}{2}(-1\pm i)+1\right)},$$

$$(5.41)$$

where the normalisation is equal to

$$P(S) = N_{g\alpha} + N_0 + 2\left(N_{\frac{1}{2}g\alpha(1+\pm i)} + N_{\frac{1}{2}g\alpha\left(\frac{\sqrt{2}}{2}(1\pm i)+1\right)} + N_{\frac{1}{2}g\alpha\left(\frac{\sqrt{2}}{2}(-1\pm i)+1\right)}\right).$$

$$(5.42)$$

### Success rate
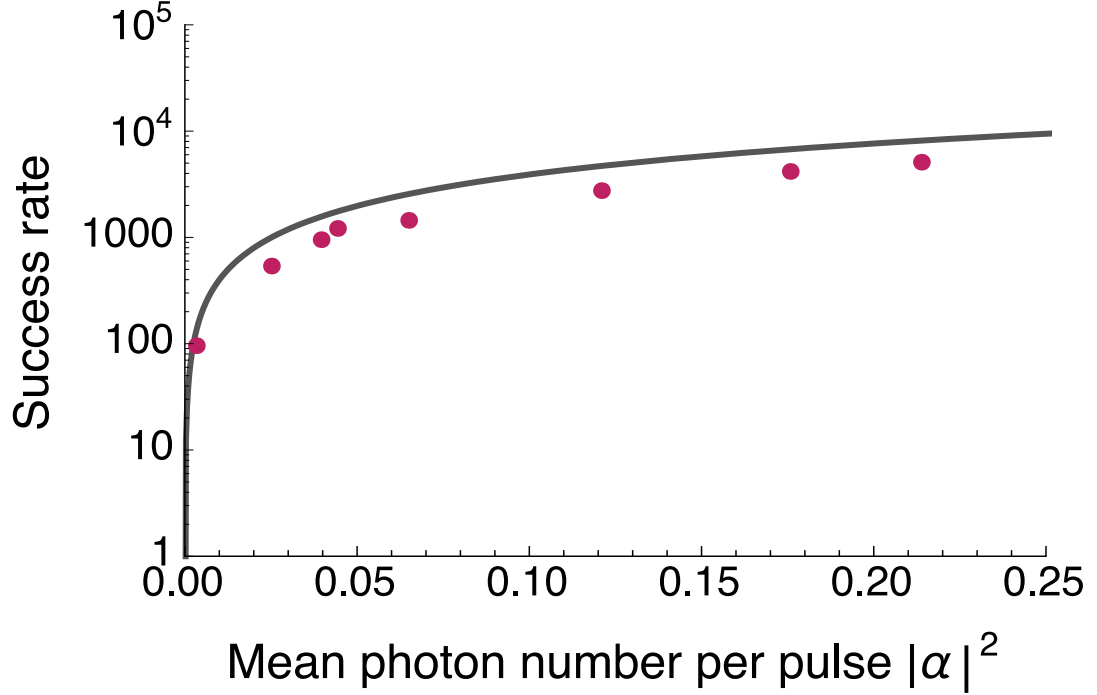


Figure 5.13: The success rate is very high ($5101\ \mathrm{s}^{-1}$ at $|\alpha|^2 = 0.21$ and $1$ MHz pulse repetition frequency) and it increases with the mean photon number per pulse, $|\alpha|^2$, as photon subtraction becomes more likely. The solid line is the theoretical prediction based on experimental parameters.

We evaluate the success rate by adding the counts registered at detector $D_1$, given that detector $D_0$ did not fire,

$$\text{Success rate} = n_1^{\alpha} + n_1^{-\alpha} + n_1^{i\alpha} + n_1^{-i\alpha}$$
$$+ n_1^{\frac{\sqrt{2}}{2}\alpha(1+i)} + n_1^{\frac{\sqrt{2}}{2}\alpha(1-i)} + n_1^{\frac{\sqrt{2}}{2}\alpha(-1+i)} + n_1^{\frac{\sqrt{2}}{2}\alpha(-1-i)}. \qquad (5.43)$$

The success rate has the same trend is in the previous two sets. We find that the state comparison amplifier produces $5101$ amplified states per second of mean photon number $|\alpha|^2 = 0.21$ (Figure 5.13).

## Fidelity

The fidelity of the output state with the target state is given by

$$\text{Fidelity} = \langle g\alpha|\hat{\rho}_{output}|g\alpha\rangle$$

$$
= \langle g\alpha| \left( \frac{N_{g\alpha}}{P(S)}|g\alpha\rangle\langle g\alpha| + \frac{N_0}{P(S)}|0\rangle\langle 0| \right.
$$

$$
+ \frac{N_{g\alpha(1+\pm i)/2}}{P(S)} \left| \frac{1}{2}g\alpha(1+i) \right\rangle \left\langle \frac{1}{2}g\alpha(1+i) \right|
$$

$$
+ \frac{N_{g\alpha(1+\pm i)/2}}{P(S)} \left| \frac{1}{2}g\alpha(1-i) \right\rangle \left\langle \frac{1}{2}g\alpha(1-i) \right|
$$

$$
+ \frac{N_{\frac{1}{2}g\alpha\left(\frac{\sqrt{2}}{2}(1\pm i)+1\right)}}{P(S)} \left| \frac{1}{2}g\alpha\left(\frac{\sqrt{2}}{2}(1+i)+1\right) \right\rangle \left\langle \frac{1}{2}g\alpha\left(\frac{\sqrt{2}}{2}(1+i)+1\right) \right|
$$

$$
+ \frac{N_{\frac{1}{2}g\alpha\left(\frac{\sqrt{2}}{2}(1\pm i)+1\right)}}{P(S)} \left| \frac{1}{2}g\alpha\left(\frac{\sqrt{2}}{2}(1-i)+1\right) \right\rangle \left\langle \frac{1}{2}g\alpha\left(\frac{\sqrt{2}}{2}(1-i)+1\right) \right|
$$

$$
+ \frac{N_{\frac{1}{2}g\alpha\left(\frac{\sqrt{2}}{2}(-1\pm i)+1\right)}}{P(S)} \left| \frac{1}{2}g\alpha\left(\frac{\sqrt{2}}{2}(-1+i)+1\right) \right\rangle \left\langle \frac{1}{2}g\alpha\left(\frac{\sqrt{2}}{2}(-1+i)+1\right) \right|
$$

$$
+ \left. \frac{N_{\frac{1}{2}g\alpha\left(\frac{\sqrt{2}}{2}(-1\pm i)+1\right)}}{P(S)} \left| \frac{1}{2}g\alpha\left(\frac{\sqrt{2}}{2}(-1-i)+1\right) \right\rangle \left\langle \frac{1}{2}g\alpha\left(\frac{\sqrt{2}}{2}(-1-i)+1\right) \right| \right) |g\alpha\rangle,
$$

$$(5.44)$$

$$
\text{Fidelity} = \frac{N_{g\alpha}}{P(S)} + \frac{N_0}{P(S)}e^{-g^2|\alpha|^2} + 2\frac{N_{g\alpha(1+\pm i)/2}}{P(S)}e^{-\frac{1}{2}g^2|\alpha|^2}
$$

$$
+ 2\left( \frac{N_{\frac{1}{2}g\alpha\left(\frac{\sqrt{2}}{2}(1\pm i)+1\right)}}{P(S)}e^{-\frac{1}{4}g^2|\alpha|^2\left(2-\sqrt{2}\right)} + \frac{N_{\frac{1}{2}g\alpha\left(\frac{\sqrt{2}}{2}(-1\pm i)+1\right)}}{P(S)}e^{-\frac{1}{4}g^2|\alpha|^2\left(2+\sqrt{2}\right)} \right)
$$

$$(5.45)$$

The state produced by the quantum optical state comparison amplifier has a high fidelity with the target amplified state (Figure 5.14). The fidelity drops (from $0.99$ to $0.92$) with higher mean photon numbers.

## Target State Fraction

The target state fraction is equal to

$$\text{Target state fraction} = \frac{N_{g\alpha}}{P(S)}, \tag{5.46}$$

where the probability of success, $P(S)$, is given in (5.42). Post-selecting on the photon subtraction measurement increases the probability to have the target state in the output from $12.5\%$ up to $24\%$ (Figure 5.15).
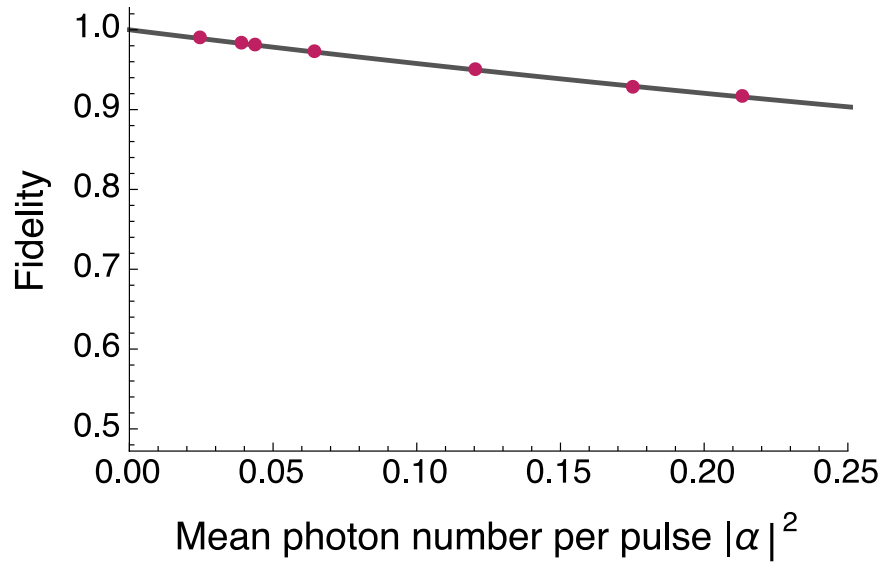
Figure 5.14: The state produced by the quantum optical state comparison amplifier has a high fidelity with the target state. The average standard error is $\pm 0.0013$. The solid line is the theoretical prediction based on experimental parameters.
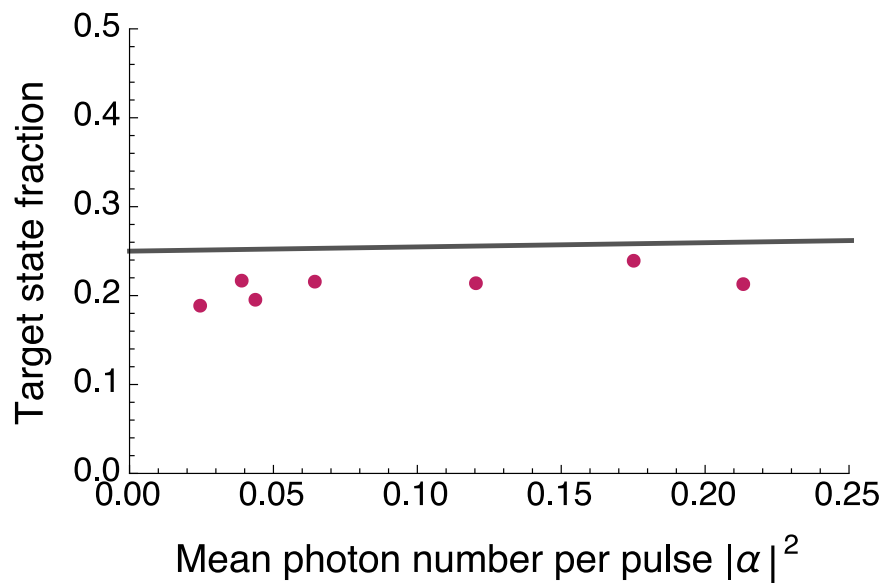


Figure 5.15: The quantum optical state comparison amplifier produced the desired amplified state about $25\%$ of times, which is twice as many times compared to the case where the conditioning on the photon subtraction measurement is not taken into account. The average standard error is $\pm 0.0173$. The solid line is the theoretical prediction based on experimental parameters.

## 5.3  Discussion

### 5.3.1  Comparison with other schemes

Table 5.1: Comparison of the experimental performance of the state comparison amplifier (SCAMP) with other non-deterministic amplifiers.
(For each scheme the top line shows the range (or maximum value) of capabilities, subsequent lines show the performance for specific $|\alpha|^2$ or $g^2$ values.)

| Protocol (source rate) | Gain $g^2$ | $|\alpha|^2$ | Fidelity | | | Success rate $(\mathrm{s}^{-1})$ |
|---|---|---|---|---|---|---|
| | | 0.01 - 1.0 | N=2 | N=4 | N=8 | N=2 (4,8) |
| SCAMP (pulsed diode laser at 1MHz) | 1.8 in this exp. | 0.25 | >0.99 | ~0.9 | ~0.9 | > 6 000 |
| | | 0.30 | 0.985 | 0.86 | - | > 7 000 |
| | | 0.50 | 0.980 | 0.80 | - | > 11 000 |
| | | 0.94 | 0.975 | - | - | > 26 000 |
| Q. Scissors (SPDC 2.5 s⁻¹) | 2 - 4 | <0.1 | <93.6% | | | ~25 |
| | 2.05 | 0.02 | 92.9% | | | - |
| [Xiang et al., 2010] | 3.85 | 0.02 | 93.6% | | | - |
| Photon addition and subtraction (mode-locked laser at 82MHz) | ≤4 ($\downarrow$ with $|\alpha|^2$) | ≤1.4 | ~1 max. | | | ~20 - ~70 ($\uparrow$ with $|\alpha|^2$) |
| | ~2.56 | ≤0.65 | >90% | | | - |
| [Zavatta et al., 2011] | ~2.56 | 1.0 | 70% | | | ~70 |
| Random thermal noise (cw diode laser at 100kHz) | >1 ($\uparrow$ with no. of photons resolved) | 0.4 - 2.1 | <1 ($\uparrow$ with no. of photons resolved) | | | $P(S) = 20\%$ ($\downarrow$ with no. of photons resolved) |
| | | 0.5 | ~0.96 | | | 3.5% |
| [Müller et al., 2012] | | 1.0 | ~0.88 | | | 10% |

### 5.3.2  Summary

In this chapter we described the experimental implementation for the quantum optical state comparison amplifier. We examined the performance of the device for a fixed gain, $g^2 = 1.8$, and varying mean photon number per pulse. The input coherent state was chosen at random from a set of two, four and eight coherent states (Figure 5.1).

We used a laser of pulse repetition frequency $1\,\mathrm{MHz}$ to launch the coherent states. We attenuated them to a maximum mean photon number per pulse of $|\alpha|^2 = 1.0$ to avoid damaging the detectors. Experimental imperfections reduced this number further, to $|\alpha|^2 = 0.6$ for the four state system and $|\alpha|^2 = 0.21$ for the eight state system.

For the two state system the state comparison amplifier has an outstanding experimental performance. The fidelity of the output state with the target state is very high ($> 0.98$), (Figure 5.7). We found that the desired target state was produced about $97\%$ of the times (Figure 5.8). The state comparison amplifier adds very little noise to the signal: we found a negative equivalent input noise which compares very well with the ideal value for a noiseless non-deterministic amplifier (Figure 5.9). The state comparison amplifier produced more than $26000$ amplified states per second for an input of mean photon number of $|\alpha|^2 = 1.0$, a rate which is remarkably high (Figure 5.6).

The behaviour of the state comparison amplifier for the four state and eight state systems is similar to the theoretical performance of the phase symmetric system (Chapter 4, Subsection 4.2.2). The state comparison amplifier produces an output state with high fidelity which decreases slightly with increasing mean photon number per pulse (Figures 5.11, 5.14). As with the two state system, post-selecting the output on the photon subtraction measurement doubles the probability to have the target state in the output, *e.g.* it increases from $25\%$ to almost $50\%$ for the four state system, and from $12.5\%$ to almost $25\%$ for the eight state system. The success rate is also similar to the two state system; the state comparison amplifier produces more than $14000$ amplified states per second for a mean photon number near $|\alpha|^2 = 0.6$ for the four state system and more than $5000$ amplified states at $|\alpha|^2 = 0.2$ for the eight state system (Figures 5.10, 5.13).

Despite the experimental imperfections, the experimental results verify that the quantum optical state comparison amplifier produces an output with very high fidelity with the target state in agreement with the theoretical predictions. The simplicity in the experimental set-up gives the state comparison amplifier a further advantage over other non-deterministic amplifiers. As the state comparison amplifier does not rely on complex quantum resources, it can achieve very high success rates (Table 5.1). Based on these qualities, the state comparison amplifier makes a good candidate for a trusted quantum repeater to increase the transmission distance of signals used in quantum communications systems with known phase alphabets, such as quantum key distribution [Lütkenhaus and Shields, 2009] or quantum digital signatures [Clarke et al., 2012; Collins et al., 2014].

## 5.A  Input chosen from a set of 4 coherent states: derivation of formulae

### 5.A.1  The output state density operator

For an input state chosen at random from a set of four coherent states, the density operator of the output state has the following form

$$\hat{\rho}_{output} = P_{g\alpha}|g\alpha\rangle\langle g\alpha| + P_0|0\rangle\langle 0|$$

$$+ P_{\frac{1}{2}g\alpha(1+i)}\left|\frac{1}{2}g\alpha(1+i)\right\rangle\left\langle\frac{1}{2}g\alpha(1+i)\right|$$

$$+ P_{\frac{1}{2}g\alpha(1-i)}\left|\frac{1}{2}g\alpha(1-i)\right\rangle\left\langle\frac{1}{2}g\alpha(1-i)\right|, \qquad (5.47)$$
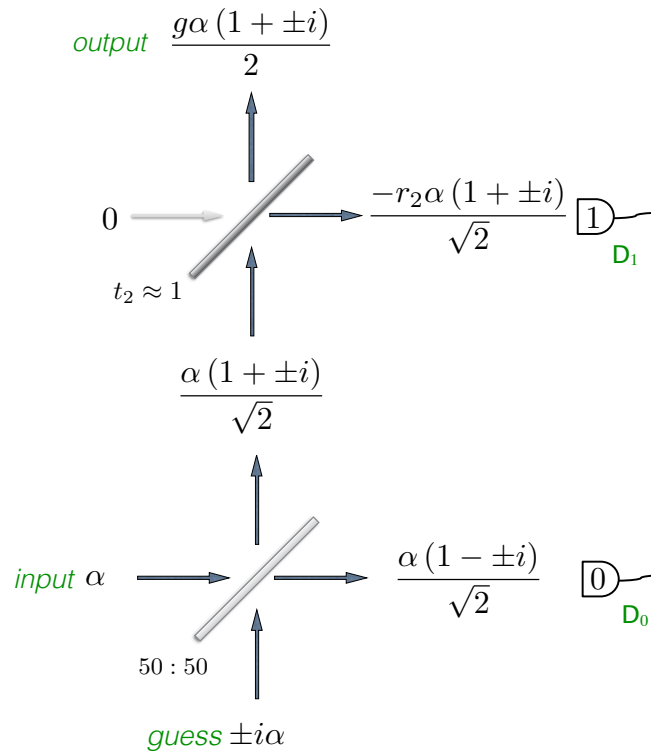


Figure 5.16: Coherent amplitude transformation through the quantum optical state comparison amplifier for the guess state $|\pm i\alpha\rangle$.

The nominal gain is given by $g = t_2/r_1$, where $r_1 = 1/\sqrt{2}$ in this implementation.

where the last two states are due to the input states $|\pm i\alpha\rangle$, (Figure 5.16), and all probabilities are normalised.
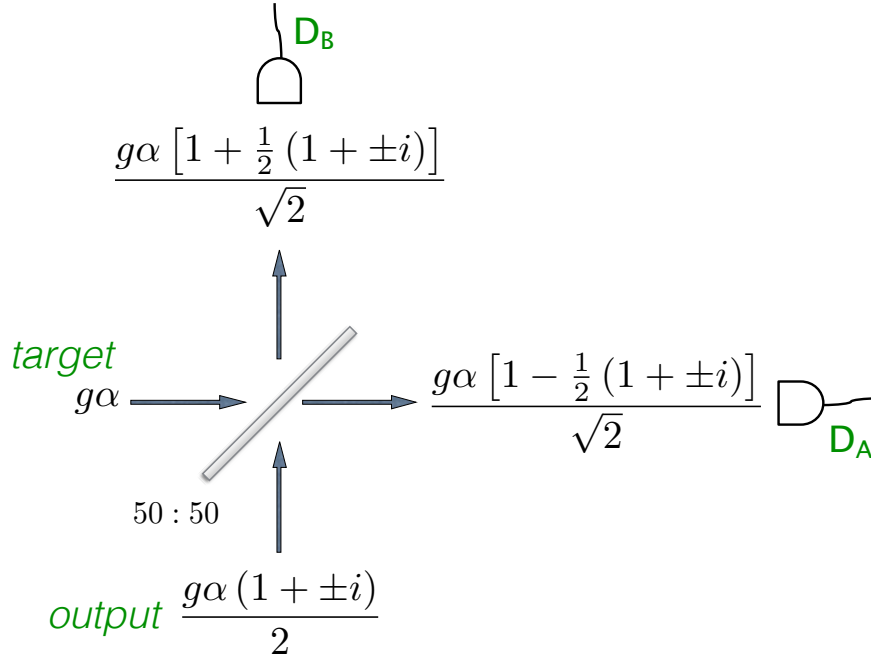
Figure 5.17: The states output states $\left|\frac{1}{2}g\alpha\left(1+\pm i\right)\right\rangle$ are interfered with the target state $|g\alpha\rangle$ for an analysis measurement.

The probability that detector $D_B$ fires and detector $D_A$ does not fire, given that the output of the state comparison amplifier is state $\left|\frac{1}{2}g\alpha\left(1+\pm i\right)\right\rangle$, is given by

$$P\left(1,0|g\alpha\left(1+\pm i\right)/2\right) = \left(1 - e^{-\eta g^2|\alpha|^2\frac{1}{2}|1+\frac{1}{2}(1+\pm i)|^2}\right)e^{-\eta g^2|\alpha|^2\frac{1}{2}|1-\frac{1}{2}(1+\pm i)|^2}$$
$$= \left(1 - e^{-\eta g^2|\alpha|^2\frac{5}{4}}\right)e^{-\eta g^2|\alpha|^2\frac{1}{4}}, \tag{5.48}$$

Similarly, we find that the probability that detector $D_B$ does not fire and detector $D_A$ does, given that the output of the state comparison amplifier is state $\left|\frac{1}{2}g\alpha\left(1+\pm i\right)\right\rangle$, is given by

$$P\left(0,1|g\alpha\left(1+\pm i\right)/2\right) = e^{-\eta g^2|\alpha|^2\frac{1}{2}|1+\frac{1}{2}(1+\pm i)|^2}\left(1 - e^{-\eta g^2|\alpha|^2\frac{1}{2}|1-\frac{1}{2}(1+\pm i)|^2}\right)$$
$$= e^{-\eta g^2|\alpha|^2\frac{5}{4}}\left(1 - e^{-\eta g^2|\alpha|^2\frac{1}{4}}\right). \tag{5.49}$$

The probability that both detectors fire, given that the output state is $\left|\frac{1}{2}g\alpha\left(1+\pm i\right)\right\rangle$, is

$$P\left(1,1|g\alpha\left(1+\pm i\right)/2\right) = \left(1 - e^{-\eta g^2|\alpha|^2\frac{1}{2}|1+\frac{1}{2}(1+\pm i)|^2}\right)\left(1 - e^{-\eta g^2|\alpha|^2\frac{1}{2}|1-\frac{1}{2}(1+\pm i)|^2}\right)$$
$$= \left(1 - e^{-\eta g^2|\alpha|^2\frac{5}{4}}\right)\left(1 - e^{-\eta g^2|\alpha|^2\frac{1}{4}}\right). \tag{5.50}$$

We use the notation $n_A^{g\alpha(1+\pm i)/2}$ and $n_B^{g\alpha(1+\pm i)/2}$ to indicate the counts at $D_A$ and $D_B$, respectively, when the output is $\left|\frac{1}{2}g\alpha\left(1+\pm i\right)\right\rangle$. We want to find the number

of pulses, $N_{g\alpha(1+\pm i)/2}$, that generated these counts. The number of pulses is related to the number of counts in the following way:

$$n_A^{g\alpha(1+\pm i)/2} = [P(0,1|g\alpha(1+\pm i)/2) + P(1,1|g\alpha(1+\pm i)/2)] N_{g\alpha(1+\pm i)/2}$$
$$= \left(1 - e^{-\eta g^2 |\alpha|^2 \frac{1}{4}}\right) N_{g\alpha(1+\pm i)/2} \tag{5.51}$$

and similarly, for the number of pulses that generated the counts at $D_B$,

$$n_B^{g\alpha(1+\pm i)/2} = [P(1,0|g\alpha(1+\pm i)/2) + P(1,1|g\alpha(1+\pm i)/2)] N_{g\alpha(1+\pm i)/2}$$
$$= \left(1 - e^{-\eta g^2 |\alpha|^2 \frac{5}{4}}\right) N_{g\alpha(1+\pm i)/2}. \tag{5.52}$$

Therefore the number of pulses that generated the counts at $D_A$ and $D_B$ when the *output* state was $|\frac{1}{2}g\alpha(1+\pm i)\rangle$, is given by

$$N_{g\alpha(1+\pm i)/2} = \frac{n_A^{g\alpha(1+\pm i)/2}}{1 - e^{-\eta g^2 |\alpha|^2 \frac{1}{4}}} = \frac{n_B^{g\alpha(1+\pm i)/2}}{1 - e^{-\eta g^2 |\alpha|^2 \frac{5}{4}}}. \tag{5.53}$$

Finally, we take weighted averages for $N_{g\alpha(1+\pm i)/2}$, so that

$$N_{g\alpha(1+\pm i)/2} = w_A \frac{n_A^{g\alpha(1+\pm i)/2}}{1 - e^{-\eta g^2 |\alpha|^2 \frac{1}{4}}} + w_B \frac{n_B^{g\alpha(1+\pm i)/2}}{1 - e^{-\eta g^2 |\alpha|^2 \frac{5}{4}}}, \tag{5.54}$$

where

$$w_A = \frac{n_A^{g\alpha(1+\pm i)/2}}{n_A^{g\alpha(1+\pm i)/2} + n_B^{g\alpha(1+\pm i)/2}},$$

$$w_B = \frac{n_B^{g\alpha(1+\pm i)/2}}{n_A^{g\alpha(1+\pm i)/2} + n_B^{g\alpha(1+\pm i)/2}}. \tag{5.55}$$

We express the probabilities in the density operator, (5.47), in terms of the number of pulses, as

$$P_{g\alpha} = \frac{N_{g\alpha}}{N_{g\alpha} + N_0 + 2N_{g\alpha(1+\pm i)/2}},$$

$$P_0 = \frac{N_0}{N_{g\alpha} + N_0 + 2N_{g\alpha(1+\pm i)/2}}$$

$$P_{\frac{1}{2}g\alpha(1+i)} = P_{\frac{1}{2}g\alpha(1-i)} = \frac{N_{g\alpha(1+\pm i)/2}}{N_{g\alpha} + N_0 + 2N_{g\alpha(1+\pm i)/2}} \tag{5.56}$$

Therefore the output state operator is equal to

$$\hat{\rho}_{output} = \frac{N_{g\alpha}}{N_{g\alpha} + N_0 + 2N_{g\alpha(1+\pm i)/2}} |g\alpha\rangle\langle g\alpha|$$
$$+ \frac{N_0}{N_{g\alpha} + N_0 + 2N_{g\alpha(1+\pm i)/2}} |0\rangle\langle 0|$$
$$+ \frac{N_{g\alpha(1+\pm i)/2}}{N_{g\alpha} + N_0 + 2N_{g\alpha(1+\pm i)/2}} \left|\frac{1}{2}g\alpha(1+i)\right\rangle\left\langle\frac{1}{2}g\alpha(1+i)\right|$$
$$+ \frac{N_{g\alpha(1+\pm i)/2}}{N_{g\alpha} + N_0 + 2N_{g\alpha(1+\pm i)/2}} \left|\frac{1}{2}g\alpha(1-i)\right\rangle\left\langle\frac{1}{2}g\alpha(1-i)\right|. \tag{5.57}$$

## 5.A.2   Equivalent input noise

We define the equivalent input noise as

$$N_{eq} = \frac{(\Delta\hat{X})^2_{output}}{g^2_{eff}} - (\Delta\hat{X})^2_{input},$$

$$= \frac{(\Delta\hat{X})^2_{output}\langle\hat{X}\rangle^2_{input}}{\langle\hat{X}\rangle^2_{output}} - (\Delta\hat{X})^2_{input}. \tag{5.58}$$

For our output state we find,

$$
\begin{aligned}
\langle\hat{X}\rangle_{output} &= \mathrm{Tr}\{\hat{\rho}_{output}\hat{X}_{output}\}\\
&= \frac{1}{2}\mathrm{Tr}\Bigg\{\left(\hat{a}^\dagger + \hat{a}\right)\left(P_{g\alpha}|g\alpha\rangle\langle g\alpha| + P_0|0\rangle\langle 0|\right.\\
&\quad + P_{\frac{1}{2}g\alpha(1+i)}\left|\frac{1}{2}g\alpha(1+i)\right\rangle\left\langle\frac{1}{2}g\alpha(1+i)\right|\\
&\quad + P_{\frac{1}{2}g\alpha(1-i)}\left.\left|\frac{1}{2}g\alpha(1-i)\right\rangle\left\langle\frac{1}{2}g\alpha(1-i)\right|\right)\Bigg\}\\
&= \frac{1}{2}P_{g\alpha}\left(g\alpha^* + g\alpha\right)\\
&\quad + \frac{1}{2}P_{\frac{1}{2}g\alpha(1+i)}\left(\frac{1}{2}g\alpha^*(1-i) + \frac{1}{2}g\alpha(1+i)\right)\\
&\quad + \frac{1}{2}P_{\frac{1}{2}g\alpha(1+i)}\left(\frac{1}{2}g\alpha^*(1+i) + \frac{1}{2}g\alpha(1-i)\right)\\
&= P_{g\alpha}\,g|\alpha|\\
&\quad + \frac{1}{2}P_{\frac{1}{2}g\alpha(1+i)}\left(\frac{1}{2}g\alpha^*(1-i+1+i) + \frac{1}{2}g\alpha(1+i+1-i)\right)\\
&= P_{g\alpha}\,g|\alpha| + \frac{1}{2}P_{\frac{1}{2}g\alpha(1+i)}\left(g\alpha^* + g\alpha\right)\\
&= P_{g\alpha}\,g|\alpha| + P_{\frac{1}{2}g\alpha(1+i)}g|\alpha|
\end{aligned}
$$

$$\tag{5.59}$$

where we used the relation $P_{\frac{1}{2}g\alpha(1+i)} = P_{\frac{1}{2}g\alpha(1-i)}$. Therefore

$$\langle\hat{X}\rangle^2_{output} = \left(P_{g\alpha} + P_{\frac{1}{2}g\alpha(1+i)}\right)^2 g^2|\alpha|^2. \tag{5.60}$$

Then

$$\langle \hat{X}^2 \rangle_{output} = \mathrm{Tr}\{\hat{\rho}_{output}\hat{X}^2_{output}\}$$

$$= \frac{1}{4}\mathrm{Tr}\Bigg\{ \left( \hat{a}_i^{\dagger 2} + \hat{a}_i^2 + 2\hat{a}_i^\dagger \hat{a}_i + 1 \right) (P_{g\alpha}|g\alpha\rangle\langle g\alpha| + P_0|0\rangle\langle 0|$$

$$+ P_{\frac{1}{2}g\alpha(1+i)}\left|\frac{1}{2}g\alpha(1+i)\right\rangle\left\langle\frac{1}{2}g\alpha(1+i)\right|$$

$$+ P_{\frac{1}{2}g\alpha(1-i)}\left|\frac{1}{2}g\alpha(1-i)\right\rangle\left\langle\frac{1}{2}g\alpha(1-i)\right| \Bigg) \Bigg\}$$

$$= \frac{1}{4}\Bigg[ P_{g\alpha}\left( g^2\alpha^{*2} + g^2\alpha^2 + 2g^2|\alpha|^2 + 1 \right) + P_0\,(1)$$

$$+ P_{\frac{1}{2}g\alpha(1+i)}\left( \frac{-2i}{4}g^2\alpha^{*2} + \frac{2i}{4}g^2\alpha^2 + g^2|\alpha|^2 + 1 \right)$$

$$+ P_{\frac{1}{2}g\alpha(1+i)}\left( \frac{2i}{4}g^2\alpha^{*2} + \frac{-2i}{4}g^2\alpha^2 + g^2|\alpha|^2 + 1 \right)\Bigg]$$

$$= \frac{1}{4}\Bigg[ P_{g\alpha}\left( 4g^2|\alpha|^2 + 1 \right) + 1 - P_{g\alpha} - 2P_{\frac{1}{2}g\alpha(1+i)} + P_{\frac{1}{2}g\alpha(1+i)}\left( 2g^2|\alpha|^2 + 2 \right)\Bigg]$$

$$= \frac{1}{4}\Bigg[ P_{g\alpha}4g^2|\alpha|^2 + 1 + P_{\frac{1}{2}g\alpha(1+i)}2g^2|\alpha|^2 \Bigg]$$

$$= \left( P_{g\alpha} + \frac{1}{2}P_{\frac{1}{2}g\alpha(1+i)} \right)\, g^2|\alpha|^2 + \frac{1}{4}. \tag{5.61}$$

Therefore the variance is equal to

$$(\Delta\hat{X})^2_{output} = \left( P_{g\alpha} + \frac{1}{2}P_{\frac{1}{2}g\alpha(1+i)} \right)\, g^2|\alpha|^2 + \frac{1}{4} - \left( P_{g\alpha} + P_{\frac{1}{2}g\alpha(1+i)} \right)^2\, g^2|\alpha|^2. \tag{5.62}$$

Then the equivalent input noise is equal to

$$N_{eq} = \frac{(\Delta\hat{X})^2_{output}\langle\hat{X}\rangle^2_{input}}{\langle\hat{X}\rangle^2_{output}} - (\Delta\hat{X})^2_{input}$$

$$= \frac{\left[\left( P_{g\alpha} + \frac{1}{2}P_{\frac{1}{2}g\alpha(1+i)} \right)\, g^2|\alpha|^2 + \frac{1}{4} - \left( P_{g\alpha} + P_{\frac{1}{2}g\alpha(1+i)} \right)^2\, g^2|\alpha|^2\right]|\alpha|^2}{\left( P_{g\alpha} + P_{\frac{1}{2}g\alpha(1+i)} \right)^2\, g^2|\alpha|^2} - \frac{1}{4}$$

$$= \frac{\left( P_{g\alpha} + \frac{1}{2}P_{\frac{1}{2}g\alpha(1+i)} \right)\, |\alpha|^2}{\left( P_{g\alpha} + P_{\frac{1}{2}g\alpha(1+i)} \right)^2} + \frac{1}{4\left( P_{g\alpha} + P_{\frac{1}{2}g\alpha(1+i)} \right)^2 g^2} - |\alpha|^2 - \frac{1}{4}. \tag{5.63}$$

Let $P_{g\alpha} \approx 2 \times P_{\frac{1}{2}g\alpha(1+i)}$,

$$N_{eq} \approx \frac{\left(P_{g\alpha} + \frac{1}{2} \times \frac{1}{2}P_{g\alpha}\right) |\alpha|^2}{\left(P_{g\alpha} + \frac{1}{2}P_{g\alpha}\right)^2} + \frac{1}{4\left(P_{g\alpha} + \frac{1}{2}P_{g\alpha}\right)^2 g^2} - |\alpha|^2 - \frac{1}{4}$$

$$\approx \frac{5|\alpha|^2}{9P_{g\alpha}} + \frac{1}{9P_{g\alpha}^2 \, g^2} - |\alpha|^2 - \frac{1}{4}. \tag{5.64}$$

For $g^2 = 1.8$, the equivalent input noise becomes

$$N_{eq} \approx \frac{5|\alpha|^2}{9P_{g\alpha}} + \frac{5}{81P_{g\alpha}^2} - |\alpha|^2 - \frac{1}{4}, \tag{5.65}$$

and for the probability $P_{g\alpha} \approx 0.5$, it is equal to

$$N_{eq} \approx \frac{10|\alpha|^2}{9} + \frac{20}{81} - |\alpha|^2 - \frac{1}{4}$$

$$\approx \frac{1}{9}|\alpha|^2 - \frac{1}{324}. \tag{5.66}$$

Therefore the equivalent input noise is negative for values $|\alpha|^2$:

$$\frac{1}{9}|\alpha|^2 - \frac{1}{324} < 0$$

$$|\alpha|^2 < \frac{1}{36} \approx 0.03. \tag{5.67}$$

In our experiment the smallest mean input photon number per pulse is $|\alpha|^2 = 0.05$
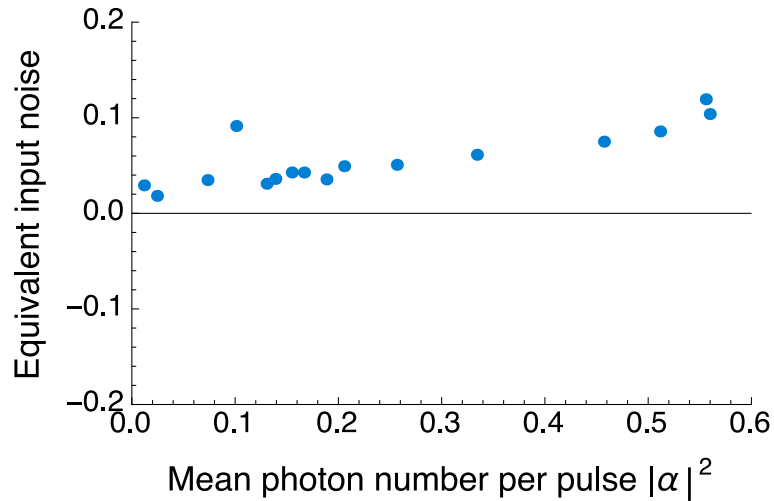


Figure 5.18: The equivalent input noise is positive and very close to zero ($0.06$ on average)

(Figure 5.18).

# PART II

## Information content in optical states

# Gaussian Entropy-Minimising States (GEMS)

T HE ORBITAL ANGULAR MOMENTUM OF LIGHT provides an effectively unlimited basis for encoding information. Beams carrying orbital angular momentum (OAM) have the potential to be used extensively for the transmission of information.

The challenge remains to extract this information with the highest precision possible. Uncertainty relations provide the fundamental limits on measurements of incompatible observables, such as orbital angular momentum and angle. Observables that satisfy the lower bound of an uncertainty relation yield more accurate measurement results.

The intelligent states satisfy the lower bound of the usual Heisenberg uncertainty relation in terms of position and linear momentum, making them the minimum uncertainty states [Aragone et al., 1974]. However, the intelligent states do not satisfy the lower bound of the uncertainty relation for angular position and orbital angular momentum variables, because in this case the lower bound is state dependent. The states that satisfy this bound are the constrained minimum uncertainty product (CMUP) states [Pegg et al., 2005]. However, these states are very complex and they are not practical to produce and handle.

We propose a new form of orbital angular momentum and angular position states, which have a Gaussian distribution in the orbital angular momentum basis and a distribution of overlapping Gaussians in the angle basis. These states are well-defined throughout the whole range of angular uncertainty and they provide a lower uncertainty product than the intelligent states. Furthermore, we study their properties in terms of their entropic uncertainty relation and we compare their values to numerically optimised states. We find that our proposed states have a lower entropic uncertainty than the intelligent states and they are a practical approximation of the minimum uncertainty states.

A peer-reviewed version of this work can be found in the *Journal of Optics* **16**, 105404 [Yao, Brougham, Eleftheriadou, Padgett, and Barnett, 2014].

This chapter is organised as follows,

**Introduction** We start by introducing the orbital angular momentum of light and then we introduce the uncertainty product for angular position and orbital angular momentum. We introduce the states that satisfy the equality in the uncertainty product, the intelligent states, and the states that minimise the uncertainty product, the constrained minimum uncertainty product (CMUP) states.

**Gaussian Entropy-Minimising States (GEMS)** In this section we propose a new form of angular position and orbital angular momentum state. We show that these states provide a lower uncertainty product than the intelligent states and are well-defined throughout the whole angular uncertainty range in contrast to the CMUP states. Furthermore, we introduce the entropic uncertainty relation for angular position and orbital angular momentum states. We find that our proposed states give a lower entropic uncertainty than the intelligent states. Finally, we compare the entropic uncertainty of our states with numerically minimised states and we find that for all practical purposes our states have the minimum entropic uncertainty.

**Conclusion** We summarise the main results and the properties of our proposed states.

## 6.1 Introduction

This section serves as an introduction to the concepts we mentioned at the beginning of the chapter, before we proceed to introduce the Gaussian-Entropy-Minimising-States (GEMS) in the following section.

### 6.1.1 The orbital angular momentum of light

Light as an electromagnetic wave can have different polarisations, such as linear or circular. Associated with the circular polarisation is the spin angular momentum: light has a spin angular momentum equal to $\pm\hbar$ per photon; the sign depending on whether the light is right or left circularly polarised. Linearly polarised light does not have spin angular momentum.

Distinctly different and independent of the spin angular momentum is the orbital angular momentum (OAM) of light. Light beams can have helical phase fronts and associated with the rotation of the phase fronts is the orbital angular momentum of light: light carries an OAM equal to $m\hbar$ per photon, where $m$ is an integer; the phase fronts rotate clockwise or anti-clockwise depending on the sign of $m$ (Figure 6.1). Plane waves (m=0) do not have orbital angular momentum.

Allen et al. [1992] realised that any beam with an azimuthal phase dependence, of the form $u(r,\varphi,z) = u_0(r,z)e^{im\varphi}$, carries orbital angular momentum. In particular, such a beam is best described by Laguerre-Gaussian ($LG_{pm}$) modes where $p$ is the number of concentric dark rings (in addition to the central singularity when $m \neq 0$) (Figure 6.2). Furthermore, any arbitrary beam can be described by a linear
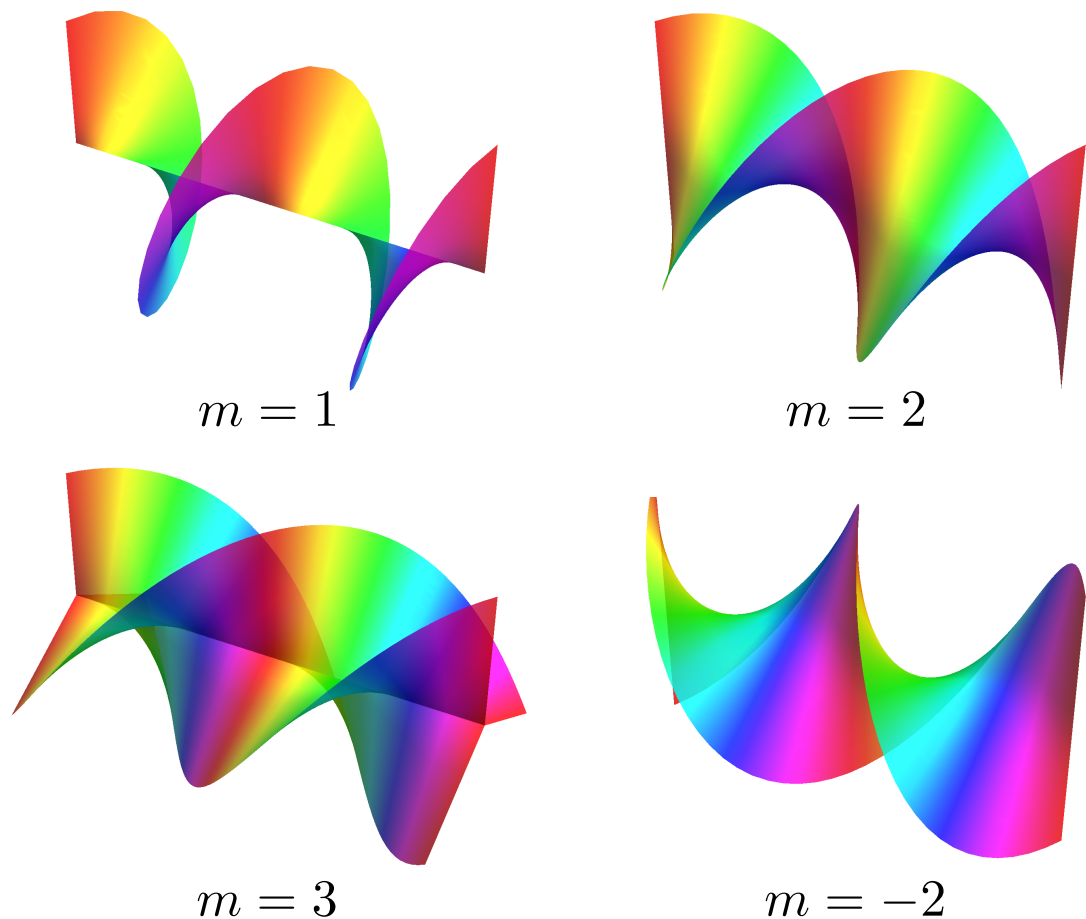
Figure 6.1: Helically phased beams have an orbital angular momentum (OAM) of $\pm m\hbar$ per photon. Positive $m$ corresponds to clockwise rotating phase fronts, while negative $m$ corresponds to anti-clockwise rotation.

superposition of Laguerre-Gaussian modes or a combination of Hermite-Gaussian modes [Beijersbergen et al., 1993; Tamm and Weiss, 1990].

Helical beams can be generated in a number of ways [Allen et al., 2003; Yao and Padgett, 2011]: either they are produced directly inside the laser [Harris et al., 1994] or mode converters transform Hermite-Gaussian modes into Laguerre-Gaussian modes. Allen et al. [1992] used mode converters formed from cylindrical lenses [Beijersbergen et al., 1993]. They work by first decomposing a Hermite-Gaussian mode into a set of Hermite-Gaussian modes, which when rephased and recombined they give a particular Laguerre-Gaussian mode. The advantage of this technique is that it converts higher order Hermite-Gaussian modes into pure Laguerre-Gaussian modes with high efficiency.

Another type of mode converter is the spiral phase plate [Beijersbergen et al., 1994; Turnbull et al., 1996]. This is an optical element with one planar surface whose thickness progressively increases with the angle around the centre, also known

$$LG_{01} \qquad LG_{11} \qquad LG_{0-4} + LG_{04} \quad LG_{10} + LG_{06}$$
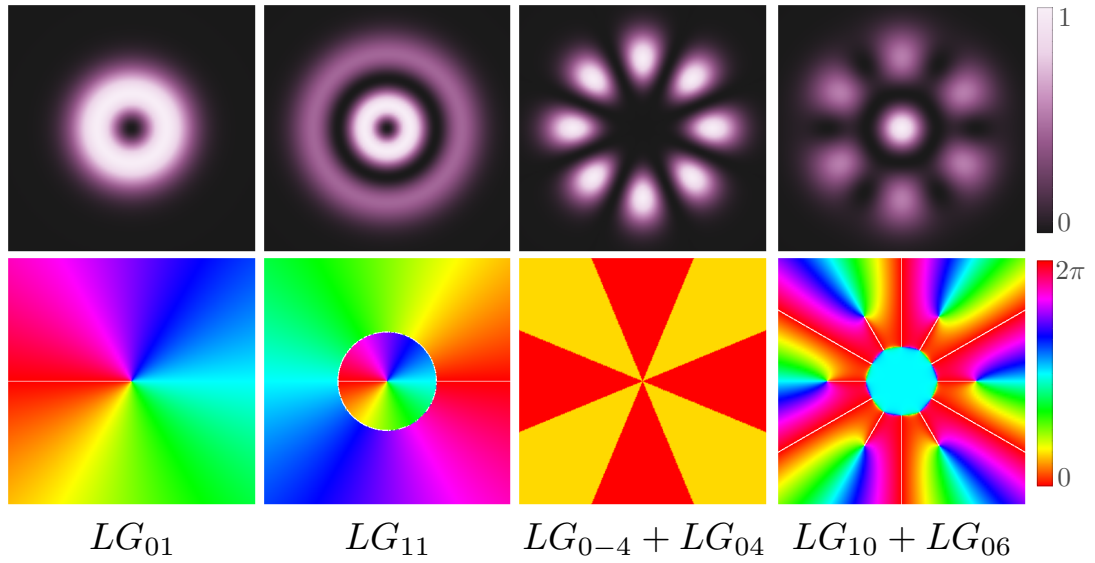
Figure 6.2: Laguerre-Gaussian ($LG_{pm}$) modes, and a linear superposition thereof, carry orbital angular momentum. The top row shows the normalised intensity profiles and the bottom row the phase profiles. $p$ corresponds to the number of concentric rings (in addition to the central singularity if it exists).

as the azimuthal angle, so that the other surface of the element is helical. The Hermite-Gaussian mode that is incident on the planar surface of the phase plate covers different path lengths inside the medium. Consequently, as it exits the spiral phase plate, the phase profile of the resulting wavefront varies with the azimuthal angle. The phase dislocation leads to destructive interference along the beam axis, and thus the helical wavefront has a phase singularity in the centre. The step height of the spiral phase plate must be an integer number of wavelengths for this to happen, so these devices must be designed with very high precision.

However, helical beams are generated with more flexibility when using diffractive optical elements, such as computer generated holograms [Bazhenov et al., 1990; Heckenberg et al., 1992]. These holograms are usually forked diffraction gratings which are constructed by adding the phase profile of the helical beam to be generated and a linear phase ramp. The widespread availability of spatial light modulators (SLMs), which can be easily programmed to act as holograms, makes this method for generating helical beams very practical.

More interesting, though, is the generation of helical beams by spontaneous parametric down conversion (SPDC) [Mair et al., 2001; Leach et al., 2010]. Down converted photon pairs are entangled in orbital angular momentum and angular position. As orbital angular momentum spans a high-dimensional state space, a greater amount of information can be encoded on each photon compared to encoding information on the two-dimensional state space of its polarisation. This opens up the possibility to use OAM carrying beams in quantum information protocols [Vaziri et al., 2002; Molina-Terriza et al., 2004].

### 6.1.2 Angular uncertainty relation

Orbital angular momentum and angular position are conjugate variables and so there is an uncertainty principle associated with the precision with which they can be measured simultaneously. For linear position, $x$, and linear momentum, $p$, which are continuous and unbounded conjugate variables, the uncertainty relation is given by [Heisenberg]

$$\Delta x \Delta p \geq \hbar/2. \tag{6.1}$$

On the other hand, the angular position is periodic and bounded and the orbital angular momentum is discrete. When we have an orbital angular momentum eigenstate, $\Delta m = 0$, the angular position is completely undefined: it can take any value between $0$ and $2\pi$ with equal probability. In this case, the variance in angular position takes its maximum value

$$
\begin{aligned}
(\Delta \varphi)^2 &= \int_{-\pi}^{\pi} \mathrm{d}\varphi \; \varphi^2 P(\varphi) \\
&= \frac{1}{2\pi} \left[ \frac{\varphi^3}{3} \right]_{-\pi}^{\pi} = \frac{\pi^2}{3},
\end{aligned}
\tag{6.2}
$$

and so the uncertainty is $\Delta\varphi = \pi/\sqrt{3}$. An uncertainty relation of the form of (6.1) fails for small $\Delta m$, as it must be equal to zero, $\Delta m \Delta \varphi = 0$. Therefore, we require a different form of the uncertainty relation for orbital angular momentum and angular position variables.

The uncertainty relation for angular position (or angle), $\varphi$, and orbital angular momentum, $m$, is given by [Robertson, 1934; Barnett and Pegg, 1990],

$$\Delta m \Delta \varphi \geq \frac{1}{2} \left| 1 - 2\pi P(\theta) \right|, \tag{6.3}$$

where $P(\theta) = |\psi(\theta)|^2$ is the probability density at the boundary of the chosen $2\pi$ angular range. In contrast to the uncertainty relation for linear position and linear momentum, (6.1), which has a constant lower bound, the lower bound of (6.3) is state dependent. Consequently, the states that minimise the uncertainty product in linear position and linear momentum, (6.1), do not necessarily minimise the uncertainty product in angular position and orbital angular momentum, (6.3). On the other hand, the contained minimum uncertainty product (CMUP) states have been shown to minimise the uncertainty product, (6.3), but they are not easy to produce and handle. We briefly describe these states in the following subsections before we introduce a new form of states that circumvents these problems.

### 6.1.3 Intelligent states

The intelligent states are the states that satisfy the equality in an uncertainty relation [Aragone et al., 1974],

$$\Delta x \Delta p = \hbar/2, \tag{6.4}$$

$$\Delta m \Delta \varphi = \frac{1}{2} \left| 1 - 2\pi P(\theta) \right|. \tag{6.5}$$

For linear position, $x$, and linear momentum, $p$, they are also the minimum uncertainty states and have Gaussian probability distributions. However, they are not the minimum uncertainty states for angular position and orbital angular momentum because of the state dependent lower bound of the uncertainty principle, $P(\theta)$.

For angular position and momentum, the intelligent states are given by the angle wavefunction

$$\psi(\varphi)_{\text{Int}} = (\lambda/\pi)^{1/4} \left[ \text{erf}\left(\pi/\sqrt{\lambda}\right) \right]^{-1/2} \exp\left(-\frac{\lambda\varphi^2}{2}\right), \qquad (6.6)$$

[Franke-Arnold et al., 2004], where $\text{erf}$ is the error function, $\text{erf}(x) = (2/\sqrt{\pi}) \int_0^x e^{-t^2} dt$ [Gradshteyn and Ryzhik, 2007]. Intelligent states have the form of a truncated Gaussian distribution in this representation, (6.6), (Figure 6.3). Usually we choose the probability distribution $P(\theta)$ that gives the smallest variance, *i.e.* the angular range is $-\pi \leq \varphi < \pi$, and so the Gaussian is centred at $\varphi = 0$ and it has a discontinuity at $\pm\pi$.
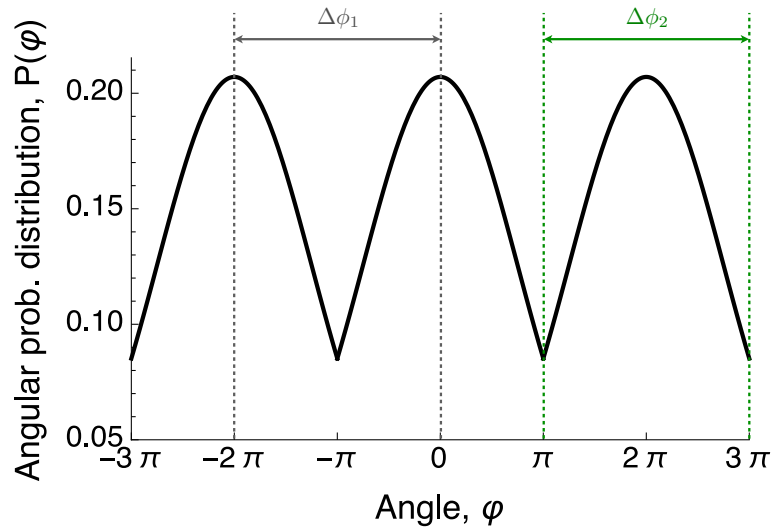


Figure 6.3: The angular probability distribution for the intelligent states is a Gaussian distribution centred at $\varphi = 0$ and truncated at $\pm\pi$. We choose the range $-\pi \leq \varphi < \pi$ to minimise the angular variance, $(\Delta\phi_2)^2 < (\Delta\phi_1)^2$.

It follows that the variances in angular position and orbital angular momentum are [Franke-Arnold et al., 2004]

$$(\Delta\varphi)^2 = \int_{-\pi}^{\pi} d\varphi \, \varphi^2 \, |\psi_{\text{Int}}|^2 = \frac{1}{2\lambda} - \sqrt{\frac{\pi}{\lambda}} \frac{e^{-\lambda\pi^2}}{\text{erf}\left(\pi\sqrt{\lambda}\right)}$$

$$(\Delta m)^2 = \sum_{m'=-\infty}^{\infty} m^2 |c_m|^2 = \lambda^2 \left(\Delta\varphi\right)^2, \qquad (6.7)$$
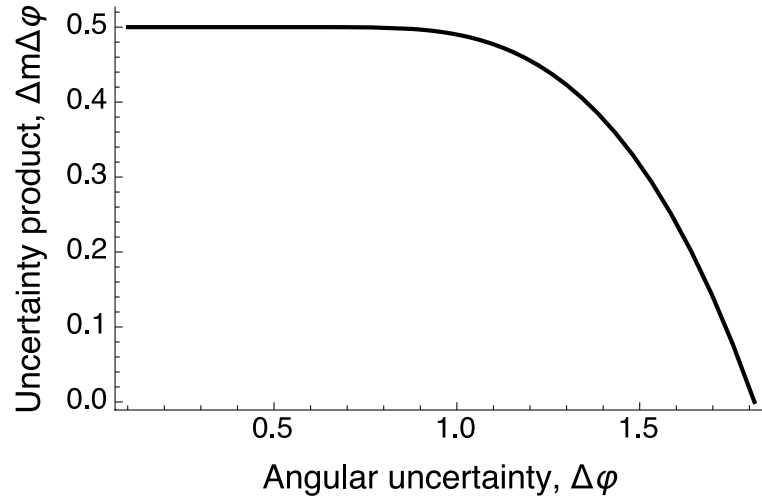
Figure 6.4: The uncertainty product for the intelligent state, $\Delta\varphi\Delta m$, varies between $0.5$ for very small angular uncertainty, $\Delta\varphi$, to zero at the maximum angular uncertainty, $\Delta\varphi = \pi/\sqrt{3} \approx 1.81$, in which case we have an OAM eigenstate.

from which we can find the uncertainty product $\Delta\varphi\Delta m$, (6.5).

As it is expected, the uncertainty product, (6.5), is zero when the uncertainty in the angle is maximum, at $\Delta\varphi = \pi/\sqrt{3} \approx 1.81$, because of $P(\theta) = 1/(2\pi)$ (Figure 6.4). On the other hand, for small uncertainty in the angle $\Delta\phi$, the probability $P(\theta) \to 0$ and the uncertainty product tends to $1/2$.

### 6.1.4 Constrained minimum uncertainty product (CMUP) states

The states which minimise the uncertainty relation for a given $\Delta m$ or $\Delta\phi$ are the constrained minimum uncertainty product (CMUP) states. The exact solution of their eigenvalue equation found in Pegg et al. [2005] is expressed in terms of a confluent hypergeometric function. The first order perturbation solution is

$$\psi(\varphi)_{\text{CMUP}} = \frac{1}{\sqrt{2\pi}} \left[ 1 + \frac{\lambda}{6} \left( \frac{\varphi^4}{2} - \pi^2\varphi^2 + \frac{7\pi^4}{30} \right) \right], \tag{6.8}$$

where $\lambda$ is a Langrange multiplier related to the angular width of the states [Pegg et al., 2005]. It follows that the uncertainty in the angle, $\Delta\varphi$, to the first order in $\lambda$, is

$$\Delta\varphi = \frac{\pi}{\sqrt{3}} \left( 1 - \frac{8\pi^4}{315}\lambda \right) \tag{6.9}$$

and the uncertainty relation is

$$\Delta m \Delta\varphi = \frac{\lambda\pi^4}{\sqrt{3}} \sqrt{\frac{8}{945}} \left( 1 - \frac{8\pi^4}{315}\lambda \right). \tag{6.10}$$
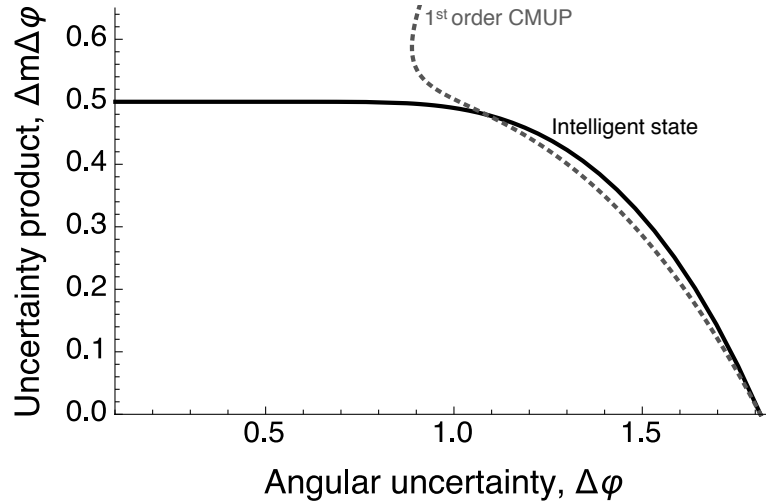
Figure 6.5: The uncertainty product for the first order CMUP state, $\Delta\varphi\Delta m$, is smaller than the uncertainty product for the intelligent states for a big range of angular uncertainty, $\Delta\varphi$. The CMUP state blows up for small $\Delta\varphi$.

The uncertainty relation for the first order solution of the CMUP states, (6.10), is smaller than the uncertainty relation for the intelligent states, for the angular range $1 < \Delta\varphi < \pi/\sqrt{3}$ (Figure 6.5). However, the first (and second) order solution blows up for small $\Delta\varphi$ [Pegg et al., 2005].

## 6.2   Gaussian Entropy-Minimising States (GEMS)

In this section we propose a new form of orbital angular momentum and angle states. We compare their uncertainty product, $\Delta m\Delta\varphi$, to the one for the intelligent states and the first order solution of the CMUP states. Furthermore, we examine their entropic uncertainty relation and we compare it numerically with the entropic uncertainty of the intelligent states. Finally, we compare our states with states obtained by a minimisation algorithm to determine whether our proposed states are indeed the minimum states.

### 6.2.1   Definition

We propose the orbital angular momentum state with a Gaussian distribution in the angular momentum basis,

$$|\psi\rangle = \sum_{m=-\infty}^{\infty} c_m |m\rangle = \sum_{m=-\infty}^{\infty} \sqrt{N(a)} e^{-am^2} |m\rangle, \tag{6.11}$$

where $a$ is real and positive. We require this state to be normalised, therefore

$$\sum_{m'=-\infty}^{\infty} |c_m|^2 = \sum_{m'=-\infty}^{\infty} \left| \sqrt{N(a)} e^{-am^2} \right|^2 = 1,$$

(6.12)

$$\Rightarrow N(a) = \left( \sum_{m'=-\infty}^{\infty} e^{-2am^2} \right)^{-1}$$
$$= \left[ \vartheta_3 \left( 0, e^{-2a} \right) \right]^{-1},$$

(6.13)

where $\vartheta_3 (u,q) = \sum_{n=-\infty}^{\infty} q^{n^2} e^{2inu}$ is an elliptic theta function of the third kind [Cover and Thomas, 2012]. Put differently, we can write the orbital angular momentum wavefuction as

$$\psi(m) = \langle m | \psi \rangle = \sum_{m=-\infty}^{\infty} \sqrt{N(a)} e^{-am^2}$$
$$= \frac{1}{\sqrt{\vartheta_3 \left( 0, e^{-2a} \right)}} \sum_{m=-\infty}^{\infty} e^{-am^2}.$$

(6.14)

The orbital angular momentum and angle are related by a discrete Fourier transform. It follows that the angle waverfunction is given by

$$\psi(\varphi) = \langle \varphi | \psi \rangle = \frac{1}{\sqrt{2\pi}} \sum_{m=-\infty}^{\infty} c_m \, e^{im\varphi}$$
$$= \frac{1}{\sqrt{2\pi \vartheta_3 \left( 0, e^{-2a} \right)}} \sum_{m=-\infty}^{\infty} e^{-am^2} e^{im\varphi}$$
$$= \frac{\vartheta_3 \left( \frac{\varphi}{2}, e^{-a} \right)}{\sqrt{2\pi \vartheta_3 \left( 0, e^{-2a} \right)}}.$$

(6.15)

It is not intuitive to extract a physical meaning from the state in this form, (6.15). By applying the Poisson sum-rule [Cover and Thomas, 2012] we can express the state as

$$\psi(\varphi) = \frac{1}{\sqrt{2a \vartheta_3 \left( 0, e^{-2a} \right)}} \sum_{n=-\infty}^{\infty} \exp \left\{ -\frac{1}{4a} (\varphi - 2n\pi)^2 \right\},$$

(6.16)

which is a distribution of equal overlapping Gaussians (Figure 6.6).

The width of the Gaussians is determined by the parameter $a$ (Figure 6.7). In particular, the full width at half maximum (FWHM) is equal to $4\sqrt{\ln(2)a}$ (see Appendix 6.A). As $a$ increases, the Gaussian distribution becomes broader in the angle representation. Consequently the angular uncertainty, $\Delta\varphi$, increases and so the uncertainty in orbital angular momentum, $\Delta m$, decreases. In fact, when the angular uncertainty reaches its maximum value $\Delta\varphi = \pi/\sqrt{3}$, we have an orbital angular
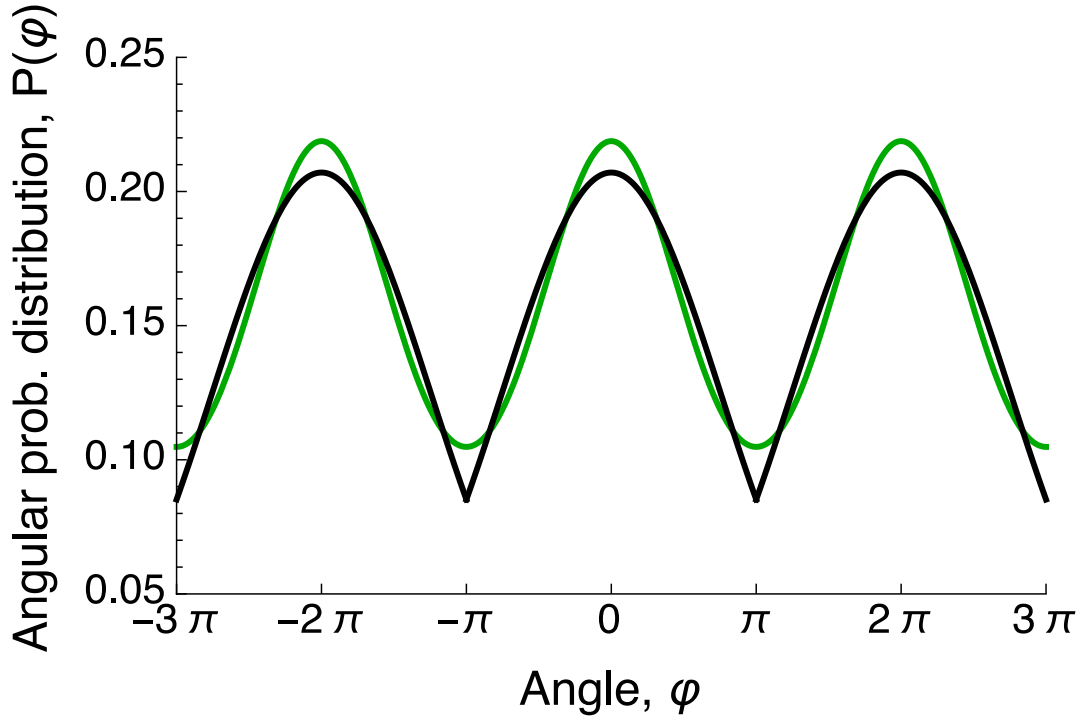
Figure 6.6: The angular probability distribution for the overlapping Gaussian states is similar to the angular probability distribution for the intelligent states, without a discontinuous derivative at $\pm\pi$. This plot is for an angular variance $\Delta\phi = 1.61$.

momentum eigenstate with $\Delta m = 0$. This means that the distribution in orbital angular momentum changes from an almost flat and continuous distribution, for very small $a$, to a sharply peaked distribution (an OAM eigenstate) as $a$ increases.

Therefore we expect the uncertainty product, (6.3), for our states to vary between $1/2$ and $0$ as the angular uncertainty, $\Delta\varphi$, increases.

## 6.2.2 Uncertainty product, $\Delta m \Delta \varphi$

In order to find the uncertainty product, $\Delta m \Delta \varphi$, we need to calculate the variances in angular position and orbital angular momentum,

$$(\Delta\varphi)^2 = \int_{-\pi}^{\pi} \mathrm{d}\varphi \, \varphi^2 P(\varphi) \tag{6.17}$$

$$(\Delta m)^2 = \sum_{m=-\infty}^{\infty} m^2 P(m), \tag{6.18}$$

where $P(\varphi) = \left|\psi(\varphi)\right|^2$ and $P(m) = |c_m|^2$.

For our overlapping Gaussian states the variance in the angular position is given
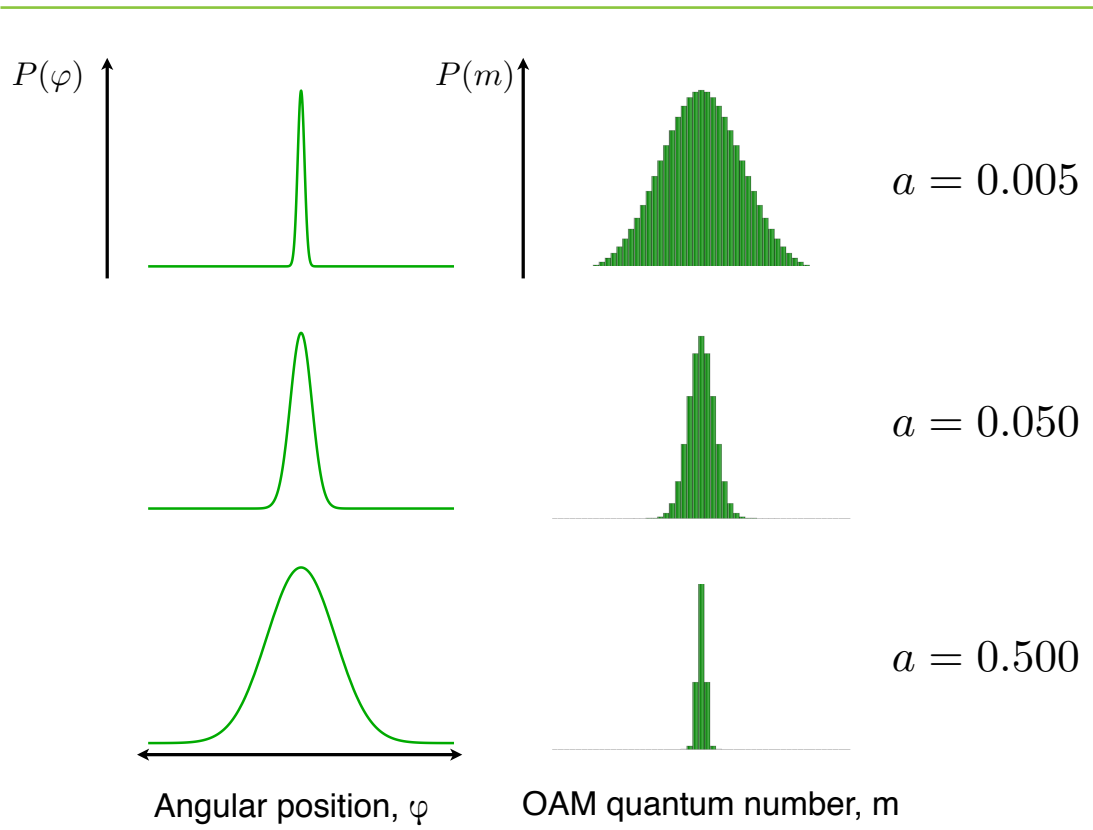
Figure 6.7: As $a$ increases, the Gaussians become broader in the angle representation. On the other hand, the distribution in orbital angular momentum becomes more peaked with increasing $a$.

by

$$(\Delta\varphi)^2 = \frac{1}{2\pi\vartheta_3\left(0, e^{-2a}\right)} \int_{-\pi}^{\pi} \mathrm{d}\varphi\, \varphi^2 \sum_{m=-\infty}^{\infty} e^{-am^2} e^{im\varphi} \sum_{m'=-\infty}^{\infty} e^{-am'^2} e^{-im'\varphi}, \quad (6.19)$$

which we calculate (see Appendix 6.B) to be

$$(\Delta\varphi)^2 = \frac{\pi^2}{3} + \frac{2}{\vartheta_3\left(0, e^{-2a}\right)} \times \sum_{\substack{m,m'=-\infty \\ m \neq m'}}^{\infty} \frac{(-1)^{m-m'}}{(m-m')^2} e^{-a(m^2+m'^2)}, \quad (6.20)$$

and the variance in orbital angular momentum is equal to

$$(\Delta m)^2 = \sum_{m=-\infty}^{\infty} m^2 |\sqrt{N(a)}e^{-am^2}|^2,$$

$$= N(a) \sum_{m=-\infty}^{\infty} m^2 e^{-2am^2}$$

$$= -\frac{N(a)}{2}\frac{\mathrm{d}}{\mathrm{d}a}\left(\frac{1}{N(a)}\right)$$

$$= -\frac{1}{2\vartheta_3\left(0, e^{-2a}\right)}\frac{\mathrm{d}}{\mathrm{d}a}\vartheta_3\left(0, e^{-2a}\right). \tag{6.21}$$

By taking the square of the variances in (6.20) and (6.21), we calculate the uncertainty relation $\Delta m \Delta \varphi$. We found that the overlapping Gaussian states have a lower uncertainty product than the intelligent states (Figure 6.8). In contrast to the CMUP states, the overlapping Gaussian states are well-defined throughout the whole range of angular uncertainty, $\Delta \phi$ (Figure 6.8).
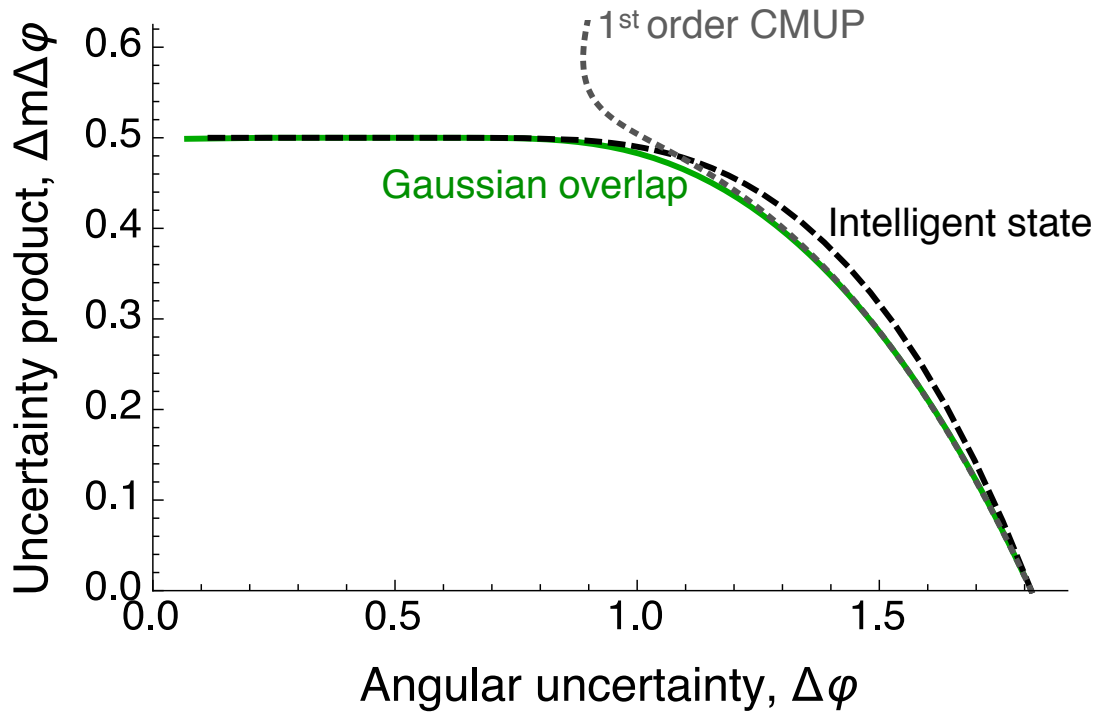


Figure 6.8: The overlapping Gaussian states have a lower uncertainty product than the intelligent states and are well-defined throughout the whole range of angular uncertainty, $\Delta \phi$.

### 6.2.3  Entropic uncertainty relation, $H_m + H_\varphi$

When we consider angular position and orbital angular momentum observables it is preferred to express the uncertainty relation in terms of the entropy of these observables. Entropic relations do not suffer from the issue of angle periodicity and the lower bound is not state dependent as it is in the uncertainty product (6.5). Furthermore, entropic relations are used in quantum communications theory as a measure of information content. In particular, entropic bounds quantify the secure information capacity per photon or the maximum secure information rate in quantum key distribution protocols [Leach et al., 2012].

The entropic uncertainty for continuous and unbounded conjugate variables, such as linear position, $x$, and linear momentum, $p$, is given by [Białynicki-Birula and Mycielski, 1975]

$$H_x + H_p \geq \ln(1 + \ln \pi) = \ln(e\pi) \,, \tag{6.22}$$

where the entropies are defined as

$$H_x = -\int_{-\infty}^{\infty} \mathrm{d}x |\psi(x)|^2 \ln \left(|\psi(x)|\right)^2$$
$$H_p = -\int_{-\infty}^{\infty} \mathrm{d}p |\psi(p)|^2 \ln \left(|\psi(p)|\right)^2 \,. \tag{6.23}$$

However, the entropic uncertainty of bounded and discrete variables, such as angular position, $\varphi$, and orbital angular momentum, $m$, respectively, has a different lower bound [Bialynicki-Birula, 1984],

$$H_\varphi + H_m \geq \ln(2\pi) \,, \tag{6.24}$$

where the entropies are defined as

$$H_\varphi = -\int_{-\pi}^{\pi} \mathrm{d}\varphi \, |\psi(\varphi)|^2 \ln \left(|\psi(\varphi)|^2\right) \tag{6.25}$$

$$H_m = -\sum_{m=-\infty}^{\infty} |c_m|^2 \ln \left(|c_m|^2\right) \,. \tag{6.26}$$

## Entropic uncertainty relation for the overlapping gaussian states

The orbital angular momentum entropy for our Gaussian state is

$$
\begin{aligned}
H_m &= -\sum_{m=-\infty}^{\infty} |c_m|^2 \ln\left(|c_m|^2\right) \\
&= -\sum_{m=-\infty}^{\infty} N(a)e^{-2am^2} \ln\left(N(a)e^{-2am^2}\right) \\
&= -\sum_{m=-\infty}^{\infty} N(a)e^{-2am^2} \left[\ln\left(N(a)\right) - 2am^2\right] \\
&= -N(a)\ln\left(N(a)\right)\sum_{m=-\infty}^{\infty} e^{-2am^2} + 2aN(a)\sum_{m=-\infty}^{\infty} m^2 e^{-2am^2} \\
&= -\ln\left(N(a)\right) + 2a\left(\Delta m\right)^2 \\
&= \ln\left[\vartheta_3(0, e^{-2a})\right] + 2a\left(\Delta m\right)^2
\end{aligned}
\tag{6.27}
$$

where the variance is given in (6.21).

We have not been able to find an analytical expression for the angle entropy, $H_\varphi$ for the whole range of angular uncertainty, $\Delta\varphi$. However, we can calculate limiting forms for the minimum and maximum ranges of the angular uncertainty, $\Delta\varphi$.

In the limit of very narrow Gaussian peaks, $a \to 0$, when there is very small angular uncertainty, $\Delta\varphi$, the orbital angular momentum distribution tends towards a continuum (Figure 6.7). In this limit we expect the entropic uncertainty to behave like the one for linear position and linear momentum, (6.22).

As the Gaussian peaks in the angle representation become well separated, we can approximate the wavefunction so that we consider only the peak centred at $\varphi = 0$,

$$
\psi(\varphi) \approx \sqrt{\frac{N(a)}{2a}} \exp\left\{-\frac{\varphi^2}{4a}\right\},
\tag{6.28}
$$

where the normalisation becomes

$$
\int_{-\pi}^{\pi} \mathrm{d}\varphi\, |\psi(\varphi)|^2 \equiv 1
$$

$$
\frac{N(a)}{2a}\int_{-\pi}^{\pi} \mathrm{d}\varphi\, \exp\left\{-\frac{\varphi^2}{2a}\right\} = 1
$$

$$
\frac{N(a)}{2a}\sqrt{2a\pi} = 1
$$

$$
\Rightarrow N(a) = \sqrt{\frac{2a}{\pi}}.
\tag{6.29}
$$

Note that in this limit of very small $a$ we can change the limits of the integrals from $\{-\pi, \pi\}$ to $\{-\infty, \infty\}$. The angle wavefunction is thus given by

$$
\psi(\varphi) \approx (2a\pi)^{-1/4} \exp\left\{-\frac{\varphi^2}{4a}\right\}.
\tag{6.30}
$$

It is useful to find the variance in angular position,

$$
\begin{aligned}
(\Delta\varphi)^2 &= \int_{-\pi}^{\pi} \mathrm{d}\varphi \; \varphi^2 |\psi(\varphi)|^2 \\
&= \frac{1}{\sqrt{2a\pi}} \int_{-\pi}^{\pi} \mathrm{d}\varphi \; \varphi^2 \exp\left\{-\frac{\varphi^2}{2a}\right\} \\
&= \frac{1}{\sqrt{2a\pi}} \sqrt{2\pi} \, a^{3/2} \\
&= a,
\end{aligned}
\tag{6.31}
$$

and the one in orbital angular momentum,

$$
\begin{aligned}
(\Delta m)^2 &= \sum_{m=-\infty}^{\infty} m^2 |c_m|^2 \\
&= \sum_{m=-\infty}^{\infty} m^2 |\sqrt{N(a)} e^{-am^2}|^2 \\
&= N(a) \sum_{m=-\infty}^{\infty} m^2 e^{-2am^2} \\
&= -\frac{N(a)}{2} \frac{\mathrm{d}}{\mathrm{d}a}\left(\frac{1}{N(a)}\right) \\
&= +\frac{\sqrt{a}}{\sqrt{2\pi}} \frac{\sqrt{\pi}}{\sqrt{2}\, 2a^{3/2}} \\
&= \frac{1}{4a}.
\end{aligned}
\tag{6.32}
$$

The entropy in angular position for this approximated state, (6.25), is equal to

$$
\begin{aligned}
H(\varphi) &= -\int_{-\pi}^{\pi} \mathrm{d}\varphi \, |\psi(\varphi)|^2 \ln\left(|\psi(\varphi)|^2\right) \\
&= -\int_{-\pi}^{\pi} \mathrm{d}\varphi \, \frac{1}{\sqrt{2a\pi}} \exp\left\{-\frac{\varphi^2}{2a}\right\} \ln\left(\frac{1}{\sqrt{2a\pi}} \exp\left\{-\frac{\varphi^2}{2a}\right\}\right) \\
&= -\frac{1}{\sqrt{2a\pi}} \ln\left(\frac{1}{\sqrt{2a\pi}}\right) \int_{-\pi}^{\pi} \mathrm{d}\varphi \, \exp\left\{-\frac{\varphi^2}{2a}\right\} + \frac{(\Delta\varphi)^2}{2a} \\
&= -\frac{1}{\sqrt{2a\pi}} \ln\left(\frac{1}{\sqrt{2a\pi}}\right) \sqrt{2a\pi} + \frac{1}{2} \\
&= \ln\left(\sqrt{2a\pi}\right) + \frac{1}{2} \\
&= \frac{1}{2} \ln\left(2ea\pi\right).
\end{aligned}
\tag{6.33}
$$

The entropy in angular momentum in this limit is equal to

$$H(m) = -\ln(N(a)) + 2a(\Delta m)^2$$
$$= \frac{1}{2}\ln\left(\frac{\pi}{2a}\right) + \frac{1}{2}$$
$$= \frac{1}{2}\ln\left(\frac{e\pi}{2a}\right), \tag{6.34}$$

and so the entropic uncertainty relation is

$$H(\varphi) + H(m) = \frac{1}{2}\ln(2ea\pi) + \frac{1}{2}\ln\left(\frac{e\pi}{2a}\right)$$
$$= \ln(e\pi), \text{ as required.} \tag{6.35}$$

On the other hand, in the limit of very broad Gaussian peaks in angular position, $a \to \infty$, we expect the entropic uncertainty to reach the lower bound of (6.24).

The angle wavefunction becomes

$$\psi(\varphi) = \sqrt{\frac{N(a)}{2\pi}} \sum_{m=-\infty}^{\infty} e^{-am^2} e^{im\varphi}$$
$$= \sqrt{\frac{N(a)}{2\pi}} \left[1 + \sum_{m=1}^{\infty} e^{-am^2} \cos(m\varphi)\right]$$
$$\to \sqrt{\frac{N(a)}{2\pi}}. \tag{6.36}$$

The state must be normalised, therefore

$$\int_{-\pi}^{\pi} \mathrm{d}\varphi\, |\psi(\varphi)|^2 \equiv 1$$
$$\int_{-\pi}^{\pi} \mathrm{d}\varphi\, \frac{N(a)}{2\pi} = 1$$
$$\Rightarrow N(a) = 1. \tag{6.37}$$

The entropy in angular position is

$$H_\varphi = -\int_{\pi}^{\pi} \mathrm{d}\varphi\, |\psi(\varphi)|^2 \ln|\psi(\varphi)|^2$$
$$= -\int_{\pi}^{\pi} \mathrm{d}\varphi\, \frac{1}{2\pi}\ln\left(\frac{1}{2\pi}\right) \tag{6.38}$$
$$= -\ln\left(\frac{1}{2\pi}\right) = \ln(2\pi). \tag{6.39}$$

As it is expected in this large $a$ limit, the entropy in orbital angular momentum is zero,

$$H_m = -\ln(N(a)) + 2a(\Delta m)^2$$
$$\to -\ln(N(a)) = 0. \tag{6.40}$$

Therefore the entropic uncertainty relation is equal to

$$H_m + H_\varphi = \ln(2\pi), \text{ as required.} \qquad (6.41)$$

In this way, we have demonstrated that our states tend towards the two expected entropic uncertainty bounds, (6.22) and (6.24), at the two limits of angular uncertainty $\Delta\varphi$.

## Numerical comparison

Although we do not have an analytical solution for the angular entropy $H_\varphi$, we can still compare numerically the entropic uncertainty, $H_m + H_\varphi$, of the overlapping Gaussian states and the intelligent states.
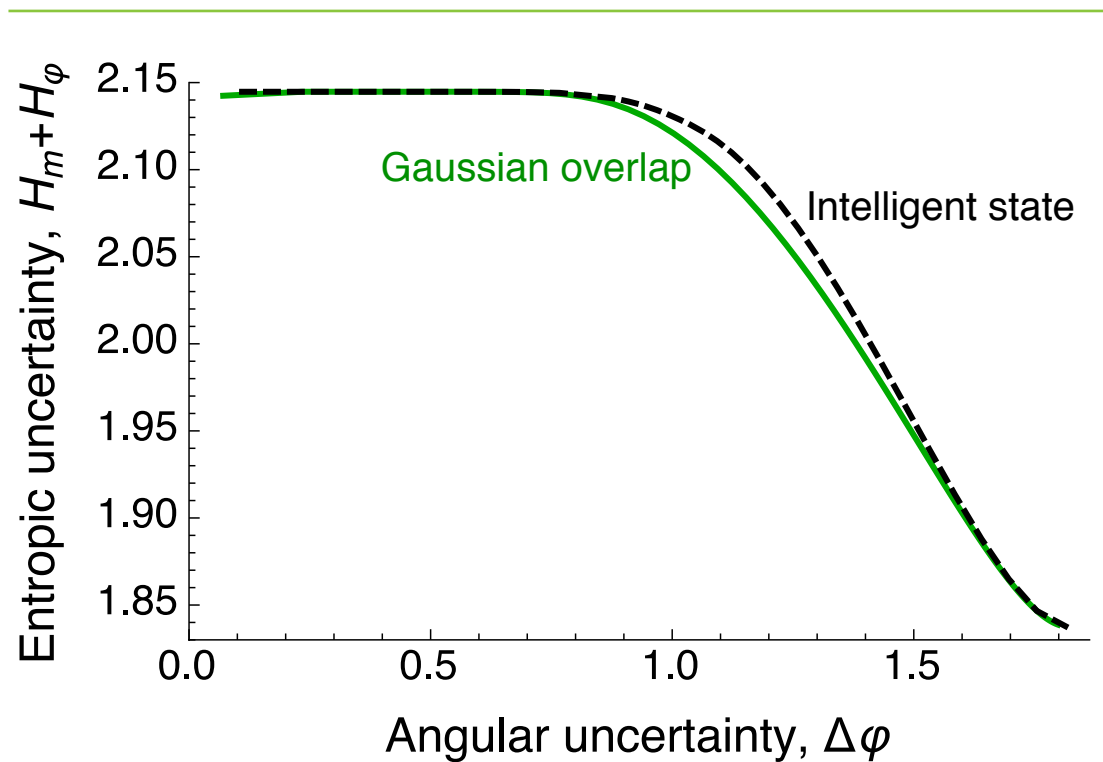


Figure 6.9: The overlapping gaussian states have a lower entropic uncertainty than the intelligent states, over a large range of angular uncertainty $\Delta\varphi$.

We found that the overlapping Gaussian states have a lower entropic uncertainty than the intelligent states over a large range of angular uncertainty, $\Delta\varphi$, (Figure 6.9). Both the overlapping Gaussian states and the intelligent states tend towards the limits $\ln(e\pi) = 2.14$ and $\ln(2\pi) = 1.84$, as the angular uncertainty, $\Delta\varphi$, increases.

## Entropic minimum

We perform a numerical optimisation to minimise the entropic uncertainty, $H_m + H_\varphi$, in order to determine the difference in the entropic uncertainty of our overlapping

Gaussian states and the numerically minimised sum. The numerical optimisation algorithm was written by Prof. Miles J. Padgett.

The algorithm used is an iterative optimisation of the cost function (the entropic sum, $H_m + H_\varphi$). We verified that our optimisation is global by running the iteration many times with a randomised optimisation pathway and confirming that the various solutions converged to the same answer.

The numerical optimisation showed no significant difference ($\sim 0.1\%$) between the entropic uncertainty for the overlapping gaussian states and the numerically minimised sum (Figure 6.10), thus suggesting that the overlapping Gaussian states are the minimum states.
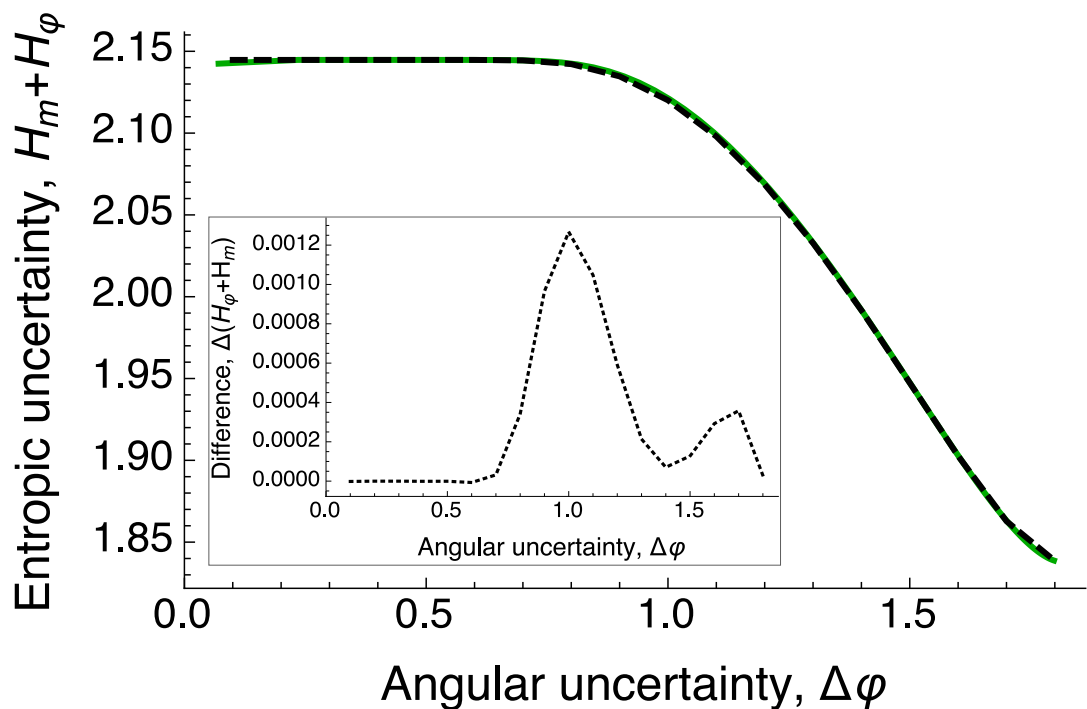


Figure 6.10: The overlapping Gaussian states have an almost identical entropic uncertainty to the numerically minimised sum.

The inset shows that the difference in the entropic uncertainty for the overlapping Gaussian states and the numerically minimised sum is of the order of $0.1\%$.

## 6.3   Conclusion

In this chapter we introduced a new form of orbital angular momentum and angle states. These states have Gaussian amplitudes in the orbital angular momentum representation and consist of a sum of overlapping Gaussians in the angle representation. Our proposed states have a lower uncertainty product than the intelligent states (Figure 6.8). They are also well-defined throughout the whole angular uncertainty range, in contrast to the CMUP states (Figure 6.8).

The entropic uncertainty of our overlapping Gaussian states is lower than the entropic uncertainty of the intelligent states (Figure 6.9). We found no significant difference between the entropic uncertainty of the overlapping Gaussian states and the numerically minimised states, suggesting that, for all practical purposes, the overlapping Gaussian states are the minimum states (Figure 6.10).

As these states are less complex than the CMUP states and have lower uncertainties than the intelligent states, both in terms of the uncertainty product $\Delta m \Delta \varphi$ and the entropic uncertainty $H(m) + H(\varphi)$, they have the potential to be used in quantum communications protocols that exploit the high-dimensional entanglement of the orbital angular momentum and the angle properties of photons.

## 6.A Full width at half maximum

For a Gaussian function given by

$$f(x) = \alpha \exp \left\{ -\frac{(x-b)^2}{2c^2} \right\}, \tag{6.42}$$

the full width at half maximum (FWHM) is equal to

$$\text{FWHM} = 2\sqrt{2\ln(2)}c. \tag{6.43}$$

Therefore for our state

$$\psi(\varphi) = \frac{1}{\sqrt{2a\vartheta_3\left(0, e^{-2a}\right)}} \sum_{n=-\infty}^{\infty} \exp\left\{ -\frac{1}{4a}\left(\varphi - 2n\pi\right)^2 \right\}, \tag{6.44}$$

we have that

$$2c^2 = 4a \Rightarrow c = \sqrt{2a}, \tag{6.45}$$

and so the full width at half maximum is equal to

$$\text{FWHM} = 2\sqrt{2\ln(2)}\sqrt{2a}$$
$$= 4\sqrt{\ln(2)a} \tag{6.46}$$

## 6.B Angular variance $(\Delta\varphi)^2$ for GEMS

For the angle states the variance is given by

$$(\Delta\varphi)^2 = \int_{-\pi}^{\pi} \mathrm{d}\varphi\, \varphi^2 |\psi(\varphi)|^2$$
$$= \frac{1}{2\pi\vartheta_3\left(0, e^{-2a}\right)} \int_{-\pi}^{\pi} \mathrm{d}\varphi\, \varphi^2 \sum_{m=-\infty}^{\infty} e^{-am^2} e^{im\varphi} \sum_{m'=-\infty}^{\infty} e^{-am'^2} e^{-im'\varphi}. \tag{6.47}$$

We can expand $\varphi^2$ in a Fourier series, such that

$$\varphi^2 = \frac{1}{2\pi} \sum_{n=-\infty}^{\infty} \alpha_n e^{in\varphi}, \tag{6.48}$$

where the Fourier coefficients are

$$\alpha_n = \int_{-\pi}^{\pi} \mathrm{d}\varphi\, \varphi^2 e^{-in\varphi}. \tag{6.49}$$

It follows that

$$\alpha_n = -\frac{\mathrm{d}^2}{\mathrm{d}n^2} \int_{-\pi}^{\pi} \mathrm{d}\varphi\, e^{-in\varphi}$$
$$= -\frac{\mathrm{d}^2}{\mathrm{d}n^2} \left[ \frac{e^{-in\varphi}}{-in} \right]$$
$$= -\frac{\mathrm{d}^2}{\mathrm{d}n^2} \left[ \frac{2\sin(n\pi)}{n} \right]$$
$$= \frac{2\pi}{n^2}(-1)^n, \tag{6.50}$$

and so (6.48) becomes

$$\varphi^2 = \sum_{n=-\infty}^{\infty} \frac{1}{n^2} (-1)^n e^{in\varphi}. \tag{6.51}$$

By substituting (6.51) into (6.47) we get

$$(\Delta\varphi)^2 = \frac{1}{2\pi\vartheta_3\left(0, e^{-2a}\right)} \int_{-\pi}^{\pi} \mathrm{d}\varphi \sum_{n=-\infty}^{\infty} \frac{(-1)^n}{n^2} e^{in\varphi} \sum_{m=-\infty}^{\infty} e^{-am^2} e^{im\varphi} \sum_{m'=-\infty}^{\infty} e^{-am'^2} e^{-im'\varphi}$$

$$= \frac{1}{2\pi\vartheta_3\left(0, e^{-2a}\right)} \sum_{n=-\infty}^{\infty} \sum_{m=-\infty}^{\infty} \sum_{m'=-\infty}^{\infty} \int_{-\pi}^{\pi} \mathrm{d}\varphi \frac{(-1)^n}{n^2} e^{-a(m^2+m'^2)} \underbrace{e^{in\varphi} e^{i(m-m')\varphi}}_{=2\pi\delta_{n,m-m'}}$$

$$= \frac{1}{\vartheta_3\left(0, e^{-2a}\right)} \sum_{m=-\infty}^{\infty} \sum_{m'=-\infty}^{\infty} \frac{(-1)^{m-m'}}{(m-m')^2} e^{-a(m^2+m'^2)} \tag{6.52}$$

This has a singularity at $m = m' \Rightarrow m = 0$. We note that the zeroth Fourier coefficient is

$$\alpha_0 = \int_{-\pi}^{\pi} \mathrm{d}\varphi \; \varphi^2$$

$$= \left[\frac{\varphi^3}{3}\right]_{-\pi}^{pi} = \frac{2\pi^3}{3}, \tag{6.53}$$

and so

$$\varphi_0^2 = \frac{\alpha_0}{2\pi} = \frac{\pi^2}{3}, \tag{6.54}$$

which has a variance

$$(\Delta\varphi_0)^2 = \frac{1}{2\pi\vartheta_3\left(0, e^{-2a}\right)} \int_{-\pi}^{\pi} \mathrm{d}\varphi \frac{\pi^2}{3} \sum_{m=-\infty}^{\infty} e^{-2am^2}$$

$$= \frac{1}{2\pi\vartheta_3\left(0, e^{-2a}\right)} 2\pi \frac{\pi^2}{3} \sum_{m=-\infty}^{\infty} e^{-2am^2},$$

$$= \frac{\pi^2}{3} \tag{6.55}$$

where we have used

$$\sum_{m'=-\infty}^{\infty} e^{-2am^2} = \vartheta_3\left(0, e^{-2a}\right), \tag{6.56}$$

Therefore we can write the variance as

$$(\Delta\varphi)^2 = \frac{\pi^2}{3} + \frac{2}{\vartheta_3\left(0, e^{-2a}\right)} \times \sum_{\substack{m,m'=-\infty \\ m \neq m'}}^{\infty} \frac{(-1)^{m-m'}}{(m-m')^2} e^{-a(m^2+m'^2)}. \tag{6.57}$$

## Conclusion

I N SUMMARY, in the first part of this thesis we presented a protocol for probabilistic amplification of coherent states and its experimental realisation and in the second part we proposed a new form of orbital angular momentum and angle states. This chapter is a brief overview of the characteristics and the main results of our proposals.

We proposed a method to amplify coherent states non-deterministically, based on coherent state comparison and photon subtraction. We post-selected the output state on no detection events in the state comparison measurement and a detection event in the photon subtraction measurement. The nominal gain depends only on the characteristics of the two beamsplitters: it is given by $g = t_2/r_1$, where $r_1$ is the reflection coefficient of the state comparison beamsplitter and $t_2$ is the transmission coefficient of the photon subtraction beamsplitter. Dark counts were so low as to allow us to assume that none were there and we found that our protocol is relatively insensitive to detector quantum efficiency.

We found that the fidelity of the amplified state with the ideal target state is very high. In particular, for an input state chosen from a binary alphabet, when the comparison beamsplitter is $50 : 50$, the theoretical fidelity of the output state with the target state is $100\%$. The gain in this special case is $g^2 = 1.8$, if the photon subtraction beamsplitter has transmissivity $t^2 = 0.9$. Our protocol does not use any quantum resources and consequently has a high probability of success. The probability of success increases with gain ($\sim 10 - 40\%$) and it can be increased at a cost to the fidelity. Both the fidelity and the probability of success increase with the input state amplitude.

The simplicity of our protocol made it possible to realise it experimentally. We tested the state comparison amplifier for a fixed gain ($g^2 = 1.8$) and varying mean photon number per pulse. We ran the experiment for three sets of input states: a binary set, four and eight coherent states. We found that the performance of the last two sets is similar to the theoretical performance of the phase covariant set. For all sets both the fidelity and the success rate were very high. In particular for the two state set, the fidelity is $> 98\%$ and the success rate is $> 26000$ amplified states per

second. We found that both the theoretical and the experimental performance of our protocol compare favourably with other non-deterministic amplification methods.

In the second part of the thesis we proposed a new form of orbital angular momentum and angle states, that consist of a sum of overlapping Gaussians in the angle representation. We found that our states are well-defined throughout the whole angular range, in contrast to the CMUP states. We compared their uncertainty product and their entropic uncertainty with the intelligent states and we found that in both cases the overlapping Gaussian states have a smaller uncertainty. Furthermore, we compared their entropic uncertainty with numerically optimised states and we found that they do not have a significant difference ($\sim 1\%$), suggesting that, for all practical purposes, they are the minimum states.

Our findings highlight the potential that the quantum optical state comparison amplifier offers an option for the development of quantum optical repeaters and the overlapping Gaussian states are the ideal states to use in protocols involving high-dimensional entanglement in the orbital angular momentum basis.

# Bibliography

E. Eleftheriadou, S. M. Barnett, and J. Jeffers, "Quantum optical state comparison amplifier," *Phys. Rev. Lett.*, vol. 111, p. 213601, Nov 2013.

A. M. Yao, T. Brougham, E. Eleftheriadou, M. J. Padgett, and S. M. Barnett, "Entropic uncertainty minimum for angle and angular momentum," *Journal of Optics*, vol. 16, no. 10, p. 105404, 2014.

**Chapter 2:**.

S. Barnett and P. M. Radmore, *Methods in theoretical quantum optics*. Oxford University Press, 2002.

W. P. Schleich, *Quantum optics in phase space*. John Wiley & Sons, 2011.

G. Grynberg, A. Aspect, and C. Fabre, *Introduction to quantum optics: from the semi-classical approach to quantized light*. Cambridge university press, 2010.

R. J. Glauber, "Coherent and incoherent states of the radiation field," *Phys. Rev.*, vol. 131, pp. 2766–2788, Sep 1963.

R. Loudon, *The quantum theory of light*, 3rd ed. Oxford university press, 2000.

E. Andersson, M. Curty, and I. Jex, "Experimentally realizable quantum comparison of coherent states and its applications," *Physical Review A*, vol. 74, no. 2, p. 022304, 2006.

P. L. Kelley and W. H. Kleiner, "Theory of electromagnetic field measurement and photoelectron counting," *Phys. Rev.*, vol. 136, pp. A316–A334, Oct 1964.

**Chapter 3:**.

H. Haus and J. Mullen, "Quantum noise in linear amplifiers," *Physical Review*, vol. 128, no. 5, p. 2407, 1962.

W. K. Wootters and W. H. Zurek, "A single quantum cannot be cloned," 1982.

C. M. Caves, "Quantum limits on noise in linear amplifiers," *Physical Review D*, vol. 26, no. 8, p. 1817, 1982.

T. Ralph and A. Lund, "Quantum communication measurement and computing proceedings of 9th international conference," 2009.

D. T. Pegg, L. S. Phillips, and S. M. Barnett, "Optical state truncation by projection synthesis," *Phys. Rev. Lett.*, vol. 81, pp. 1604–1606, Aug 1998.

C. H. Bennett, G. Brassard, C. Crépeau, R. Jozsa, A. Peres, and W. K. Wootters, "Teleporting an unknown quantum state via dual classical and einstein-podolsky-rosen channels," *Phys. Rev. Lett.*, vol. 70, pp. 1895–1899, Mar 1993.

S. Babichev, J. Ries, and A. Lvovsky, "Quantum scissors: Teleportation of single-mode optical states by means of a nonlocal single photon," *EPL (Europhysics Letters)*, vol. 64, no. 1, p. 1, 2003.

G.-Y. Xiang, T. Ralph, A. Lund, N. Walk, and G. J. Pryde, "Heralded noiseless linear amplification and distillation of entanglement," *Nature Photonics*, vol. 4, no. 5, pp. 316–319, 2010.

F. Ferreyrol, M. Barbieri, R. Blandino, S. Fossier, R. Tualle-Brouri, and P. Grangier, "Implementation of a nondeterministic optical noiseless amplifier," *Physical review letters*, vol. 104, no. 12, p. 123603, 2010.

J. Jeffers, "Nondeterministic amplifier for two-photon superpositions," *Physical Review A*, vol. 82, no. 6, p. 063828, 2010.

P. Marek and R. Filip, "Coherent-state phase concentration by quantum probabilistic amplification," *Physical Review A*, vol. 81, no. 2, p. 022302, 2010.

H.-J. Kim, S.-Y. Lee, S.-W. Ji, and H. Nha, "Quantum linear amplifier enhanced by photon subtraction and addition," *Physical Review A*, vol. 85, no. 1, p. 013839, 2012.

J. Fiurášek, "Engineering quantum operations on traveling light beams by multiple photon addition and subtraction," *Physical Review A*, vol. 80, no. 5, p. 053822, 2009.

A. Zavatta, J. Fiurášek, and M. Bellini, "A high-fidelity noiseless amplifier for quantum light states," *Nature Photonics*, vol. 5, no. 1, pp. 52–60, 2011.

M. A. Usuga, C. R. Müller, C. Wittmann, P. Marek, R. Filip, C. Marquardt, G. Leuchs, and U. L. Andersen, "Noise-powered probabilistic concentration of phase information," *Nature Physics*, vol. 6, no. 10, pp. 767–771, 2010.

C. R. Müller, C. Wittmann, P. Marek, R. Filip, C. Marquardt, G. Leuchs, and U. L. Andersen, "Probabilistic cloning of coherent states without a phase reference," *Physical Review A*, vol. 86, no. 1, p. 010305, 2012.

J. Jeffers, "Optical amplifier-powered quantum optical amplification," *Physical Review A*, vol. 83, no. 5, p. 053818, 2011.

**Chapter 4:**.

P. J. Clarke, R. J. Collins, V. Dunjko, E. Andersson, J. Jeffers, and G. S. Buller, "Experimental demonstration of quantum digital signatures using phase-encoded coherent states of light," *Nature communications*, vol. 3, p. 1174, 2012.

G. N. Watson, *A treatise on the theory of Bessel functions*. Cambridge university press, 1995.

S. D. Bartlett, T. Rudolph, and R. W. Spekkens, "Reference frames, superselection rules, and quantum information," *Reviews of Modern Physics*, vol. 79, no. 2, p. 555, 2007.

**Chapter 5:**.

A. Kumar and A. K. Ghatak, *Polarization of light with applications in optical fibers*. SPIE Press, 2011, vol. 246.

P. J. Clarke, R. J. Collins, P. A. Hiskett, M.-J. García-Martínez, N. J. Krichel, A. McCarthy, M. G. Tanner, J. A. O'Connor, C. M. Natarajan, S. Miki *et al.*, "Analysis of detector performance in a gigahertz clock rate quantum key distribution system," *New Journal of Physics*, vol. 13, no. 7, p. 075008, 2011.

A. Spinelli, L. Davis, and H. Dautet, "Actively quenched single-photon avalanche diode for high repetition rate time-gated photon counting," *Review of scientific instruments*, vol. 67, no. 1, pp. 55–61, 1996.

G. Buller and R. Collins, "Single-photon generation and detection," *Meas. Sci. Technol*, vol. 21, no. 1, p. 012002, 2010.

R. J. Collins, R. H. Hadfield, and G. S. Buller, "Commentary: New developments in single photon detection in the short wavelength infrared regime," *Journal of Nanophotonics*, vol. 4, no. 1, pp. 040 301–040 301, 2010.

M. Wahl, H.-J. Rahn, T. Röhlicke, G. Kell, D. Nettels, F. Hillger, B. Schuler, and R. Erdmann, "Scalable time-correlated photon counting system with multiple independent input channels," *Review of Scientific Instruments*, vol. 79, no. 12, p. 123113, 2008.

K. Gordon, V. Fernandez, G. Buller, I. Rech, S. Cova, and P. Townsend, "Quantum key distribution system clocked at 2 ghz," *Optics Express*, vol. 13, no. 8, pp. 3015–3020, 2005.

N. Lütkenhaus and A. Shields, "Focus on quantum cryptography: theory and practice," *New Journal of Physics*, vol. 11, no. 4, p. 045005, 2009.

R. J. Collins, R. J. Donaldson, V. Dunjko, P. Wallden, P. J. Clarke, E. Andersson, J. Jeffers, and G. S. Buller, "Realization of quantum digital signatures without the requirement of quantum memory," *Physical review letters*, vol. 113, no. 4, p. 040502, 2014.

**Chapter 6:**.

C. Aragone, G. Guerri, S. Salamo, and J. Tani, "Intelligent spin states," *Journal of Physics A: Mathematical, Nuclear and General*, vol. 7, no. 15, p. L149, 1974.

D. T. Pegg, S. M. Barnett, R. Zambrini, S. Franke-Arnold, and M. Padgett, "Minimum uncertainty states of angular momentum and angular position," *New Journal of Physics*, vol. 7, no. 1, p. 62, 2005.

L. Allen, M. W. Beijersbergen, R. Spreeuw, and J. Woerdman, "Orbital angular momentum of light and the transformation of laguerre-gaussian laser modes," *Physical Review A*, vol. 45, no. 11, p. 8185, 1992.

M. W. Beijersbergen, L. Allen, H. E. L. O. van der Veen, and J. P. Woerdman, "Astigmatic laser mode converters and transfer of orbital angular momentum," *Opt. Commun.*, vol. 96, pp. 123–132, 1993.

C. Tamm and C. Weiss, "Bistability and optical switching of spatial patterns in a laser," *JOSA B*, vol. 7, no. 6, pp. 1034–1038, 1990.

L. Allen, S. M. Barnett, and M. J. Padgett, *Optical angular momentum*. CRC Press, 2003.

A. M. Yao and M. J. Padgett, "Orbital angular momentum: origins, behavior and applications," *Adv. Opt. Photon.*, vol. 3, no. 2, pp. 161–204, Jun 2011.

M. Harris, C. Hill, and J. Vaughan, "Optical helices and spiral interference fringes," *Optics communications*, vol. 106, no. 4, pp. 161–166, 1994.

M. Beijersbergen, R. Coerwinkel, M. Kristensen, and J. Woerdman, "Helical-wavefront laser beams produced with a spiral phaseplate," *Optics Communications*, vol. 112, no. 5, pp. 321–327, 1994.

G. Turnbull, D. Robertson, G. Smith, L. Allen, and M. Padgett, "The generation of free-space laguerre-gaussian modes at millimetre-wave frequencies by use of a spiral phaseplate," *Optics communications*, vol. 127, no. 4, pp. 183–188, 1996.

V. Y. Bazhenov, M. Vasnetsov, and M. Soskin, "Laser beams with screw dislocations in their wavefronts," *Jetp Lett*, vol. 52, no. 8, pp. 429–431, 1990.

N. Heckenberg, R. McDuff, C. Smith, H. Rubinsztein-Dunlop, and M. Wegener, "Laser beams with phase singularities," *Optical and Quantum Electronics*, vol. 24, no. 9, pp. S951–S962, 1992.

A. Mair, A. Vaziri, G. Weihs, and A. Zeilinger, "Entanglement of the orbital angular momentum states of photons," *Nature*, vol. 412, no. 6844, pp. 313–316, 2001.

J. Leach, B. Jack, J. Romero, A. K. Jha, A. M. Yao, S. Franke-Arnold, D. G. Ireland, R. W. Boyd, S. M. Barnett, and M. J. Padgett, "Quantum correlations in optical angle–orbital angular momentum variables," *Science*, vol. 329, no. 5992, pp. 662–665, 2010.

A. Vaziri, G. Weihs, and A. Zeilinger, "Experimental two-photon, three-dimensional entanglement for quantum communication," *Physical Review Letters*, vol. 89, no. 24, p. 240401, 2002.

G. Molina-Terriza, A. Vaziri, J. Řeháček, Z. Hradil, and A. Zeilinger, "Triggered qutrits for quantum communication protocols," *Physical review letters*, vol. 92, no. 16, p. 167903, 2004.

W. K. Heisenberg, *The Physical Principles of the Quantum Theory*.

H. Robertson, "An indeterminacy relation for several observables and its classical interpretation," *Physical Review*, vol. 46, no. 9, p. 794, 1934.

S. M. Barnett and D. Pegg, "Quantum theory of rotation angles," *Physical Review A*, vol. 41, no. 7, p. 3427, 1990.

S. Franke-Arnold, S. M. Barnett, E. Yao, J. Leach, J. Courtial, and M. Padgett, "Uncertainty principle for angular position and angular momentum," *New Journal of Physics*, vol. 6, no. 1, p. 103, 2004.

I. S. Gradshteyn and I. M. Ryzhik, *Table of Integrals, Series, and Products*. 8th edn ed A. Jeffrey and D. Zwillinger, Chapter 8: Special functions, p.887 Academic Press, 2007.

T. M. Cover and J. A. Thomas, *Elements of information theory*. John Wiley & Sons, 2012.

J. Leach, E. Bolduc, D. J. Gauthier, and R. W. Boyd, "Secure information capacity of photons entangled in many dimensions," *Physical Review A*, vol. 85, no. 6, p. 060304, 2012.

I. Białynicki-Birula and J. Mycielski, "Uncertainty relations for information entropy in wave mechanics," *Communications in Mathematical Physics*, vol. 44, no. 2, pp. 129–132, 1975.

I. Bialynicki-Birula, "Entropic uncertainty relations," *Physics Letters A*, vol. 103, no. 5, pp. 253–254, 1984.